A transportable optical lattice clock for metrology and geodesy

Der QUEST-Leibniz-Forschungsschule der
Gottfried Wilhelm Leibniz Universität Hannover
zur Erlangung des Grades

Doktor der Naturwissenschaften
Dr. rer. nat.

genehmigte Dissertation
von

M.Sc.-Phys. Jacopo Grotti
geboren am 13.09.1988, in Arezzo

2018

Referent	PD Dr. Christian Lisdat Physikalisch-Technische Bundesanstalt
Koreferent	Prof. Dr. Ernst M. Rasel Leibniz Universität Hannover
Tag der Disputation	04.05.2018

Abstract

This thesis reports the use of the PTB transportable optical lattice clock based on ^{87}Sr atoms in two measurement campaigns outside a quantum optics laboratory for applications in metrology and geodesy. From a metrological point of view, a transportable optical frequency standard can serve to compare optical clocks developed in different institutes, which is an important step in view of a future redefinition of the second by an optical frequency. In geodesy, it can be use for chronometric leveling, which is the determination of geopotential differences via the measurement of remote clocks' relativistic redshift [Ver83, Bje85]: A 1 cm height difference on Earth corresponds to a fractional redshift of 10^{-18}, an accuracy that is nearly reached by the best laboratory optical clocks today [Nic15, Ush15, Hun16, Al-15a, Sch17]. However, transportable clocks are required to establish this new field of research to allow for the required flexibility in the choice of the measurement sites.

The design and first realization of the transportable clock were done in the laboratory in previous works [Vog15, Vog16, Häf15a]. In this thesis, we completed and installed the system in an air conditioned car trailer [Kol17], and we used the clock in two measurement campaigns outside PTB [Gro18].
In the first campaign, we measured the gravity potential difference between the Italian metrology institute (INRIM) and the Laboratoire Soutterrain de Modane (LSM), a particle physics laboratory in France. The locations are 90 km apart and are connected via a fiber link for optical frequency transfer allowing for comparisons against INRIM's clocks. LSM and INRIM have a height difference of approximately 1000 m. At INIRM we also performed a measurement of the frequency ratio between our clock and INIRM's ^{171}Yb optical clock, a demonstration of remote optical comparisons with a transportable clock. In this campaign, the Sr clock achieved an uncertainty of 2×10^{-16} [Gro18].
In the second campaign, we used the transportable clock to measure the gravity potential difference between PTB and SYRTE-Observatorie de Paris, the French metrology institute. After a local validation with PTB's stationary ^{87}Sr lattice clock, we performed a remote comparison making use of the 1,415 km optical fiber link between the two institutes. In this campaign, we reached an uncertainty on the frequency ratio of 3.6×10^{-17}.

The clock has now been characterized to a fractional uncertainty of 2×10^{-17} (very close to the design limit of approximately 1×10^{-17}) and a fraction instability of $1.5\times10^{-15}/\sqrt{\tau}$, values that are competitive with the performances of the majority of the laboratory systems in Europe.

Keywords: transportable optical clocks, relativistic geodesy, frequency standards, metrology, chronometric leveling, lattice clock, Strontium

Zusammenfassung

In dieser Arbeit werden zwei Messkampagnen der transportablen ^{87}Sr Gitteruhr der PTB mit metrologischer und geodätischer Anwendung vorgestellt, die außerhalb der für die Quantenoptik typischen Laborbedingungen durchgeführt wurden. Vom metrologischen Gesichtspunkt aus können transportable optische Frequenznormale für den Vergleich von optischen Uhren unterschiedlicher Institute dienen, was für eine Neudefinition der Einheit Sekunde über von hoher Bedeutung ist. In der Geodäsie liegt die Anwendung im chronometrischen Nivellement, bei dem die Differenz des Geopotentials aus der relativistischen Rotverschiebung zwischen zwei Uhren bestimmt wird [Ver83, Bje85]. Auf der Erdoberfläche entspricht eine relative Rotverschiebung von 10^{-18} einer Höhendifferenz von 1 cm. Unsicherheiten in dieser Größenordnung werden von den besten Laboraufbauten erreicht [Nic15, Ush15, Hun16, Al-15a, Sch17]. Für die Flexible Anwendung in der Geodäsie werden allerdings transportable Uhren dieser Qualität benötigt.

Der Entwurf und die erste Realisierung der transportablen Uhr wurde bereits im Labor demonstriert [Vog15, Vog16, Häf15a]. In dieser Arbeit wurde der Aufbau komplettiert, in einem klimatisierten Autoanhänger installiert [Kol17] und in zwei Messkampagnen verwendet [Gro18].
In der ersten Kampagne wurde die Potentialdifferenz zwischen dem Laboratoire Souterrain de Modane (LSM), einem Labor für Teilchenphysik in Frankreich, und dem italienischen Metrologieinstitut INRIM gemessen. Beide sind 90 km entfernt und durch eine optische Faser zur Frequenzübertragung verbunden, die Vergleiche mit den Uhren am INRIM erlaubt. Zwischen LSM und INRIM liegt eine Höhendifferenz von ca. 1000 m. Am INRIM wurde außerdem das optische Frequenzverhältnis zur dortigen ^{171}Yb Gitteruhr bestimmt, was die Validierung optischer Uhren mit dem transportablen Aufbau demonstriert. In diesen Messungen wurden eine Unsicherheit der Sr Uhr von 2×10^{-16} erreicht [Gro18].
In der zweiten Kampagne wurde mit der transportablen Sr Uhr die Potentialdifferenz zwischen der PTB und dem französischen Metrologieinstitut SYRTE-Observatorie de Paris bestimmt. Nach einer lokalen Validierung mit der stationären Sr Gitteruhr der PTB wurde ein Vergleich über den 1415 km langen optischen Faserlink zwischen beiden Instituten durchgeführt. Das Frequenzverhältnis wurde mit einer Unsicherheit von 3.6×10^{-17} gemessen.
Die Uhr ist jetzt mit einer Unsicherheit von 2×10^{-17} charakterisiert, was dicht am Designziel von 1×10^{-17}) liegt, und erreicht eine Instabilität von $1.5\times10^{-15}/\sqrt{\tau}$. Beide Werte liegen auf dem Niveau der meisten optischen Uhren in Europa.

Stichworte: transportable optische Uhren, relativistische Geodäsie, Frequenzstandards, Metrologie, chronometrischen Nivellement, Gitteruhren, Strontium

Publications

Stefan Vogt, Sebastian Häfner, **Jacopo Grotti**, Silvio Koller, Ali Al-Masoudi, Uwe Sterr and Christian Lisdat.
A transportable optical lattice clock.
Journal of Physics: Conference Series **723**, 012020 (2016).

Silvio Koller, **Jacopo Grotti**, Stefan Vogt, Ali Al-Masoudi, Sören Dörscher, Sebastian Häfner, Uwe Sterr and Christian Lisdat.
Transportable Optical Lattice Clock with 7×10^{-17} Uncertainty.
Physical Review Letters **118**, 073601 (2017).

Jacopo Grotti, Silvio Koller, Stefan Vogt, Sebastian Häfner, Uwe Sterr, Christian Lisdat, Heiner Denker, Christian Voigt, Ludger Timmen, Antoine Rolland, Fred N. Baynes, Helen S. Margolis, Michel Zampaolo, Pierre Thoumany, Marco Pizzocaro, Benjamin Rauf, Filippo Bregolin, Anna Tampellini, Piero Barbieri, Massimo Zucco, Giovanni A. Costanzo, Cecilia Clivati, Filippo Levi and Davide Calonico.
Geodesy and metrology with a transportable optical clock.
Nature Physics doi: 10.1038/s41567-017-0042-3 (2018).

Contents

Chapter 1

Introduction

Metrology is defined by the International Bureau of Weights and Measures (BIPM) as "the science of measurement, embracing both experimental and theoretical determinations at any level of uncertainty in any field of science and technology". The capability to perform accurate measurements of a quantity and define reference standards is not only a fundamental part of physics and science in general, but is also of great significance in the technological progress of our society.

In this thesis I will focus on the measurement of frequency. Among all the physical quantities, frequency (ν) is the one that we can measure with the highest precision: today's state-of-the-art optical atomic clocks provide their oscillation frequency with a fractional accuracy of few parts in 10^{18} and have an instability of few parts in $10^{17}/\sqrt{\tau}$, where τ is the total averaging time [Nic15, Ush15, Hun16, Al-15a, Sch17]. Experiments are ongoing and probably optical clocks performances will improve even more in the next years.
These results are pushing towards an optical redefinition of the second in the International System of Units (SI) [Gil11, Mar14, Rie15]. The second is currently defined as exactly 9 192 631 770 oscillations of the radiation corresponding to the transition between the two hyperfine levels of the ground state of the ^{133}Cs atom. This microwave frequency is indeed determined with much less precision with respect to the frequency of the optical standards presented above: Cs fountains clocks are limited to an accuracy of few parts in 10^{16} and an instability of few parts in $10^{14}/\sqrt{\tau}$ [Cla91, Jef99, Wey00, Lev04, Szy05].

Some optical atomic transition are already accepted as a secondary representation of the second [CCT04], and the first steps for an optical realization of the second have already been taken [Le 13, Gre16, Yao18].

However, before a redefinition of the second in term of an optical frequency standard can really take place, it is necessary to test the consistency of optical frequency generated by clocks developed in different institutes. The uncertainty of the Cs fountains defining the second limits the accuracy of absolute optical frequency measurements: Their comparison can show possible inconsistency only at the 10^{-16} level. To surpass this limit, direct optical frequency ratios between remote clocks are needed. Frequency ratios, being unit-less numbers, do not depend on the realization of the second.

At the moment, the only method of frequency comparison that has enough stability to connect an compare remote optical clocks without limiting the accuracy of the measurement are optical-fiber links, which are however restricted to a continental scale. A transportable optical clock that can be moved between different laboratories could serve for clock comparisons at the level of the accuracy requested, allowing in addition the connection between institutes where a link is not yet present.

Figure 1.1 shows the different accuracy that can be reached for the comparison of ^{87}Sr

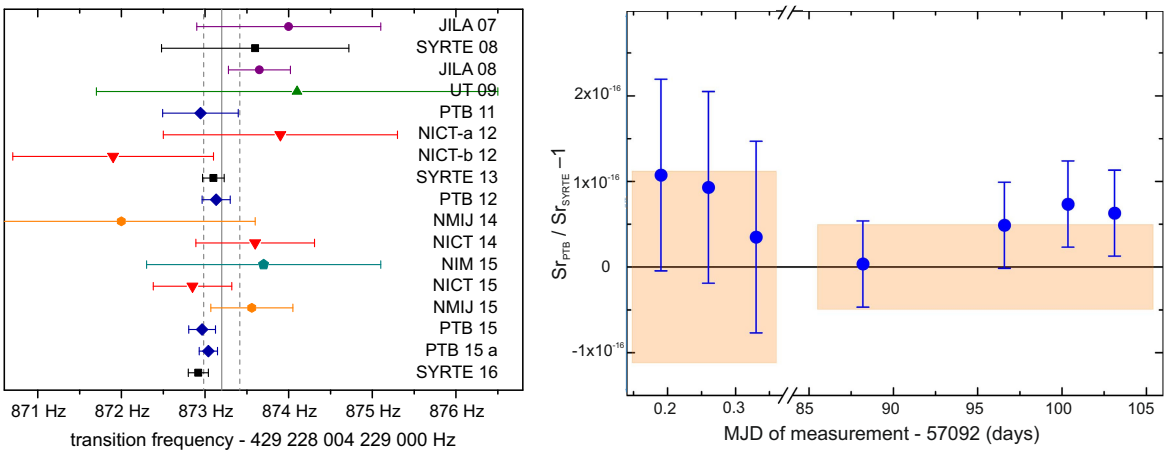

Figure 1.1: On the left: comparison of absolute frequency measurements of the ^{87}Sr clock frequency performed in different laboratories (more details in section 2.1.5). On the right: optical ratio between PTB and Syrte-Observatoire de Paris (French metrology institute) ^{87}Sr clocks trough the fiber link connecting the two institutes [Lis16].

optical clocks developed in different institutes when the absolute frequency results are compared or when a direct optical frequency ratio is performed. The beast absolute measurements reach an accuracy of $\sim$0.1 Hz ($2-3\times10^{-16}$ fractional inaccuracy, limited by the Cs fountains), while the direct ratio measured via fiber link was performed at the 5 10^{-17} inaccuracy level [Lis16].

Defining the second is not the only application where these highly precise instruments can be employed: they can also serve as benchmarks to test basic theories like general relativity and quantum electrodynamics or to confirm the invariance of fundamental constants in physics [For07, Bla08, Hun14].

Moreover, with optical clocks frequencies reaching and surpassing the 10^{-17} uncertainty, their application in relativistic geodesy is becoming feasible. Relativistic geodesy was proposed in the early 1980s [Ver83, Bje85] and refers to the determination of geopotential differences (fundamental observables in geodesy) via the measurement of remote clocks relativistic redshift $\Delta\nu_{rel}$. From the theory of general relativity it is in fact well know that time is not an absolute quantity, but depends on the relative velocity and the relative position in the gravity potential field of the observer ($\Delta U = c^2\Delta\nu_{rel}/\nu_0$, where ΔU is the geopotential difference, ν_0 is the unperturbed clock frequency and c^2 is the speed of light). In particular, to resolve a geopotential difference corresponding to 1 cm on Earth, it is necessary to determine the redshift between the clocks frequency with a fractional uncertainty of 10^{-18}. This method to measure height differences is called "chronometric leveling".

State-of-the-art standard geodesy methods (accurate GNSS positions plus gravity field modeling) provide for long distance (hundreds of kilometers) potential differences measurements with an accuracy limited to the level of 2-3 cm [Den13]. Moreover, when comparing heights measured with the GNSS/gravity modeling approach to the one measured with the spirit leveling (after correcting for the fact that the different reference points are used in different countries), inconsistencies at the decimeter level arise (see figure 1.2). Chronometric leveling can then be a third complementary method when clock reach the necessary accuracy to measure potential difference over long distances. Rela-

tivistic geodesy is expected to be a growing field for the next years: optical clocks can improve the high spatial determination of the geopotential [Lio17], at the point that in a recent geodesy paper a relativistic definition of the geoid has been presented [Phi17].

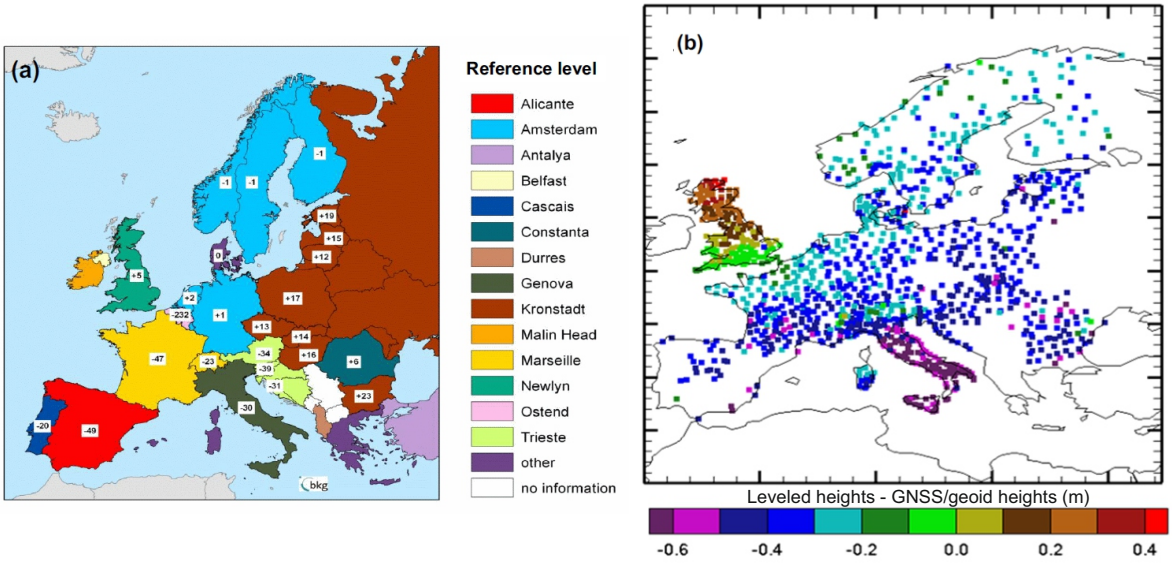

Figure 1.2: On the left: National heights system offsets with respect to the common European height system EVRF2007. On the right: discrepancy between GNSS/gravimetry and leveling measured height after offset correction [Gru14].

Currently optical clocks are stationary systems and can only be operated in the laboratory where they are built. In this work, I will present on the contrary an optical clock based on ^{87}Sr neutral atoms transformed from a bulky laboratory system into a transportable and more compact setup [Vog16, Kol17]. Such a transportable high performing frequency standard has innovative applications in optical frequency metrology and relativistic geodesy and in this thesis I will show how these fields can gain from the development of transportable optical clocks, presenting the results we obtained in two proof of principle measurement campaigns with the transportable clock [Gro18].

For relativistic geodesy, transportable optical clocks give two key advantages. First, since the more interesting locations from a geophysics point of view are remote and transition zones (where normally a metrology laboratory for optical clocks would not be build), the use of a compact transportable optical clock gives more flexibility in the choice of the

experimental site. In addition to this, the possibility to move the system permits side-by-side comparisons with the reference clock in order to cancel possible spurious effects on the redshift determination coming from the single clocks.
For applications of transportable optical clocks in relativistic geodesy a stable frequency link (not limiting the measurement accuracy) between the reference clock and the chosen remote location is needed. At the moment these requirements are fulfilled by optical fiber links: it is expected that they will become more and more common in the near future. Moreover, research is ongoing to have satellite links with the necessary stability [Lau15]. Chronometric leveling will then become a realistic prospective.

Looking at the history of transportable clocks based on cold atoms we found that in the last twenty years a few transportable microwave Cs fountains were built. In this case the motivation was to have a transportable absolute frequency standard with performances similar to the primary Cs fountains present in metrological institutes.
A transportable Cs fountain clock was developed at Syrte-Observatorie de Paris and it has been employed in some measurement campaigns [Nie00, Biz04, Fis04, Par11] to perform absolute frequency measurements. For this clock an uncertainty of $5.9 \cdot 10^{-16}$ and an instability of $1.8 \times 10^{-13}/\sqrt{\tau}$ have been reported [Abg12, Gué12]. The company μQUANS, a spin-off from Institut d'Optique and Observatoire de Paris, produced in the last years the first commercial version of this clock, for which a flicker floor at 2×10^{-15} after one day of integration is reported.
A similar transportable Cs fountain clock has been built with the same motivation at NIM (National Institue of Metrology) in China, with an uncertainty of $3 \cdot 10^{-15}$ and an instability of $9 \times 10^{-13}/\sqrt{\tau}$ [LI09].
Another application connected to the development of compact Cs fountains is their use on board of space satellites, where they can be employed to perform accurate frequency transfer over long distances. PHARAO is a compact Cs fountain clock for the ACES space mission developed with this purpose, and it is expected that it will be launched in 2018 [Lau15]. In 2016 with the CASEC mission the China Manned Space Program successfully lunched a similar clock in orbit [Li16].

However for the applications in optical frequency metrology and relativistic geodesy described before (and depicted in figure 1.3) the performances of these transportable and

compact clocks are not high enough. It is in this case necessary for the transportable clock to have an uncertainty of 10^{-17} or below and an instability in the order or below $10^{-15}/\sqrt{\tau}$, to reach this uncertainty in considerably less than one week of accumulated measurement time: These requirements can be reached only by developing transportable optical clocks.

Transferring the performances of laboratory optical clocks to their transportable versions it is indeed a difficult task, since they require a high number of lasers, a vacuum system and numerous electronic and optical components. Recently efforts in this direction have been started, aiming from one side to the development of optical clocks for space applications [Bon15c, Ori16] and on the other side to on ground transportation like the ion clock reported in [Cao16], that reaches an uncertainty of 7.7×10^{-17} and an instability of $2.3 \times 10^{-14}/\sqrt{\tau}$.

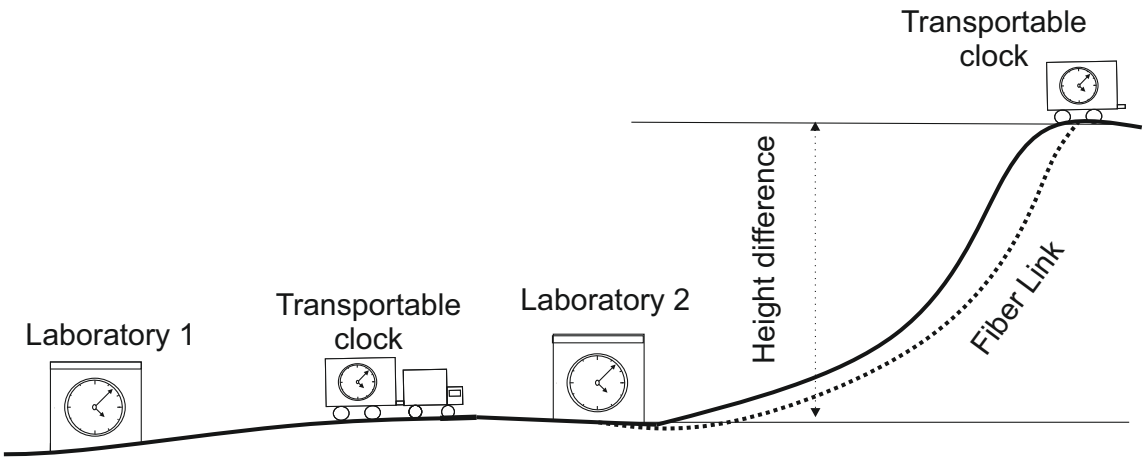

Figure 1.3: Schematic representation of the two applications where a transportable optical clock can be employed. It can serve to compare optical clocks of remote institutes between which a fiber link is not present (connection between laboratory 1 and 2 in the figure). It can also be used to to measure height (geopotential) differences, with the flexibility to choose as measurement locations also places where metrology laboratory with optical clocks are not present. Moreover, it can be transported next to the reference clock (in laboratory 2 in this case) to perform a side-by-side comparison to remove possible clock errors on the redshift determination. The two locations need to be connected by a link that does not limit the measurement accuracy (the fiber link in the figure).

The transportable clock I present in this thesis has been developed from PTB for on ground applications. Its design and first realization in the laboratory were done during the work of the previous doctoral student [Vog15]. During my doctorate we completed and installed the system in an air conditioned car trailer with which it can be transported in different locations when necessary. We characterized the system operated inside the trailer to an uncertainty of 2×10^{-17} and an instability of $1.5 \cdot 10^{-15}/\sqrt{\tau}$.
While none of the other mentioned transportable optical clocks has been used for experiments outside the laboratory, we used our system in two measurement campaigns. The transportable clock was operated in three different locations: in Modane (French Alps) and Torino (Italy) during the first campaign, and in Paris (France) for the second one.
The first campaign was a proof of principle chronometric leveling experiment to measure the gravity potential difference between two distant locations. The sites, separated by 90 km and connected by a 150 km fiber link, have an height difference of about 1000 m: One of them is the Instituto Nazionale di RIcerca Metrologica (INRIM) in Italy, where Italian atomic clocks are present to be used as reference, and the other one is the Laboratoire Souterrain de Modane (LSM), a particle physics laboratory in France, where the transportable clock was placed. LSM is a place of particular geodesy interest, since it is located in a mountain range in a transition zone between two countries (France and Italy). This underground laboratory is a challenging location from the point of view of optical clocks operation. Moreover, when we transported the clock at INIRM for the side-by-side comparison needed to complete the relativistic redshift measurement, we also performed a ratio measurement between our clock frequency and the frequency of INIRM ^{171}Yb optical clock, a demonstration of the possibility to use transportable clock for remote optical comparisons.
In the second campaign, we used the transportable clock to measure the gravity potential difference between PTB and Syrte-Observatorie de Paris, the French metrology institute. The transportable frequency was first locally compared to the stationary ^{87}Sr lattice clock at PTB. Then, we transported it in Paris, where we repeat the experiment making use of the 1,415 km optical fiber link between the two institutes.

In this thesis I will present all the work that was done during my doctorate: the installation, operation, optimization and characterization of the clock inside the trailer and its use in the two on-field missions.

I have organized the thesis as follows: The second chapter gives a more detailed picture of the optical frequency metrology and relativistic geodesy fields, showing how they can benefit from the development and use of transportable optical clocks.
In the third chapter I describe the transportable clock presenting its accuracy and stability characterization and the two comparisons we performed against the stationary optical clock of our research group in 2015 and 2017 respectively. I will point out on the problems that we encountered for the clock operation inside the car trailer and how we solved them.
In the fourth chapter, the measurement campaigns will be reported and their results will be presented.
Conclusions and outlooks will be given in chapter five.

Chapter 2

Metrology and geodesy

2.1 Frequency metrology with optical clocks

2.1.1 Principle of an atomic clock

To measure the flow of time, a clock needs to count a periodic process: For atomic clocks this is the period of an electromagnetic oscillator referenced to an atomic transition.
In the interaction with an electromagnetic field the valence electrons of an atom can be excited from one energy level E_1 to a higher one E_2 (or deexcited if they were already in an higher energy level). The possible energy states of a bound system, such as an electron in an atom, are quantized. The resonant frequency ν of an atomic oscillator is given by:

$$\nu = \frac{E_2 - E_1}{h} \tag{2.1}$$

where h is the Planck constant. The width of the resonance $\Delta\nu$ depends on the pair of energy levels that are chosen, and can be broadened by various effects.
The ratio between the atomic frequency ν and its width $\Delta\nu$ determines the quality of the atomic transition as a frequency reference: the smaller is $\Delta\nu$ in respect to ν, the more precisely the electromagnetic wave can be referred to the atomic line.
Atoms of the same species represent an universal reference, since they are all equal to each others: for this reason atomic clocks are used to define the second.

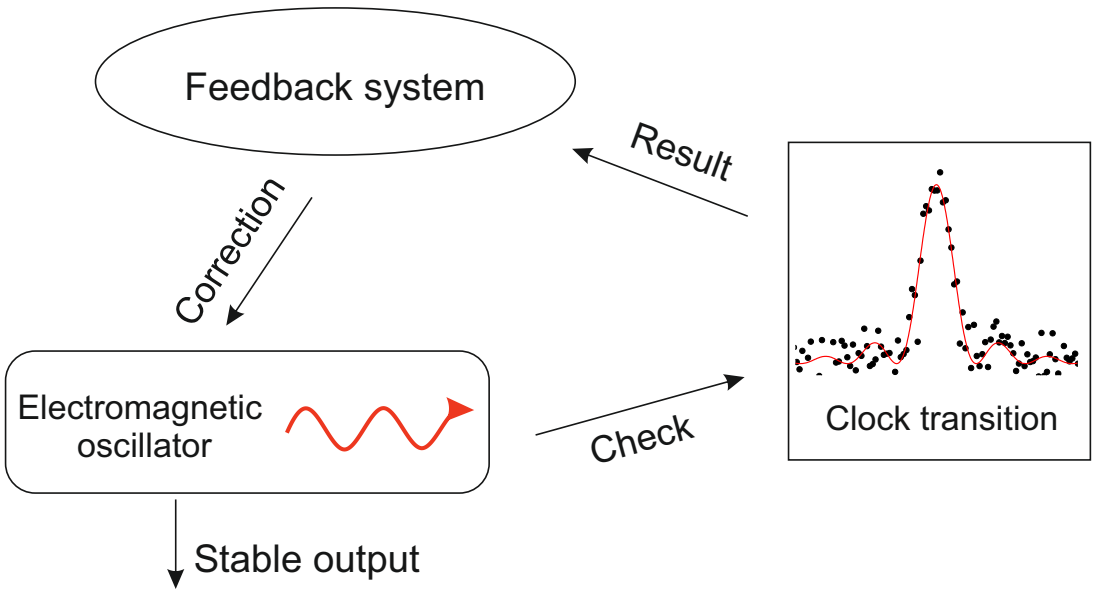

Figure 2.1: Basic principle of an atomic clock: the oscillator frequency is checked on the atom resonance and eventually corrected via the feedback system.

The working principle of an atomic clock is represented in figure 2.1: The electromagnetic oscillator is referenced via spectroscopy to the chosen atomic transition, called clock transition. This oscillators is used to interrogate the atoms in order to measure how far its frequency is from the atomic spectroscopy line. A feedback system corrects its frequency to keep it on resonance with the clock transition.

In the case of optical clocks, the electromagnetic oscillator is a laser pre-stabilized on an high quality optical cavity. Once the interrogation laser frequency is stabilized on the atomic transition it provides a frequency output that has a certain uncertainty (deviation from the true value), as any experimentally defined quantity. The total uncertainty is divided in two contributions: systematics and statistics [GUM08].
The systematic error comes from effect that present themself always in the same way in every observation of the desired quantity. These effects can be recognized and their influence can be quantified. A correction determined with a certain uncertainty can then be applied to the measurement. The combined uncertainty of all the corrections gives the total accuracy of the clock.
The statistical error on the measure comes from random variations of measured quan-

tities. These random fluctuations cannot be compensated, but the uncertainty coming from them can be reduced by averaging miltiple observations (they have zero as expected value). The stability of the clock defines the statistic error contribution to the total result.

The performances of a clock are then defined by its uncertanty and its stability. The accuracy states how well the measured clock frequency represent the real value of the frequency, while the stability gives the repeatability of the measured clock frequency over a giving averaging time τ. A graphic representation of this two concepts is given in figure 2.2.
For convenience, the (in)stability of a clock as a number is usually given at 1 second of measurement time and both accuracy and stability are given in fractional units. I follow this convention.

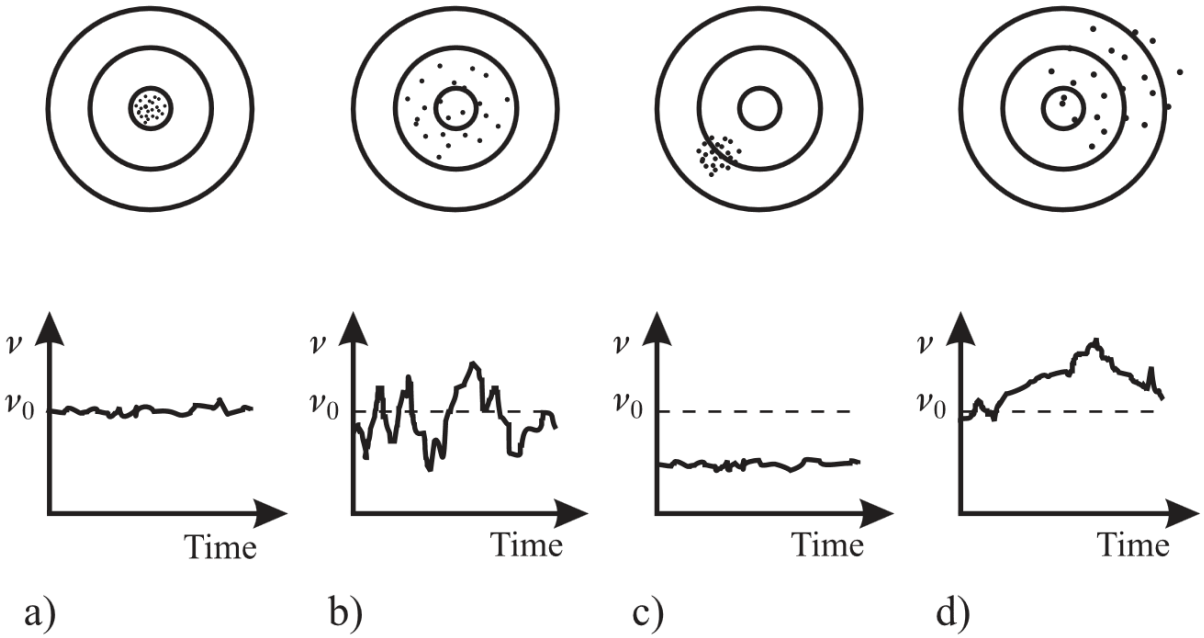

Figure 2.2: a) A clock that is both accurate and stable; b) Accurate but not stable; c) Stable but not accurate; d) A clock that is neither accurate nor stable. [Vig99]

2.1.2 Systematic effects in an optical clock

Here I will revise the systematic effects that shift the clock transition frequency from its true value [Pol13] (or, following the analogy of figure 2.2, the effects that move the shots distribution away from the center).

Doppler effect:

A well known effect that limits the spectroscopy accuracy is the Doppler shift $\delta\nu_{Dop}$ of the unperturbed atomic transition ν_0.
An atom of mass m moving with velocity $\vec{v}$ absorbs light at a frequency given by:

$$\delta\nu_{Dop} = \frac{\vec{k}\cdot\vec{v}}{2\pi} - \frac{1}{2}\nu_0\frac{\vec{v}^2}{c^2} \pm \frac{\hbar k^2}{4\pi m} \tag{2.2}$$

where $\vec{k}$ is the wave vector of the interrogation laser and c is the speed of light. The first term if the first order Doppler shift and can be reduced by reduce by reducing the atoms velocity via laser cooling [Hän75,Ash78,Phi85,Chu85,Raa87]. However for highly accurate spectroscopy this effect remain important. It is possible to use saturation spectroscopy to cancel this effect, but the two beams curvature and alignment need to be extremely well calibrated. Moreover, the second term in equation 2.2 (second order Doppler shift) is not symmetric in the velocity and can not be compensated with these techniques.
For these reasons, atoms in optical clocks are confined in a strong trapping potential (harmonic at first order) in order to reach the Lamb-Dicke regime [Dic53].
If we limit to a one-dimensional analysis and we define an harmonic trapping potential along the z direction with oscillation frequency $\omega_z = 2\pi\cdot\nu_z$, the Lamb-Dicke regime is reached when $k_z\cdot z_0 \ll 1$, where z_0 is the localization of the wave packet ($z_0 = \sqrt{\hbar/4\pi m\nu_z}$). The Lamb-Dicke parameter η is defined as:

$$\eta = \frac{2\pi}{k_z}\sqrt{\frac{h}{4\pi\nu_z}} = \sqrt{\frac{\nu_{rec}}{\nu_z}} \tag{2.3}$$

where $\nu_{rec} = \frac{\hbar k_p^2}{4\pi m}$ is the recoil frequency for the probing light with wave vector k_p.

If $\eta \ll 1$, the spectroscopy spectrum is composed by a carrier frequency that is

unperturbed from motional effects and sideband resonances at multiples of the trapping frequency ν_z:

$$\nu = \nu_0 + \pm\Delta n\nu_z \tag{2.4}$$

where n represent the motional level in the trap (more details on this will be given in the next chapter).

Interaction with magnetic fields:

The interaction of the atoms with a magnetic field B causes the well known Zeeman shift of the electronic energy. The two clock states can have different Landé factors (g) resulting in a frequency shift $\delta\nu$ of the transition. At first order the shift is given by:

$$\delta\nu^{(1)}_{Zem} = \frac{\Delta g\mu_B m_F B}{h} \tag{2.5}$$

where μ_B is the Bohr magneton and m_F is the quantum number expressing the total angular momentum projecton along the quantization axis. The first order shift is the same with opposite sign for opposite m_f states, so the average of the $\pm m_F$ states frequency gives at first order the unperturbed clock frequency.
However, the second order need to be considered. The coefficient a of its expression:

$$\delta\nu^{(2)} = aB^2 \tag{2.6}$$

can be measured experimentally.
It should be noticed that the measurement of the frequency splitting between the two interrogated m_F states gives a very precise measurement of the magnetic field B experienced by the atoms that can then be used in the evaluation of equation 2.6.

Interaction with electric fields:

The interaction of the atoms with DC and AC electric fields is also the cause of systematic shifts (Stark effect) of the clock transition given by the expression:

$$\delta\nu_{Stark} = -\frac{1}{2h}(\Delta\alpha_{DC}\vec{E_0}^{\,2} + \Delta\alpha_{AC}(\omega)\langle\vec{E}(\omega)^2\rangle) \tag{2.7}$$

where $\vec{E_0}$ and $\vec{E}(\omega)$ represent the static and dynamic electric fields, $\Delta\alpha_{DC}$ and $\Delta\alpha_{AC}$

the difference in static and dynamic polarizability of the two energy levels.

The expression of $\alpha_{AC}(\omega)$ for the generic atomic state i is given by [Bra03]:

$$\alpha_{AC,i}(\omega) = \frac{2}{\hbar} \sum_k \frac{\omega_{ik} \mid \langle k \mid \vec{d} \mid i \rangle \mid^2}{(\omega_{ik}^2 - \omega^2)} \tag{2.8}$$

where e is the electronic charge, $\langle k \mid \vec{d} \mid i \rangle$ is the dipole moment between state $\mid i \rangle$ and $\mid k \rangle$ and $\hbar\omega_{ik}$ is the energy difference between the two states. Moreover, $\lim_{\omega \to 0} \alpha_{AC,i}(\omega) = \alpha_{DC,i}$.

Blackbody radiation shift :

The thermal radiation at the ambient temperature T (black body radiation, BBR) with spectral density:

$$\rho(\omega) = \frac{2\omega^2}{\pi c^3} \frac{\hbar\omega}{e^{\hbar\omega/k_B T} - 1} \tag{2.9}$$

is also a source of a Stark shift of the clock transition. The shift can be written as:

$$\Delta\nu_{BBR}(T) = \Delta\nu_{Static} \Big(\frac{T}{T_0}\Big)^4 + \Delta\nu_{Dynamic} \Big[\Big(\frac{T}{T_0}\Big)^6 + O\Big(\frac{T}{T_0}\Big)^8 \Big] \tag{2.10}$$

whit $\Delta\nu_{Static}$, $\Delta\nu_{Dynamic}$ static and dynamic shifts measured at $T_0 = 300$ K (see [Mid12a] for Sr atoms).

Collisional shift:

Collisions between atoms can shift the transition frequency. The collision could be between the cold atoms trapped in the lattice or between the cold atoms and the hot background gas [Gib09, Gib13].

Although the first effect is obviously more relevant for clocks based on bosons, a shift dependent on atomic density has been observed also in clocks based on fermions [Cam09, Nic12]. This shift can be evaluated by performing measurements with different atomic density.

Technical shifts:
Other shifts of the clock transition can arise in the experimental way the interrogation laser is locked to the atomic transition. This shifts will be discussed in particular for our system in the next chapter.

2.1.3 Statistical error of the clock

In the ideal case the instability $\sigma(\tau)$ of a clock as a function of the total measurement time τ is given by the following formula [Hol01]:

$$\sigma(\tau) \propto \frac{1}{Q\sqrt{N}}\sqrt{\frac{T_c}{\tau}} \tag{2.11}$$

where Q is equal to $\nu/\Delta\nu$, T_c is the time needed for one measurement (cycle time), and N the number of atoms interrogated simultaneously in one measurement.
A high Q gives a stable clock, as also a short cycle times and a large number of atoms do. Thanks to their 10^5 higher working frequency with respect to microwave clocks, optical clocks can be much more stable.

A useful way to express the instability of a clock at different integration times is the two-sample Allan deviation σ_y [All66]. The Allan variance σ_y^2 is defined as:

$$\sigma_y^2 = \frac{1}{2}\left\langle(\bar{y}_{n+1,\tau} - \bar{y}_{n,\tau})^2\right\rangle \tag{2.12}$$

where

$$\bar{y}_{n,\tau} = \left\langle\frac{\delta\nu}{\nu}\right\rangle_{n,\tau} \tag{2.13}$$

is the fractional frequency averaged over sample period n of duration τ. Plotting the Allan deviation at different τ reveals the kind of noise that affects the measurement.
The sum of all noise contributions gives the total stability of the clock. These contributions come from two different sources: the first is the statistical noise in the detection process and the second stems from the fact that the atoms are interrogated for only a fraction of the cycle time (the rest of the time is spent to collect and prepare the atoms),

giving rise to a stroboscopic effect called Dick effect [Al-15a].

Detection Noise:
Detection noise contributions are connected to electronic noise and photon shot noise of the detection apparatus and intensity and frequency noise of the detection laser in the determination of the excitation probability p of the interrogated clock state.
Although this contribution can be in principle reduced with technical improvements, there is in addition a fundamental random noise source in the detection called quantum projection noise (QPN) coming from the quantum nature of the atoms. This noise contribution σ_{QPN} is given by [Ita93]:

$$\sigma_{QPN}(p) = \sqrt{p(1-p)N} \tag{2.14}$$

It is proportional to $\sqrt{N}$, and since the signal to noise ratio scale with N, it can be reduced by increasing the number of interrogated atoms. There have also been proposal to use squeezed states to go below the QPN [Mei08].

All the detection noises are assumed completely uncorrelated between the two interrogated states, except the QPN which is considered completely anti-correlated. They are summed quadratically to give the total σ_p^2 [Al-15a]. Reducing the detection noise to the QPN level is an important first step to reach the ideal case for the stability of the atomic clock (eq 2.11). However, there is always another noise that deteriorate the stability of the system: the Dick effect, that is usually the dominant factor.

Dick Effect:
This kind of noise can be seen as an aliasing phenomenon, and depends on the noise power spectral density of the interrogation laser: the noise spectral components of the oscillator at harmonic frequencies of the inverted clock cycle time are filtered by the atomic response and down-converted to low frequency noise [Dic88]. This noise contribution $\sigma_{Dick}(\tau)$ is given by:

$$\sigma_{Dick}^2(\tau) = \frac{1}{\tau} \frac{1}{\mid g_0 \mid^2} \sum_{k=1}^{\infty} S_y(k/T) \mid g_k \mid^2 \tag{2.15}$$

where $T = nT_c$ with n number of cycles, S_y is the single-sided power spectral density of the interrogation laser and g_k, g_0 weight coefficients which are the Fourier components

of a sensitivity function depending on the type of interrogation (usually Rabi or Ramsey). A crucial role is then played by the noise power spectral density of the interrogation laser and the development of ultra-stable lasers is of fundamental importance. For this reason high performance reference cavities are needed [Häf15b, Mat17a].
An other approach is to cancel the interrogation dead time, like in the zero dead-time system presented in [Sch17], where an interleaved interrogation of two cold-atom esambles is performed.

2.1.4 Optical frequency comb

Optical frequencies are much too fast for conventional electronic counters, that can work only up to the microwave spectrum. Therefore a way to connect the optical and microwave domains is needed. Some solutions adopted approaches based on harmonic frequency chains or interval bisection [Sch96,Ude97,Sch01,Ber99], but was with the invention of the optical frequency comb in 1999 that optical frequency metrology received a huge boost [Ude02].

An optical frequency comb is a mode-locked laser used as phase coherent link between different frequencies (in the optical and microwave domains) whit negligible noise contribution. Many cavity modes overlap with the gain medium and as a result the laser produces a continuous train of extremely short (femtosecond) pulses [Eck78]. The time domain picture of the pulses emitted by the laser is the multiplication of the fast electric field oscillations and an envelope function. The envelope travels with the group velocity $v_g = \frac{c}{n-\lambda \cdot dn/d\lambda}$ and the fast oscillations with the phase velocity $v_p = c/n$ (where c is the speed of light, λ is the wavelength of the laser and n is the refractive index of the medium). The difference between the two velocities leads to a slippage (de-phasing) between the two entities. In the frequency domain, this difference turns into a frequency offset f_0. Calling f_{rep} the frequency of the laser pulses emission (repetition frequency) the Fourier frequencies of the comb can be written as :

$$\nu_n = n \times f_{rep} + f_0 \tag{2.16}$$

with ν_n optical frequency of the n^{th} comb mode. The frequency of each comb "tooth" is then completely defined by the two microwave frequencies f_0 and f_{rep} and n.
In figure 2.3 the time and frequency domains of the comb are represented.

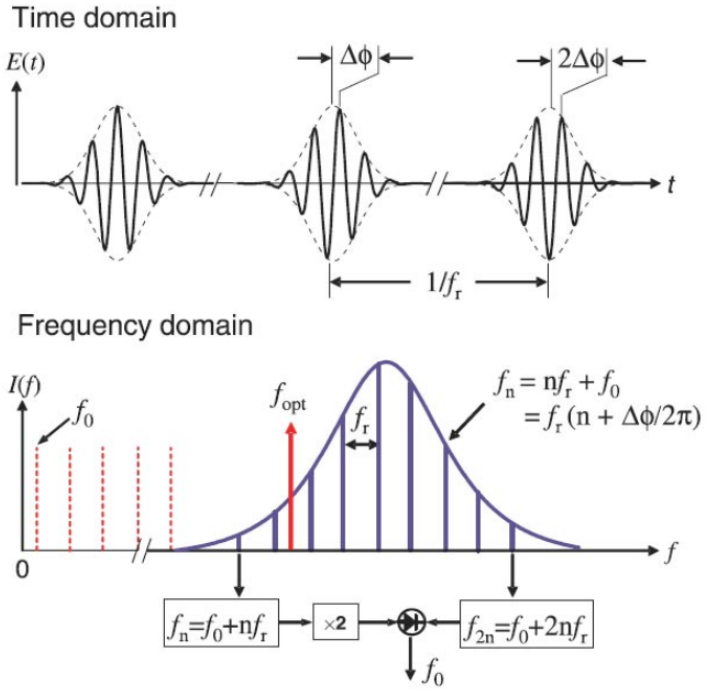

Figure 2.3: The output of an ultrafast mode-locked laser in time- and frequency-domain [Pol13]. In time-domain, at every cavity round trip the carrier and the envelope are de-phased by a quantity $\Delta\Phi$ depending on the difference between group and phase velocities. In the frequency-domain, this results in a comb of equally separated modes with an offset. In the picture it is reported the octave that is used in the self-referenced scheme to detect f_0, so that it can be stabilized. An optical frequency f_{opt} can be beaten against one of the comb modes at the offset between it and the chosen comb mode can be recored on a counter.

The frequency f_0 can be measured with the self-referencing scheme: Part of the comb light is made pass trough a frequency doubler and an optical filter for the higher frequencies. The doubled and not doubled light are then beaten on a photodiode. The detected beat note (between $2\nu_n = 2n \times f_{rep} + 2f_0$ and $\nu_{2n} = 2n \times f_{rep} + f_0$) gives exactly f_0. This is also depicted in figure 2.3. Moreover, the pulses repetition rate f_{rep} is a microwave frequency: can be measured with a photodiode and referred to a stable microwave reference. The fluctuations of f_0 need to be suppressed to a level where they contribution to the

noise is negligible. This can be done by stabilizing it to a stable optical reference. However this not necessary when the two frequencies are synchronously detected, because the knowledge of the correlation between these two frequencies permits to eliminate the fluctuations of f_0. In both cases, the comb provides a stable phase coherent link from the optical reference to any other optical frequency within the comb spectrum. Even the microwave domain can be accessed via the spacing of the comb lines.

2.1.5 Optical absolute frequencies and optical frequencies ratios

The optical frequency comb can be used to perform absolute optical frequency measurements. A (microwave) beat note f_{beat} between the interrogation laser and the closest comb tooth n can be detected on a photodiode. The frequency of the interrogation laser ν can be read as:

$$\nu = f_{beat} + n \times f_{rep} + f_0 \tag{2.17}$$

When this microwave frequencies are referenced to a primary frequency standard generating the second of the SI (a Cs fountain clock), the optical frequency is read in unit of Hz.
Several absolute frequency measurement for various optical clock transitions have been performed in metrological laboratories around the world after the invention of the comb. In particular a large number of measurement for the ^{87} Sr absolute clock frequency resulted in very good agreement between each other, leading to the inclusion of this frequency (and others optical frequencies) in the secondary representations of the second [CCT04]. Recent results for ^{87}Sr absolute clock frequency measured value are shown in figure 2.4.

In the last measurements in the graph, the biggest uncertainty contribution comes from the systematic uncertainty of the Cs fountains, that is one or two orders worse comparing to optical clocks. Moreover, the stability of the Cs fountains is two order of magnitude worse with respect to the optical frequency standards: this means that the averaging times for the latter are much shorter and the Cs clock limit the stability of the measurement.

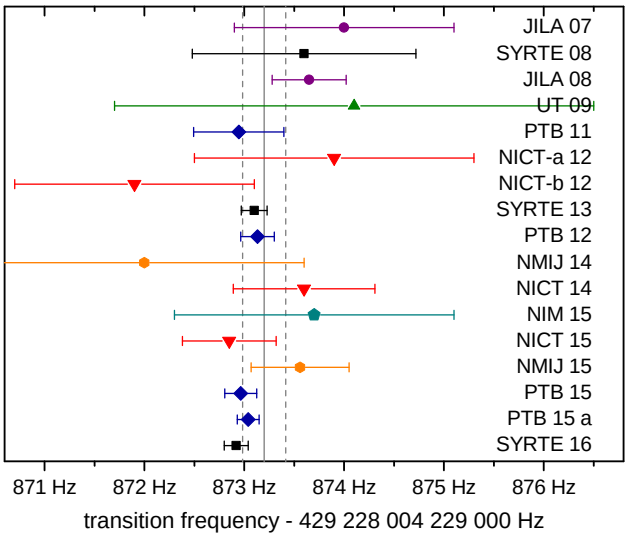

Figure 2.4: Reported results from different metrological institutes measurements of the ^{87}Sr optical absolute frequency value in the last ten years [Boy07b, Bai08, Cam08, Hon09, Fal11, Yam12, Mat12, Le 13, Fal14, Aka14a, Hac14, Lin15, Tan15, Gre16, Lod16, Hac17a, Hac17b].

The comparison of absolute optical frequency generated by different clocks can then reveal only agreements or disagreements in the 10^{-16} uncertainty range. A more stringent test is the measurement of optical frequencies ratios. Since the ratio is a unit-less number, it is not limited by the current realization of the second.

Comparing two clocks working at the same frequency (based on the same atomic specie and transition) is relatively easy: it is possible to simply measure the beat between the two interrogation lasers. On the other hand, the frequency of atomic clocks based on different atomic transitions can differer by some THz. In this case, it is necessary to use an optical comb to connect the two different parts of the optical spectrum. An example of measurement scheme was proposed in [Ste02]. Here the frequencies of the two clocks, ν_1 and ν_2, are beaten with the respective closest modes of the frequency comb, generating the two beat notes Δ_1 and Δ_2. The frequency offset f_0 of the comb is also measured trough the self-referencing measurement scheme described before.

Both Δ_1 and Δ_2 are summed to f_0 trough a mixer. The first sum is called ν_A:

$$\nu_A = f_0 + \Delta_1 = \nu_1 - n_1 f_{rep} \tag{2.18}$$

The second one is multiplied by a the ratio of the two comb modes numbers where the two frequency laser are beated, n_1/n_2, and is generated by a frequency divider. The result is called ν_B:

$$\nu_B = (f_0 + \Delta_2)\frac{n_1}{n_2} = (\nu_2 - n_2 f_{rep})\frac{n_1}{n_2} \tag{2.19}$$

Using a second mixer the difference of these two frequencies, ν_C, is then obtained:

$$\nu_C = \nu_A - \nu_B = \nu_1 - \nu_2\frac{n_1}{n_2} \tag{2.20}$$

In this way ν_C measures the (small) deviation of the ratio ν_1/ν_2 from n_1/n_2. These deviations are determined by referencing ν_c to a stable microwave reference. Since $\nu_C \ll \nu_1, \nu_2$) the requirements on the reference are more relaxed, it is not necessary to refere ν_C to a cesium-controlled hydrogen maser. Optical ratio measurements are then only limited by the accuracy of the optical clocks involved. The scheme is depicted in figure 2.5

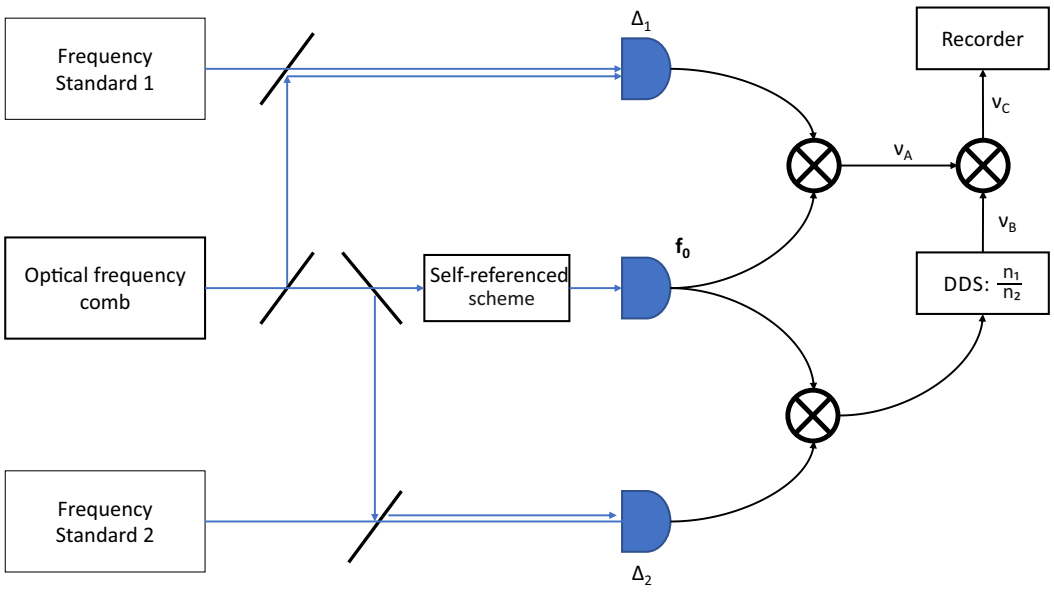

Figure 2.5: The scheme presented in [Ste02] for the measurements of optical ratios.

2.2 Remote clocks comparisons

Although the ratio measurements can be easily done between optical clocks developed in the same institute, a more general test is between systems developed independently in different institutes. The great majority of optical clocks are complicated and bulky systems at the moment: they cannot be moved from an institute to an other, and even if that is possible they have to be dismounted and mounted again, a process that requires a lot of effort. Currently the only technology that secure a stability of the frequency transfer not affecting the comparison results are optical fiber links. However, as pointed out in the introduction this links are limited to a few thousands kilometer (continental) distances. Moreover, in performing optical clocks comparison with state-of-the-art accuracy, the relativistic redshift of the clock frequency comes into play: geopotential differences between distant clock locations needs to be known with enough accuracy. For all these reasons the field of optical clock comparisons will greatly benefit from the development of transportable optical clocks.

2.2.1 Remote frequency transfer

I will revise the possible techniques for remote clock comparisons that have been developed in the last decades mainly following reference [Rie17]. A comparison of the stability of the different frequency transfer methods is showed in figure 2.6, where they are also compared to the stability of a state-of-the-art optical clock.

Satellite radio signal transfer:
On a global scale the only established method for frequency comparison is the transmission of radio signal via satellites. Here two different techniques can be utilized: the reception of signals of Global Navigation Satellite Systems (GNSS) or the exchange of signals in the microwave range between two terrestrial laboratory trough a geostationary satellite, called two-way satellite time and frequency transfer (TWSTFT) [Bau15].

In GNSS, the time signal received from the satellite clocks at the same time in different laboratories is compared with the local clocks: comparing the local clock offset to the satellite clock signal, the difference between the distant clocks can be derived. It has been shown that in some cases with this method a frequency transfer accuracy of 10^{-16} after five days of interrogation time can be reached [Pet15b].

TWSTFT has been shown to be limited to about 10^{-15} instability in most cases. Researches to improve these performances are ongoing: Efforts carrier-phase TWSTFT showed the possibility of comparison with $2 \cdot 10^{-13}$ stability at 1 second [Fuj14], with a long term stability at the 10^{-16} level, and the possible prospect of reaching the 10^{-17} level [Fuj16]. The ACES mission project to install a cold atomic cesium clock and a hydrogen maser on the International Space Station (ISS). The aim is to reduce relative frequency instabilities below 10^{-17} [Lau15] and the clock it is planned to be launched in 2018.

Although these methods do not have the necessary stability to perform optical clocks comparisons, they are currently used to compare hundreds of microwave clock around the globe for the realization of the International Atomic Time (TAI) [Pet15a].

Satellite optical signals transfer:
In the Time Transfer by Laser Link (T2L2) experiments [Sam14], a reflector array on board a satellite returns some of the light pulses emitted by a laser in a ground station. Measuring the time of emission and the return of the pulses on the ground stations (with the ground clocks) and the time of arrival on the satellite (with the satellite clock) allows to compare clocks in different ground stations. After several days of integration it is supposed to reach 10^{-17} instability level.

A better instability could be reached using a coherent optical link. Experiments on ground have demonstrated that a future coherent optical link from ground to satellite through the turbulent atmosphere could be possible [Dje10]. A theoretical instability of $2 \cdot 10^{-17}$ at 1 second has been calculated, with the possibility to reach the 10^{-18} level after few minutes [Rob16]. In a recent experiment it has been shown that two optical

timescales can be synchronized with this technique with a statistical uncertainty below 10^{-18} after 1000 s [Des16].

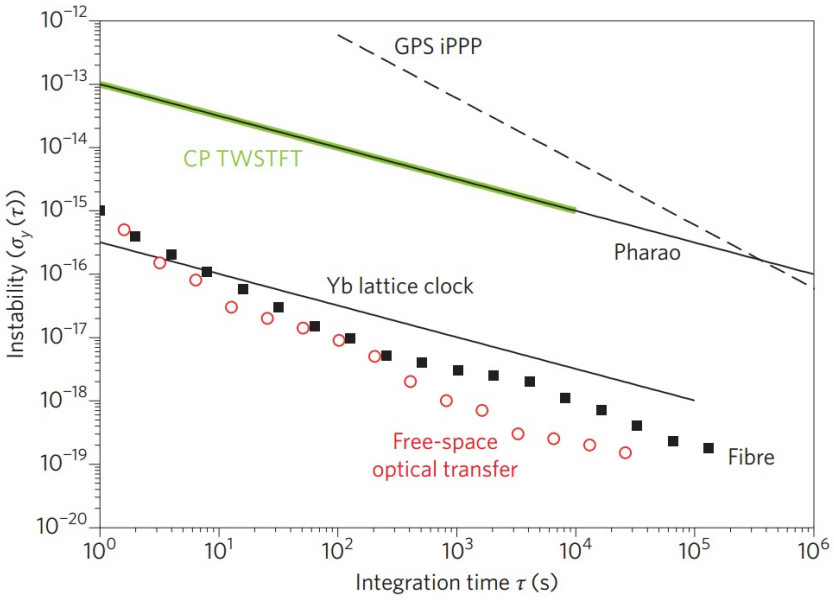

Figure 2.6: The fractional instability of the different frequency transfer techniques presented in this section as compared to the Yb lattice clock instability of reference [Hin13] as a function of the measurement time τ [Rie17]. The instability is expressed by the Allan deviation or modADEV. GPS iPPP (integer Precise Point Positioning technique [Pet15b] (modADEV), CP (carrier-phase) TWSTFT [Fuj14] (mod ADEV), Pharao [Lau15] (ADEV), Fibre link between Paris and Braunschweig [Lis16] (ADEV), free-space optical transfer [Des16] (modADEV).

Optical Fiber Links:

In the last ten years, techniques for optical frequency transfer using fiber links have greatly improved. Here an intensity modulated optical carrier around the 1.55 μm (200 THz) telecommunication window is used to transmit radio-frequency and microwave signals. The use of optical phase of the carrier at 200 THz allows to transfer in an extremely accurate and stable way optical frequencies over long distances [Lop15, Rau15]. At each institute a frequency comb is used to compare the local interrogation laser's frequency to the transfer laser. The ratio of the two local comparisons gives the ratio between the two distant optical clocks.

A fractional precision in the low 10^{-17} range can be reached after 1000 s of averaging time

giving negligible contributions to the comparison result. Several tests on fiber links have demonstrated that they can support frequency comparisons with a fractional uncertainty down to the 10^{-20} regime or below [Rau15, Ber14]. Up to now, optical fiber links have been used in several experiments, covering also more then a thousand km distance [Yam11, Pre12, Lop12, Ros12, Śli13, Cal14, Chi15, Lis16].

The optical path length of a fiber can fluctuate as a consequence of temperature fluctuations and mechanical vibrations. To solve this problem, the light does a round trip in the same fiber, in order to experience twice the perturbations. At the input end, by comparing the sent signal with the returned signal, it is possible to measure the fluctuations and thus correct for them. This configuration needs a high degree of symmetry between the forward and the backward path to work efficiently, and the laser used as light source must be a low-frequency-noise laser (when compared to the free-running fiber phase noise).
Moreover to cover long distances, the transferred frequency needs to be phase-coherently

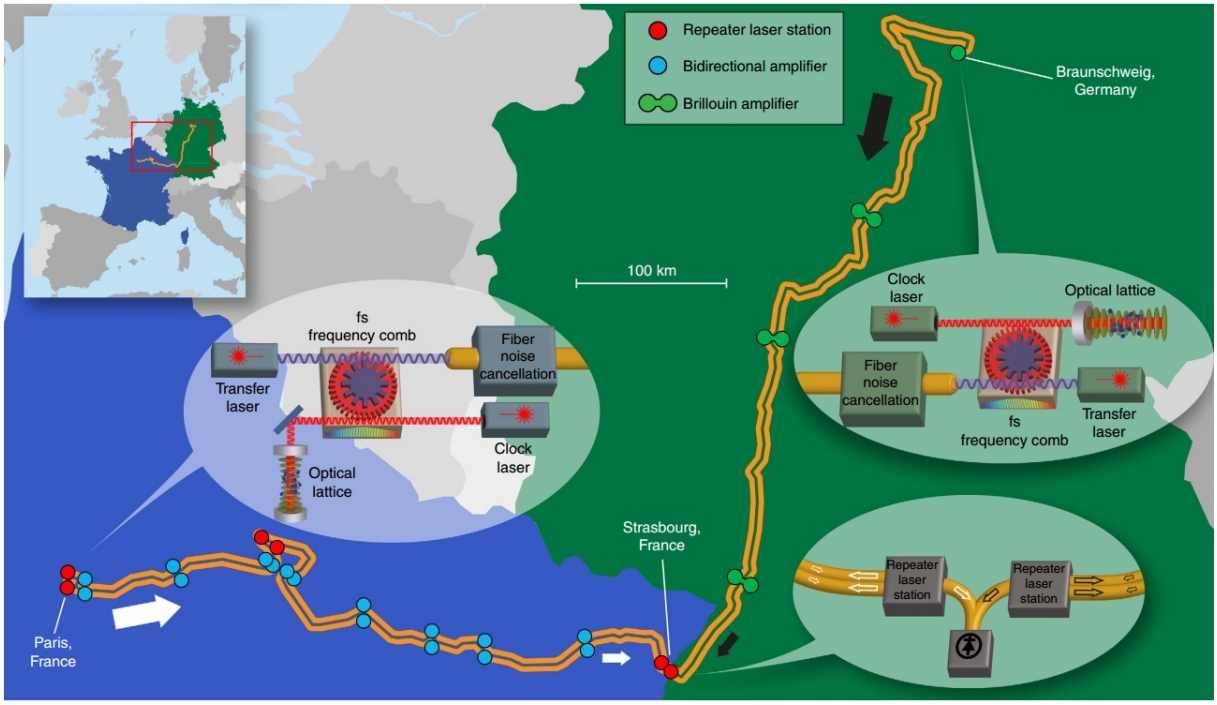

Figure 2.7: Schematic representation of the fiber link connecting PTB to Observatoire de Paris in France. In Strabourg the beat note between the two transfer lasers is recorded [Lis16].

amplified. Depending if the link is through a "dark fiber" or a "dark channel" there are different approaches for the amplifications. Using a dark fiber means having a dedicated fiber link between the laboratories: this allows extensive modification of the line to use Brillouin amplification [Rau15]. In a dark channel approach only one channel in a fiber is used in parallel to other channels used for internet traffic: here repeater stations and bidirectional amplifiers are needed due tthe many connectors and splices that the signal encounters [Chi15, Lop13].

Both approaches are in use, as for example in the 1415 km long international fiber link connecting PTB to LNE-SYRTE in Paris (see figure 2.7). The German part of the link (from Braunschweig to Strasbourg, 710 km) uses the dark fiber approach and the French part (from Paris to Strasbourg, 705 km) the dark channel approach. In Strasbourg a beat note between the two transfer lasers is recorded. This link was used in 2015 to compare the laboratory ^{87}Sr optical lattice clocks of the two institutes [Lis16] and in 2017 for an experiment involving the transportable clock.

2.2.2 Frequency comparisons and the relativity of time

When atomic clocks uncertainty started to reach the 10^{-15} level, it has become clear that to compare different clocks the frequency shift predicted by the theory of relativity needed to be estimated very carefully [Pav03].

The relativistic redshift $\delta\nu$ of an electromagnetic wave traveling from an emitter in position A to a receiver in position B both at rest in an Earth-fixed reference system co-rotating with the Earth is given by the relation:

$$\frac{\delta\nu}{\nu_B} = \frac{\nu_B - \nu_A}{\nu_B} = 1 - \frac{\delta\tau_B}{\delta\tau_A} = \frac{W_B - W_A}{c^2} + o(c^{-4}) \tag{2.21}$$

Where $W$is called geopotential and is the sum of the gravity (V) and centrifugal (Z) potentials of a point on the Earth surface.
If the point B is higher then the point A, the difference $W_B - W_A$ in equation 2.21 is

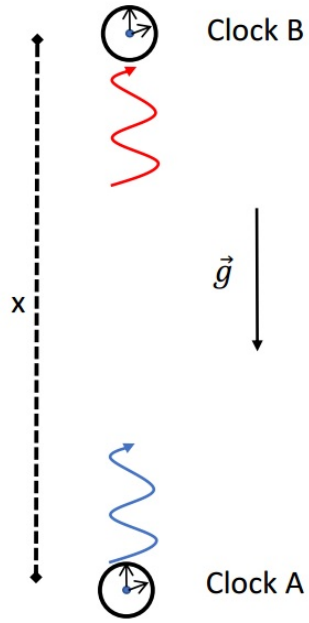

Figure 2.8: A photon emitted from A to B in the opposite direction of the gravity field is redshifted. As a consequence the clock in A seems to tick at a lower frequency.

positive and so is $\delta\nu$. In other words an observer at B will find the clock in A running slower then a local clock (its frequency is shifted to the red, see figure 2.8).

2.2.3 Transportable Atomic Clocks

From the description given before, it should become clear that the field of optical metrology is in progress, and that there are important contributions that could be given by the development of transportable optical clock systems.

Once they reach an instability at the order of $10^{-15}/\sqrt{\tau}$ or better and an uncertainty in the low 10^{-17} or better, transportable optical clocks will be of great benefit in testing the agreement of optical frequency standards at their best accuracy. The frequency of two laboratory clocks could be compared by using the transportable clock as a very accurate frequency reference that can be moved between the two places. This would be especially important to perform very distant (intercontinental) comparisons with high accuracy.

Moreover, as it was explained before, for clock comparisons in the 10^{-18} range the gravity potential difference between the two clock sites need to be know with great precision. To give an uncertainty contribution below 10^{-18} the gravity potential difference need to be known better then 0.1 m^2s^{-2} (1 cm height difference). For remote comparison, especially if they involve different countries, this is not always an easy task [Den17].
Here, transportable optical clocks can come in help again: having the possibility to be compared via a fiber link to a remote clock and then transported and compared locally, they can be employed to measure the relativistic redshift between the two locations, and consequently the gravity potential difference. This will be explained better in the next section of this chapter, where the possible applications of transportable optical clock in geodesy will be presented.

2.3 Optical clocks in geodesy

Geodesy is defined as "a branch of applied mathematics concerned with the determination of the size of Earth and the exact positions of points on its surface and with the description of variations of its gravity field" (definition taken form Merriam-Webster dictionary,www.merriam-webster.com). Optical clocks reaching fractional uncertainties in the order of 10^{-17} or better in relatively short time can be applied in geodesy to improve the knowledge of Earth's gravity field, both stationary and dynamical. This cross-disciplinary field is called relativistic geodesy. This section is dedicated to a brief introduction of fundamental geodesy concepts and to geodesy with optical clocks.

2.3.1 Representation of Earth and height determination

Different models of Earth have been used depending on the theoretical knowledge and measurement accuracy of Earth gravity potential.

In a very crude approximation Earth can be considered as a sphere: the direction of gravity is toward the center of Earth and the gravitational potential is just the potential of a sphere.
However, the rotation of Earth generates a centrifugal force that distorts this spheric shape: in this case the minimum energy shape is an ellipse rotated about the polar axis, that is called ellipsoid. The ellipsoid is a equipotential surface of Earth gravity field, thus in this approximation the gravity vector (vertical direction) is orthogonal to the ellipsoid surface.
In the real earth the mass distribution is not homogeneous due to the presence of oceans, mountains and underground inhomogeneities: The direction of the gravity vector as measured locally with a plumb line differs from the one coming from the ellipsoid model, and so does the vertical direction. The real equipotential surfaces that we can use as a reference is then the geoid. A pratical definition of the geoid is "the equipotential surface of Earth gravity field that coincide with the mean sea level in the oceans" (again from Merriam-Webster dictionary). The determination of the geoid is a crucial part of geodesy.

This is done via terrestrial gravity measurement (with gravimeter/gradiometer or spirit leveling) and via satellite measurements (as is done in the GRACE and GOCE missions). A representation of Earth as it is inferred from satellite measurements is given in figure 2.9. The geoid can differ from the ellipsoid even up to about 100 m due to local gravity anomalies.

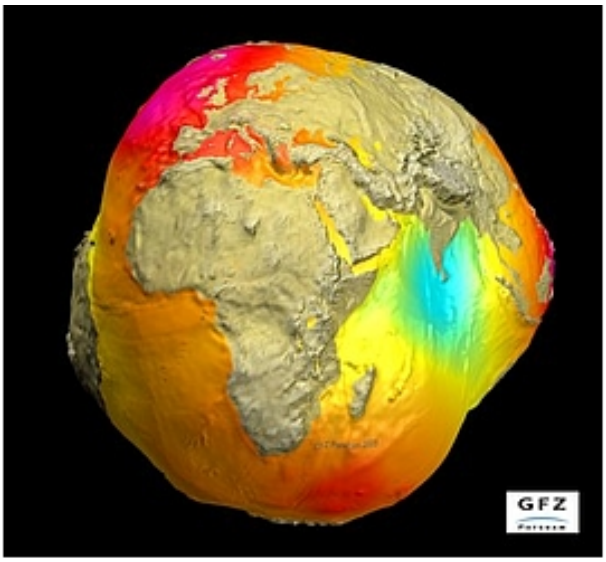

Figure 2.9: A representation of Earth as it is inferred from satellite measurements. Source: Deutsche GeoForschungsZentrum (GFZ)

For these reasons two height types arise, depending on the chosen reference surface. Orthometric heights (H) are calculated as distances from the geoid calculated along the local vertical direction (plumb line). Ellipsoid height (h) are given as distance from the ellipsoid (whose definition depends on the chosen ellipsoid model) along the direction perpendicular to the ellipsoid itself. The height difference between geoid and ellipsoid it is called geoid separation and is identified with N.

To measure othometric heights it is possible to use spirit leveling. To determine a difference H_{AB} between point A and B, vertical rods are set up at the two points and a leveling instrument (like a spirit level) is positioned between them. The difference of the two reading of the level's intersection with the vertical rods gives the H_{AB}. If the two rods are too distant from the leveling instrument, the plumb line where the horizontal

plane is referenced has not the same direction of the one at the two rods, and one does not measure the real orthometric height. To reference the height of a point to the geoid, the starting point of the leveling process needs to be at the mean sea level. Although this method is accurate at the sub-millimeter level over distances below 1 km, it is affected by systematic errors that can add up to several decimeters over distances longer then 1000 km.

Thanks to the development of GNSSs and geoid models from satellite mission (see figure 2.9), a second more accurate method over long distances can be employed. The position of two distant points can be determined in the coordinate system of the GNSS and their height difference can be consequently evaluated. However, GNSS coordinate systems measure the heights as elliposid heights (h), taking an ellipsoid model as a reference. For this reason, GNSS positions have to be corrected by the local geoid separation N which has

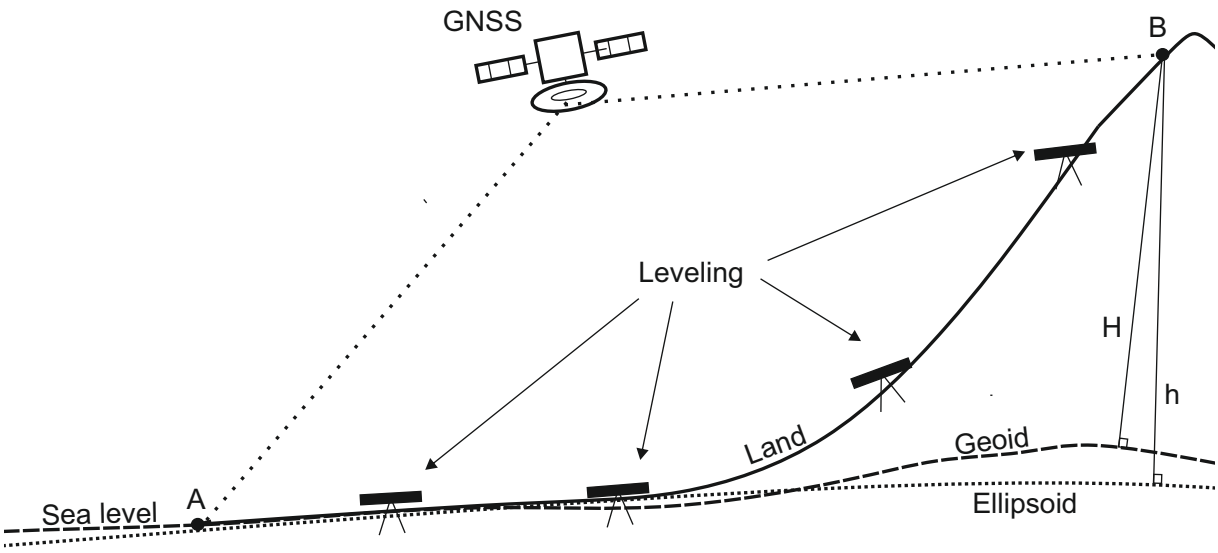

Figure 2.10: A and B are two points on the surface of Earth (represented by the continuous black line). The geoid and ellipsoid are also represented, with the geoid corresponding to the mean sea level. The two surfaces are not the same, and the height of point B over the geoid (H) is different from its height calculated over the ellipsoid (h). The orthometric height difference bewteen point A and B can be calculated via spirit leveling, which has to be performed in various step to follow the curvature of the geoid, or using GNSS satellites. However, the latter gives a difference of ellipsoid heights for the two points. To refer it to the geoid, a local geoid model is needed (from terrestrial and/or satellite data).

to be determinate by local gravity field modeling based on terrestrial and satellite data. When this approach is performed under the best possible conditions (sufficient terrestrial data for the gravity field reconstruction around the sites of interest, and state-of-the-art global satellite geopotential utilized) an accuracy of 2-3 cm over long distances is possible. [Den13, Den17].

A representation of the difference bewteen othometric and ellipsoid heights and of the spirit leveling and GNSS methods to measure heights is given in figure 2.10.

It is known that at the moment the defined position of the geoid differs between different countries. This problem is called "vertical datum problem" and as a consequence trans-national heights have a difficult determination. Moreover, across Europe the two height measurement approaches described before give results that can differ by more then 50 cm, even after applying corrections for different geoid references between nations (see figure 1.2 in the Introduction). The application of clocks in geodesy has the potential to offer an independent measurement method (with similar or even better accuracy) to help to investigate these problems.

2.3.2 Relativistic geodesy

From the discussion above it should be clear that the determination of gravity potential differences is at the core of geodesy. On the other hand, as we have seen, the frequency of clocks is directly depending on the gravity potential. So, when comparing two clocks (at rest) a direct measurement of the gravity potential difference between the points where the two clocks are is performed. This idea is at the base of chronometric leveling, as it is shown in figure 2.11.

In this case, the height of a point P is defined trough its **geopotential number** C:

$$C^i = -(W_P - W_0^i) = -\int_{P_0(i)}^{P} dW \tag{2.22}$$

where $P_0(i)$ is an arbitrary point on the zero level or height reference surface (usually as close as possible to the geoid) with the gravity potential W_0^i. The negative sign is due to the fact that in geodesy as a convention potentials are defined with the opposite sign in

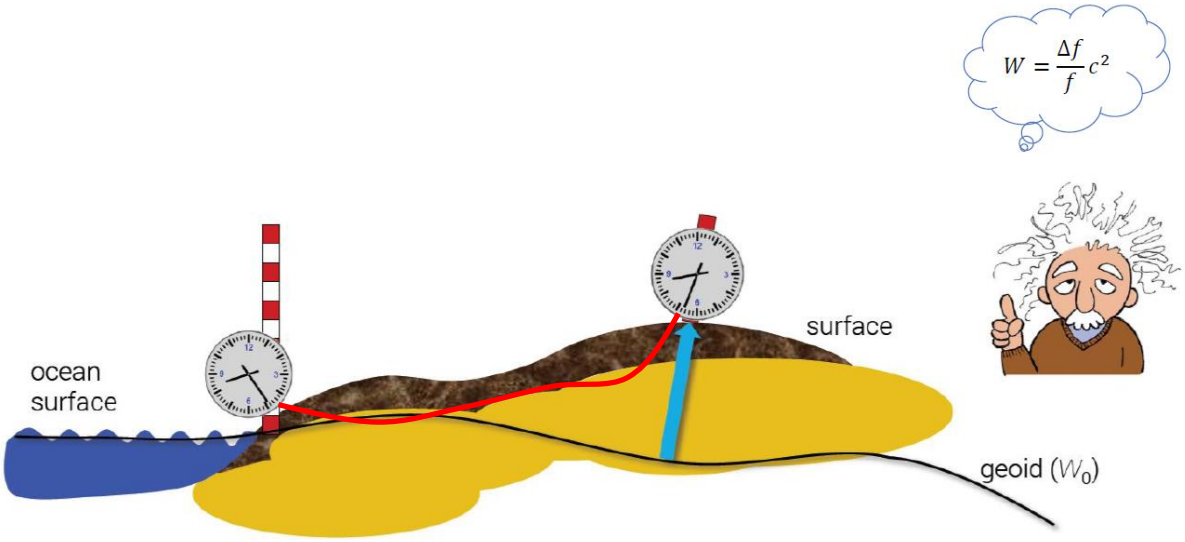

Figure 2.11: Comparing two clocks in different geopotential surfaces gives a direct measurement of the gravity potential difference. Note that a stable link connecting the two clocks is needed (in this case, the fiber link depicted in red in the figure). Source: P.O. Schmidt

respect to the definition of potentials in physics.
The first proposal of the use of clocks to establish gravity equipotential surfaces was done by Vermeer and Bjerhammar at the beginning of the 1980s [Ver83, Bje85]. In these papers they introduced the term "relativistic geodesy". They were thinking of using microwave clocks with the aim to reach an uncertainty at the 10^{-16} level in the clock frequency and masers for the long term stability.

In the last few years the Veermer and Bjerhammar hypothetical idea has been revived in a certain number of proposals papers [Bon12, Mai13, Bon15a, Bon15b, Flu16, Lio17, Mül17, Phi17], pushed by the rapid development of optical clocks that are reaching the necessary accuracy to measure geopotential differences with a competitive or even better resolution than the conventional (indirect) techniques presented above: A frequency accuracy of 10^{-18} gives a ~ 1 cm height accuracy (see equation 2.21).

A numbers of possible applications have been presented, the most important of them being probably the possibility of a redefinition of the geoid with the help of optical clocks, so that the geoid coul be directly determined by clocks without approximations coming from the model [Phi17].
Currently our best knowledge of Earth's gravitational field is coming from the reconstruction made by GRACE (Gravity Recovery and Climate Experiment) and GOCE (Gravity Filed and Steady-State Ocean Circulation Explorer) satellite data [Tap04, Pai11], with a cm accuracy at a spatial resolution of 100 km. For a shorter spatial scale, near-surface gravimetry is needed and differences up to 10 cm between the high and short spatial height resolution have been reported in areas well covered with surface data [Gru09] because of local gravity anomalies. Moreover, there is a lack of surface data especially in transition zones, like coasts, boarders between different countries and in areas of difficult access, that limit the reconstruction when one aim to the cm level accuracy. Measuring gravity potential instead of gravity itself, is smoother and more sensitive to mass sources at large scales. Optical clocks can then improve the high spatial determination of the geopotential beyond what is available with satellite data, as it is explained in [Lio17].
Other (more speculative) applications could involve earth quake prediction and vulcanology, and the monitoring of vertical surface motions due to periodic causes like solid Earth tide [Bon15a, Bon15b]. These applications would benefit from the high stability of optical clocks that can reach the 1 cm accuracy after few hours of interrogation [Nic15, Ush15, Hun16, Al-15a, Sch17]. The first experiments pointing at the idea of developing a clock network for relativistic geodesy have been performed using stationary clocks separated by 700 km in Europe [Lis16] and 15 km in Japan [Tak16] respectively, connected via fiber links, and a transportable clock can add flexibility in the choice of the experimental site. It is expected that more experiment for relativistic goedesy will follow soon.

The transportable clock presented here has part in the *geo-Q* project, an interdisciplinary project between physicist and geodesist. The aim of *geo-Q* is a better determination of Earth's gravitational field and monitoring of the global and regional mass distribution, developing on one hand quantum metrology sensors based on cold atoms, and on the other hand a better geodetic modeling, both from satellite and on ground measurements.

Chapter 3

A transportable ^{87}Sr optical lattice clock

3.1 ^{87}Sr atoms trapped in an optical lattice as frequency reference

As pointed out in the previous chapter, to accurately interrogate the narrow clock transition it is necessary to remove all the motional effects, that are the casue of Doppler shift. This is done by trapping the atoms in the Lamb-Dicke regime (section 2.1.2).

The trapping potential can be generated in two different ways. In ion clocks one positive charged atom is trapped using a combination of static and radio-frequency electric fields and is cooled via laser light [Hun16]. Ion traps offer a very controllable environment for the atom, but since they can trap only one ion the signal to noise ratio is limited. A technique to trap multiple ions for an atomic clock has been presented recently and could lead to the realization of multi-ion clocks [Kel17]. In lattice clocks [Nic15, Ush15, Al-15b, Sch17], like the one presented in this thesis, neutral atoms are trapped trough the AC Stark shift generated by a stationary optical electromagnetic wave (a laser) called optical lattice. Many neutral atoms can be trapped simultaneously in the resulting potential wells.

3.1.1 Laser cooling of ^{87}Sr atoms

The atom species that is used in this experiment is strontium (Sr), an alkaline earth atom, with two valence electrons. This results in two separate series of energy sates depending on the two electrons spins: parallel (triplet states) or anti parallel (singlet states). There are four different isotopes of Sr, three of them are bosons and one, ^{87}Sr, is a fermion with nuclear spin $I = 9/2$. The ^{87}Sr isotope has demonstrated to be a particularly good choice to build an atomic clock, because it presents a natural ultra-narrow transition (linewidth of a few mHz) that can be used as a reference for a clock [Tak05, Cou05, Cam08, Fal11]. A schematic view of the ^{87}Sr atomic levels is given in figure 3.1, where the important transitions used in the experiment are highlighted. The Russell-Sanders notation $^{2S+1}L_J$ is used to identify the energy levels, where S is the total spin, L the orbital angular momentum of the electrons and J the total electronic angular momentum of the state.

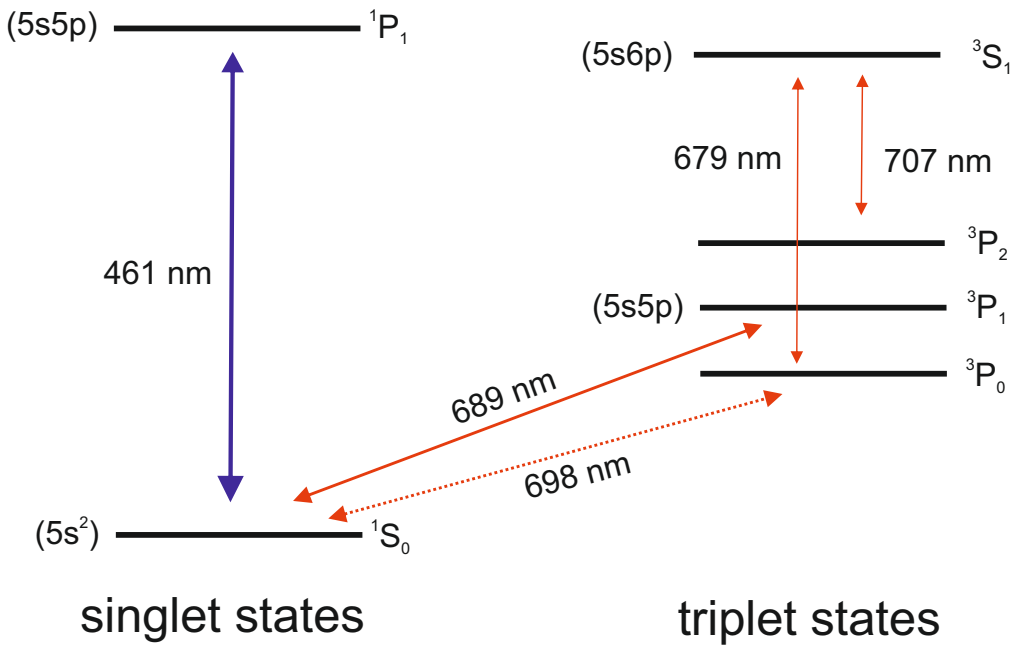

Figure 3.1: Singlet and triplet states for a ^{87}Sr atom. The line at 461 nm is used for the Zeeman slower and blue MOT, the line at 689 nm for the red MOT phase and the transition at 698 nm is the ultra-narrow clock laser transition. The two repumpers at 679 nm and 707 nm are also depicted.

To trap Sr atoms in an optical lattice, it is necessary to first reduce their temperature (kinetic energy) to few μK. To cool down the atoms to this temperature we adopt the usual procedure for this kind of atomic clocks that is largely described elsewhere (see for example [Lud08] or [Boy07a]). Here I will give just a short summary.

The source of Sr atoms is an oven heated up to 500 °C producing a collimated atomic beam with velocity of hundreds m/s. The atomic beam velocity is reduced to m/s using a Zeeman slower employing laser light at 461 nm in resonance with the dipole allowed $^1S_0 \leftrightarrow {}^1P_1$ transition (lifetime τ=5.22 ns, natural linewidth Γ=30.5 MHz [Boy07a]).
Once the atoms reach the center of the main vacuum chamber their Doppler dispersion (velocity distribution) is comparable to the line width of this transition, and they can be loaded in a magnetooptical trap (MOT). This cooling stage is called blue MOT because uses blue laser light at 461 nm. The $^1S_0 \leftrightarrow {}^1P_1$ transition is not a closed transition, since atoms can decay from level $^1P_1$ to the level $^1D_2$ and from there to level $^3P_1$ and particularly $^3P_2$, which is a metastable state. Two other lasers resonant with the transitions $^3P_2 \leftrightarrow {}^3S_1$ (707.2 nm) and $^3P_0 \leftrightarrow {}^3S_1$ (679.3 nm) must then be used to increase the lifetime of the MOT. These two laser are called re-pumper lasers. The 707.2 nm laser pumps the atoms from level $^3P_2$ to $^3S_1$. From there, they can decay into $^3P_1$ (and then eventually to the ground state) or to $^3P_0$, which has also a long life time. The second laser at 679.3 nm re-pumps them back to $^3S_1$. The presence of the repumpers experimentally enhances the MOT size by a factor of 10.
The blue MOT allows to reach a temperature in the order of few mK for the atoms. A second cooling stage, acting on the narrower transition ($\sim$ 7 kHz) $^1S_0 \leftrightarrow {}^3P_1$ at 689 nm (red laser light), is needed. Assuming pure LS coupling, this transition is forbidden since it connects a singlet state with a triplet state. However, the spin-orbit interaction allows a weak dipole transition (intercombination transition) between the two states that can be used for a (red) MOT. In addition to the cooling laser at 689 nm, a second red laser (called "stirring" laser is needed) [Muk03]. While the first one is employed for MOT laser cooling acting between the $^1S_0(F = 9/2) \leftrightarrow {}^3P_1(F = 11/2)$ states, the second one, working between the $^1S_0(F = 9/2) \leftrightarrow {}^3P_1(F = 9/2)$ states is required for optical pumping to randomize population in the different m_F. Here $F = I + J$ is the total angular momentum considering also the nuclear spin I.

3.1.2 Optical lattice trap

Once the atoms have reached a temperature of few μK, they are cold enough to be loaded in a red-detuned optical lattice trap. An optical lattice is a standing optical electromagnetic wave of wavelength λ. Due to the Stark effect, atoms are attracted to high light intensity for a red-detuned lattice. In this way a series of potential wells spaced by $\lambda/2$ arises, in which the atoms can be trapped [Gui99]. A representation of a one-dimensional lattice is given in figure 3.2.

The potential energy U of the wells can be described considering the lattice laser as a Gaussian beam that propagates along the z direction with waist $w(z)$. Using cylindrical coordinates (z and $r = \sqrt{x^2 + y^2}$) we have:

$$U(r, z) = 4U_m e^{-\frac{2r^2}{w^2(z)}} \cos^2(2\pi z/\lambda) \tag{3.1}$$

where $U_m = \frac{P\alpha}{\pi c \epsilon w^2(z)}$ (P average laser power of a single beam and α is the polarizability).

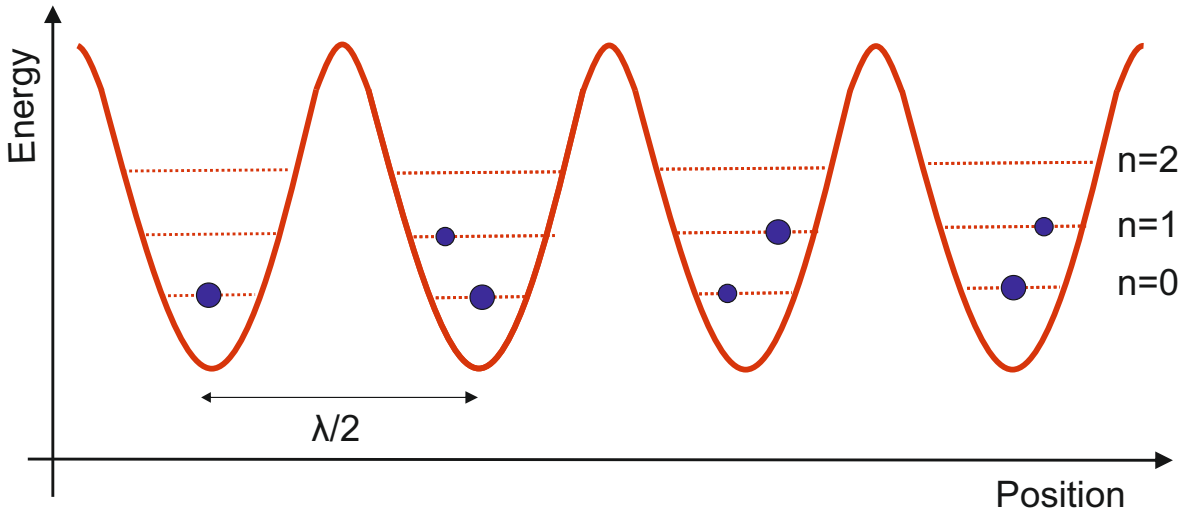

Figure 3.2: Representation of a lattice in one-dimension. The atoms are trapped in potential wells spaced by $\lambda/2$ along the laser propagation direction. This confining potential quantizes the energy of the trapped atoms (Bloch theorem, [Blo29]). The various energy bands are indicated by the band index n. Usually, the highest number of atoms is found in the $n = 0$ band.

In first approximation, this potential can be considered close to its minima as an harmonic potential in both longitudinal and radial dimensions. The resultant Hamiltonian can be solved trough the Block theorem [Blo29]. The energy spectrum presents itself in a band structure, with Bloch vectors $|n, q\rangle$ as eigenstates, where n is the band index and q is the quasi-momentum of the atom. It is possible to define then the longitudinal ν_z and radial ν_r trap frequencies at the trap waist:

$$\nu_z = \frac{1}{2\pi w_0^2}\sqrt{\frac{32\pi P\alpha}{c\epsilon_0 m\pi}} \tag{3.2}$$

$$\nu_r = \frac{1}{2\pi w_0\lambda}\sqrt{\frac{16P\alpha}{c\epsilon_0 m\pi}} \tag{3.3}$$

with m the mass of the atom. Usual values for ν_z are in the range of 50-100 kHz, and for ν_r of few hundred of Hz.

On the other hand, the same AC Stark effect of the lattice laser can be a problem for precision spectroscopy on the clock transition since it acts also on the two clock states making their energy difference (the clock transition frequency) strongly dependent on the power and frequency of this laser. In 2001 the existence of a particular frequency for the lattice light was demonstrated at which the polarizability for the ground (α_g^{E1}) and excited state (α_e^{E1}) is the same for electric dipole interaction E1 [Kat02]. The corresponding wavelength is called "magic wavelength" , for ^{87}Sr one is found at $\sim$813 nm. Keeping the lattice frequency close to the magic wavelength within a range of 100 kHz is sufficient to keep fractional shifts at typical lattice trap depth on the clock frequency due to linear polarizability below 10^{-18}.

However, second order shifts on the clock transition introduced by the lattice light should also be considered. Two photon transitions (defined by differential hyper-polarizability effect $\beta_{g(e)}I$) and Electric quadrupole ($\alpha_{g(e)}^{E2}$) or magnetic dipole ($\alpha_{g(e)}^{M1}$) transitions can also contribute and cause non negligible shifts when reaching the 10^{-17} level of uncertainty or below. The total AC Stark shift $\delta\nu_c$ introduced by the lattice light can be written in an

extended description as (following [Kat15]):

$$\begin{aligned}\delta\nu_c(I,n,\delta\nu,\xi) \approx & \left(\frac{\partial\Delta\alpha^{E1}}{\partial\nu}\delta\nu - \Delta\alpha^{qm}\right)(2n+1)\sqrt{\frac{E_{rec}}{4\alpha^{E1}}}I^{1/2} \\ & - \left[(\frac{\partial\Delta\alpha^{E1}}{\partial\nu}\delta\nu + \Delta\beta(\xi)(2n^2+2n+1)\frac{3E_{rec}}{4\alpha^{E1}}\right] I \\ & \Delta\beta(\xi)(2n+1)\sqrt{\frac{E_{rec}}{4\alpha^{E1}}}I^{3/2} - \Delta\beta(\xi)I^2\end{aligned} \tag{3.4}$$

where Δ indicated the difference between excited and ground state, $\alpha^{E1}_{g(e)} \approx \alpha^{E1}$ (we are close to the magic wavelength), $\alpha^{qm}_{g(e)} = \alpha^{E2}_{g(e)} + \alpha^{M1}_{g(e)}$), n is the band index, E_{rec} is the recoil energy in the interaction with the lattice, ξ is the degree of circular polarization of the lattice light, I is the lattice intensity and $\delta\nu$ is the detuning from the magic wavelength.

3.1.3 Precision spetroscopy on the $^1S_0$ - $^3P_0$ clock transition

The ultra-narrow ^{87}Sr transition chosen as clock transition is the one between the state $^1S_0$ and $^3P_0$ (see figure 3.1). Being both a singlet $\leftrightarrow$ triplet and a $J = 0 \leftrightarrow J = 0$ transition, this transition is in principle strictly forbidden for single photon transition. However, thanks to the hyperfine mixing of the $^3P_0$ with other states it is weakly allowed. The resulting natural linewidth is then very narrow, in the order of $2\pi\cdot$1 mHz. Moreover, being a $J = 0 \leftrightarrow J = 0$ transition, is relatively insensitive to tensorial lightshifts. For all these reasons, the transition $^1S_0 \leftrightarrow^3 P_0$ at 698 nm represents an excellent candidate for high precision spectroscopy [Tak03].

As pointed out in the previous chapter, an atom is in the Lamb-Dicke regime when its oscillation trap energy ($\hbar\nu_z$) is much higher that the recoil energy acquired in the interaction with the interrogation light photon (see equation 2.3). In this case, its spatial wave function is completely localized in a region (z_0) that is much smaller then the wavelength of the probing laser.
If we limit the analysis to the longitudinal direction and we describe the probing (interro-

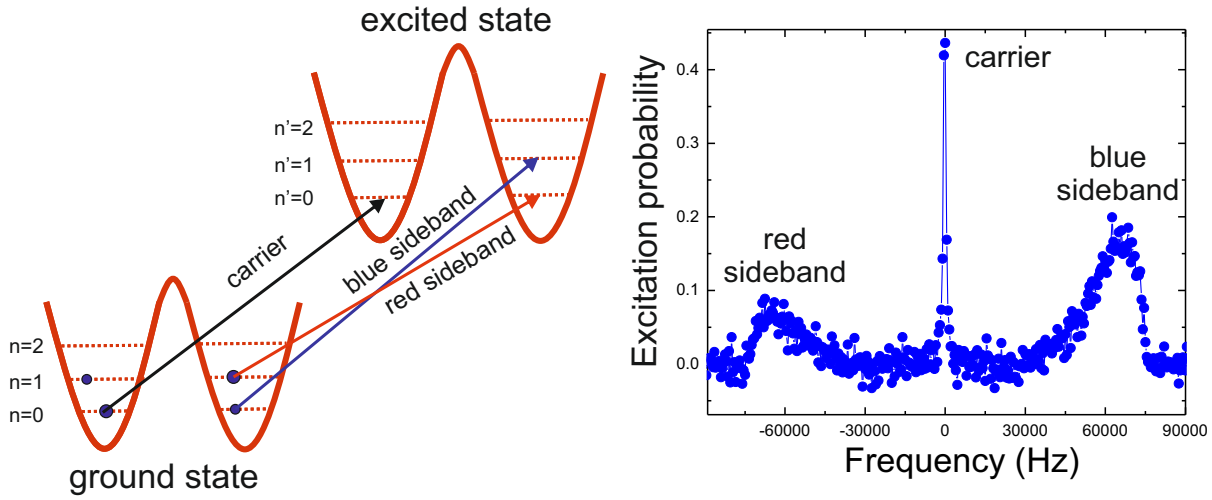

Figure 3.3: Possible transitions induced by the interaction with the probing light for the trapped atoms (left) and the recorded transition probability as a function of interrogation laser frequency (sideband spectrum, right).

gation laser) light as a plane wave traveling along the z axis ($e^{ik_p z}$), the dipole interaction is proportional to the term

$$\langle n_i \mid e^{ik_p z} \mid n_j \rangle \tag{3.5}$$

that describes the coupling between different band indexes.
When $\eta_z \ll 1$ (Lamb-Dicke regime), $e^{ik_p z} \sim 1 + ik_p z$ for $z < z_0$ and the the transition probability is proportional to:

$$\mid \langle n_i \mid e^{ik_z z} \mid n_j \rangle \mid^2 \sim \delta^2_{n_i n_j} + \eta_z^2 (n_i \delta^2_{n_{i+1} n_j} + (n_i + 1)\delta^2_{n_{i-1} n_j}) \tag{3.6}$$

The absorption spectrum is then composed by a strong carrier ($n_i = n_j$) and two sidebands at frequency $\pm\nu_z$, suppressed by the factor η_z^2.

In figure 3.3 are represented the different possible transitions for the trapped atoms induced by the interaction with the probing light and a sideband spectrum recorded in our system.
The Doppler shift is removed and the internal and external degrees of freedom are decoupled. What could shift the carrier frequency in this situation is the line pulling from the sidebands. If $\gamma_0 \ll \nu_z$ with γ_0 width of the carrier, we are in the resolved sideband regime, and the line pulling is negligible.
For the radial motion of the atoms in the lattice ν_r is in the order of some Hz: This time

the sidebands are closer to the carrier. However aligning the probe light parallel to the lattice beam allows a suppression of η_r by a factor $\delta\theta$ where $\delta\theta$ is the the misalignment between the two beams in radiant.
The real potential well is not an harmonic potential for both the longitudinal and radial direction. The real sidebands are then broadened due to the anharmonicity of the trap, especially because of the coupling between the longitudinal bands and the high number of populated radial bands.
A good estimation of the oscillation frequency ν_z can be obtained by the measured sideband frequency difference, taken from the outer edge of each sideband. The longitudinal temperature T_z can be obtained by the ratio r between blue and red sideband amplitudes and assuming a Boltzmann distribution between the lattice bands:

$$T_z = \frac{h\nu_z}{k_B \ln(r)} \tag{3.7}$$

Once the atoms are trapped in the lattice it is then possible to perform spectroscopy on the carrier transition. In our system we excite the transition using Rabi pulses [Bav86]. We detect the status of the atoms with a normalized-electron shelving detection technique [Fal11]. For atoms in the Lamb-Dicke regime the linewidth of this transition is only Fourier

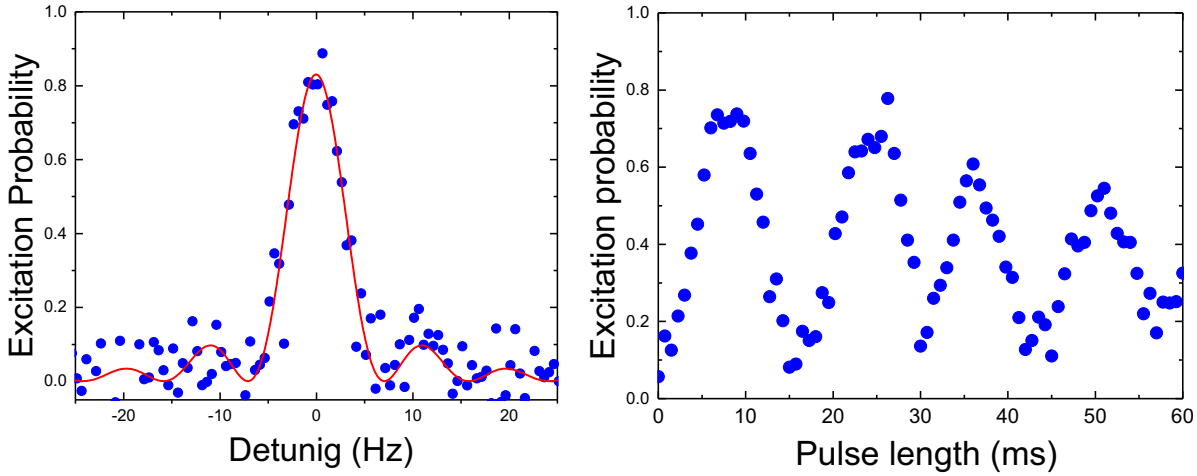

Figure 3.4: On the left: A 6 Hz ^{87}Sr clock transition line (excitation probability as a function of laser detuning from the transition). The blue dots are the measured value during the scan, and the red line is a fit with a sinc function. On the right: recorded Rabi oscillation (excitation probability as a function of interrogation time)

limited. In figure 3.4 a 6 Hz line and a Rabi oscillation detected in our system are shown.

To remove motional effects it is necessary that the wave function of the atom is completely localized in single a well. However, if the Stark effect from the lattice light is the only force involved, the potentials of adjacent wells are degenerate and the atoms can tunnel from one well to the other. This is the cause of broadening and shifts on the carrier transition. To suppress this effect it is possible to use highly intense trapping light, but this could be the cause of other shifts on the transition (see equation 3.4). An elegant solution has been proposed in [Lem05], and consists in tilting the lattice direction respect to gravity (or even to put it vertical) so to add the gravity potential. In this way the degeneracy of the states in adjacent wells is lifted, severely limiting the tunneling between them.
The new eigenstates of the atomic wave function are then Wannier-Stark states $\mid W_m\rangle$, where m is a quantum number characterizing the state [Wan60]. The great majority of optical lattice clocks adopt today this solution.

3.1.4 Laser lock to the clock transition

To lock the interrogation laser to the clock transition in order to use it as a frequency standard, it is necessary to measure its detuning from the center of the transition, generate an error signal and feed it back to the laser to correct its frequency. To determine the center frequency of the transition, we set the interrogation laser frequency value to interrogate two opposite sides of the line. The detected excitation probability (p_e) is converted into frequency offset of the interrogation laser ν [Dic88, Al-15a] using the formula:

$$\frac{\delta p_e}{\delta \nu} \approx \pm 2\pi \times 0.30 T_\pi \tag{3.8}$$

where T_π is the interrogation time and the term π denotes that we use a Rabi interrogation. The center frequency of the line is calculated from the mean of these two frequency offsets. The reference laser frequency is corrected such to keep the two interrogation points at the two extremes of the line full width half maximum of the line. The longer is the coherent interrogation time, the more sensitive is the measurement to frequency excursions and the more stable is the clock.

When the atoms are trapped in the lattice the compensating magnetic fields are set such

that the atoms experience a zero B field in their location. However, it is very difficult to really zero the magnetic field experienced by the atoms. Due to the Zeeman effect, the hyperfine states of the ground and excited clock states loose their degeneracy and are shifted: as a consequence the transition is broadened and shifted if the states population is unequal.

To solve this problem we adopt the solution presented in [Hap72]. Before probing the clock transition, a bias magnetic filed is applied orthogonal to the lattice axis, and the stirring light at 689 nm is shined on the atoms to optical pump them in one of the extreme Zeeman sub-levels $m_F = \pm 9/2$ of the $^1S_0$ ground state. The +/- sign depends on the σ_+ or σ_- polarization of the stirring light. By alternating the stirring light polarization every two consecutive experimental cycles, we detected first the line center for one extreme m_F and then the for other one. The mean of the two line centers gives the transition frequency unperturbed from the 1st order Zeeman shift. To determine the correction for the interrogation laser detuning is then necessary to repeat four experiment cycles. In

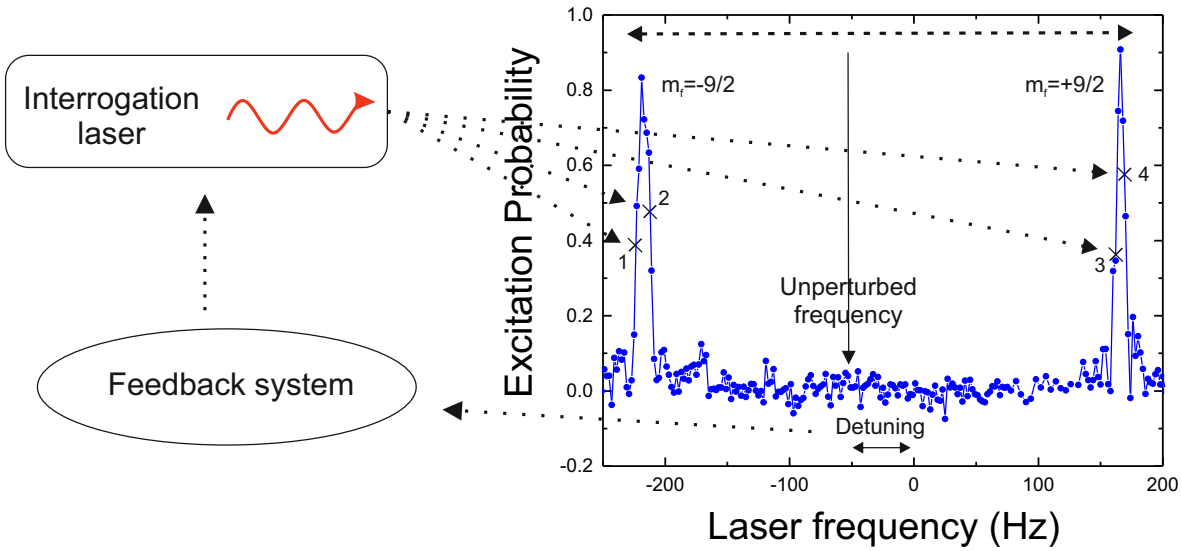

Figure 3.5: Before a frequency correction can be applied to the interrogation laser, four experimental cycles are needed. The first two interrogate the left and right side of the $m_f = -9/2$ state (after spinpolarization with σ_- stirring light), and the second one the left and right side of the $m_f = +9/2$ state (after spin-polarization with σ_+ stirring light). The center of the two lines can be then calculated, and their mean gives the clock transition frequency unperturbed by the Zeeman shift at first order. Note that in this figure the detuning is exaggerated, usual corrections are in the order of 1 Hz.

each of them, the frequency of the interrogation light going to the atoms is shifted with an AOM to interrogate the right point in the sequence (see figure 3.5).

In every cycle after the optical pumping in the desired m_F state we remove the remaining atoms in the unwanted Zeeman sub-levels to prevent line pulling from them. First we excite the atoms of the chosen Zeeman state with a π-pulse from $^1S_0$ to $^3P_0$ ($\Delta m_F = 0$) on the clock transition in a (relatively strong) bias magnetic field of about 1.9 mT. In this way all the m_f states are very well separated from each other. After this, we blow away the atoms remaining in the $^1S_0$ state (independently on their m_f) by a pulse of the 461 nm laser. This process of m_f state selection is called clean-up.
We then excite the clock transition with the necessary Rabi frequency to reach the narrower line possible and we the detected the atoms state after the interrogation. We first detect the atoms in the $^1S_0$ ground state by exciting the $^1S_0$ - $^1P_1$ transition at 461 nm. When all the atoms in the ground state are blown away by the detection process, we use the repumper light to pump the atoms in $^3P_0$ back to the ground state, and we repeat the same process on the $^1S_0$ - $^1P_1$ line to detect atoms in the excited state. After all the atoms are again blown away, a third detection pulse is performed to detected the background to be subtracted in the two measurements.

3.2 Transportable optical lattice clock

In this section, I will describe the experimental apparatus of our transportable clock. The transportable clock components have been built by Stefan Vogt during his doctorate study, and more technical details can be found in his thesis [Vog15] and in reference [Vog16]. The interrogation laser with the transportable reference cavity has been built by Sebstian Häfner [Häf15a]. I will give a short description of these components. The reader interested in more details can reference to the cited publications.

Figure 3.6: After initial tests in the laboratory, we moved the optical clock components inside a car trailer (left). A view of the car trailer from the outside is showed in the figure on the right. It can be pulled by a van and has an air conditioning system.

When I started my doctorate at PTB, the system was placed in the laboratory and few components were still missing to make it independently operational, like the reference cavity to lock the lattice laser. Moreover during the tests we made, initially in the laboratory and then in the trailer that is used for transportation, the need of some changes became clear. I will describe these changes.

3.2.1 Experimental apparatus

The transportable optical clock apparatus can be divide in four different parts: The physics package, the laser systems for laser cooling and trapping, an ultra-stable interrogation laser, and the electronic components together with the computer computer system to control the experimental sequence and perform the feedback control on the interrogation laser [Kol17]. The mass of the experimental apparatus is approximately 800 kg.
It should be noted that in contrast to other transportable optical lattice clocks that are being developed in other projects for space applications, where mass, size and power consumption of the system is of prime importance, our goal is more oriented on developing a clock with stability and uncertainty as close as possible to state-of-the-art laboratory systems.

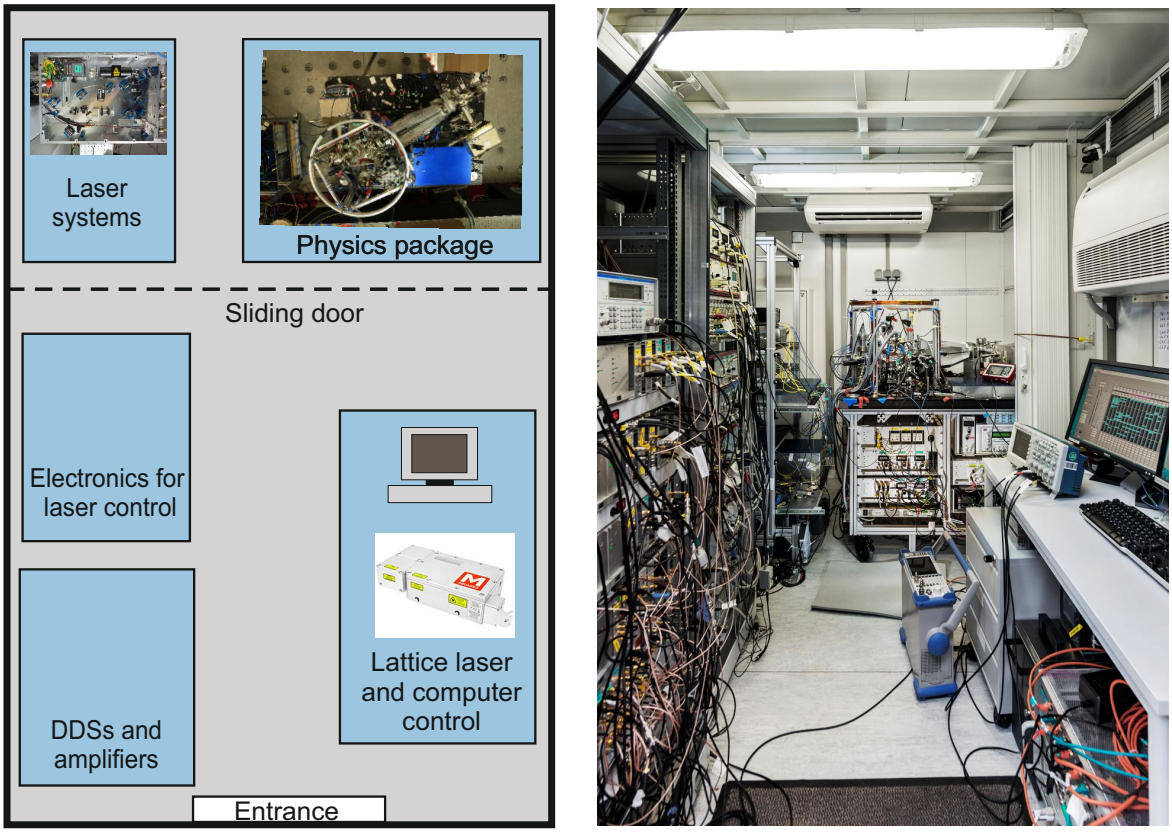

Figure 3.7: A scheme of the experiment disposition inside the container (left) and a picture of the interior of the container (right). The lattice laser was not yet installed when the picture was taken.

All the components, except the interrogation laser, are placed inside the car trailer, which is a container with interior dimension of 2.2 m × 3 m × 2.2 m that can be pulled by a small van (see figure 3.6). The mass of the loaded trailer is approximately 3000 kg. The container walls are thermally insulated and an air conditioning system is installed inside to keep the temperature stable within 1-2 K. The interrogation laser and its ultra-stable cavity are placed outside the trailer on concrete floor. This is needed because the floor of the container is subjected to vibrations that degrade the clock laser cavity performances.

The disposition of the components inside the container is depicted in figure 3.7. In the back of the trailer, the physics package and the laser systems with their reference cavities are placed. Optical breadboards and cavities are arranged in a rack with five wooden drawers. They are fixed to the drawers with rubber isolation posts to suppress the transmission of vibrations. In the front-left of the container, there are two racks containing the necessary electronics and on the front-right the lattice laser system and the computer for experiment control and feedback generation to the clock laser are placed. A sliding door separates the front from the back. In this way the physic package is better sheltered from the heat produced by the electronics and from the light that could disturb the fluorescence detection.

Physics package:
The physics package is where the atomic ensamble is generated, collected and interrogated. An atomic beam is produced in an oven. Successively the atoms are cooled and trapped into the optical lattice for spectroscopy in the main chamber. The vacuum and oven chambers are connected by the 50 cm long Zeeman slower. The pressure inside the main chamber is of the order of 10^{-9} mbar. The oven chamber is connected to the slower by a 2-mm-diameter pin hole: In this way the main chamber is protected from the black body radiation (BBR) of the oven. In addition, the pin-hole acts as differential pumping between the two chambers (pressure difference of about one order of magnitude). Two 40 l/s ion pumps are adopted to maintain the vacuum. To completely shield the main chamber from the oven radiation during spectroscopy we use a rotating shutter with a servo motor. The shutter closes the view to the oven during atomic interrogation.
The whole physics package is mounted on an optical breadboard with the size of 120 cm × 90 cm.

To provide temperature homogeneity of the chamber, the Zeeman slower's magnetic field is generated using permanent magnets instead of electric coils. The coils for the MOT's magnetic fields are very efficiently water cooled. The cooling water is stabilized to better than 100 mK by a thermostat, which has also the effect to effectively stabilize the temperature of a large part of the vacuum system. The winding exposed to the chamber are cooled first, and their temperature is the best controlled [Vog16].

Laser system:

Laser light generation, splitting, shifting and modulation is done in five compact aluminum breadboards (45 cm $\times$ 30 cm), and makes use of diode ECDL lasers and compact optical components, except for the lattice light, which is generated by a Ti:Sapphire laser. The blue (461 nm) laser light is generated by doubling the light from a 922 nm laser diode with a second harmonic generation (SHG) crystal. In the breadboards, half-inch optics are used together with acousto-optic modulators (AOMs) and mechanical shutters.

To stabilize the frequency of the lasers, all of them, except the two repumper lasers, are locked to individual ultra low expansion (ULE) cavities of 10 cm length. A frequency modulation of several 100 MHz is applied to the 707 nm repumper to cover the hyperfine structure of ^{87}Sr. The 922 nm laser ULE cavity is housed in a simple vacuum chamber with a passive heat shield. This is enough because the blue cooling transition has linewidth in the order of 30 MHz: the requirements om its stability are more relaxed. The external temperature of the cavity is stabilized by thermoelectric coolers (TEC). The red cooling laser and lattice laser ULE cavities are also placed in a vacuum chamber but there, an additional temperature stabilized internal heat shield is used: The laser stabilization must be performed at the kHz level. The stirring laser is phase-locked to the red cooling laser, since their frequency difference is only 1.46 GHz, and can be generated via a synthesizer. The finesse of the cavity for the red cooling laser is high ($F = 240000$), while the other two have a finesse of $F = 1000$.

To lock to the cavities, we adopt a Pound-Drever-Hall (PDH) locking scheme [Dre83]. In particular, with a fiber coupled low power EOM we first generate two sidebands on the laser carrier frequency and then we generate two additional sidebands on each sideband. The PDH lock is then perform using one of the carrier sidebands. In this way we have an easy and wide tuneability of the laser frequency.

Interrogation laser:
The interrogation laser has to be as stable as possible to reduce the Dick effect [Dic88] and at the same time allow long interrogation pulses, which are both important conditions to improve the stability of the clock (see section 2.1.3). This means that the cavity used to pre-stabilize it has much higher requirements then the previous ones. Moreover, in the case of a transportable clock the cavity has also to be compact and robust for the transport.
In our system, the compromise is reached by the use of a 12 cm ULE spacer with fused silica mirrors [Vog11], [Häf15a]. The mounting of the cavity (via wire-bar attached to Invar pins that are glued into holes in the spacer) is optimized for low vibration sensitivity [Häf15a, Ste11]. The sensitivity to accelerations in three orthogonal directions is $k = (0.3, 4.3, 11.6) \cdot 10^{-10}/\mathrm{g}$. Placing the cavity on an active vibration isolation platform, the thermal noise floor of the resonator setup $4 \cdot 10^{-16}$ is reached for timescales of 1 s up to a few 10 s. This cavity is also housed in a vacuum chamber, with internal and external temperature stabilization.
The laser board of this laser has been changed during this work from the initial one where standard optical components were used to a much compact one by an other student who is working also on an a new transportable reference cavity based on microcristalline mirrors with the goal to reach a thermal noise floor of 1×10^{-16} for short timescales. The new optical board can be placed during operation on the top of the ULE cavity itself, resulting in a very compact system.

Figure 3.8 shows a scheme with the three output of the interrogation laser board: one for the pre-stabilization to the transportable cavity, one to interrogate the atomic clock transition and one acting as the output of the system (that can be used for clock comparisons).

The switch AOM generates the Rabi pulses for interrogation and switches between different frequencies in order to interrogate the two different side of the opposite m_F states. As said, the interrogation laser board and cavity are placed outside the car trailer and the light is delivered to the physics package via an optical fiber. The interrogation light is delivered to the atoms through the back of the lattice laser's back-reflection mirror. This mirror has very has low transmission and is used as reference mirror for the optical path length stabilization [Fal12]. The interrogation laser light is reflected back into the fiber

and its de-phasing with respect to a short interferometer arm on the clock laser board is measured as a beat note on a photodiode (see figure 3.8). This beat note is tracked (after a filtering and amplifying process) through a tracking oscillator and phase-compared to a fixed rf frequency generated by a DDS. The phase-comparator output is fed to a VCO that clocks the DDS generating the signal for the switch AOM. In this way the phase of the interrogation light is stabilized directly at the position of the atoms. To check for cycle slips of the detector, we split the beat signal and track it with a second independent tracking oscillator. The frequencies of the two tracking oscillator are divided by digital

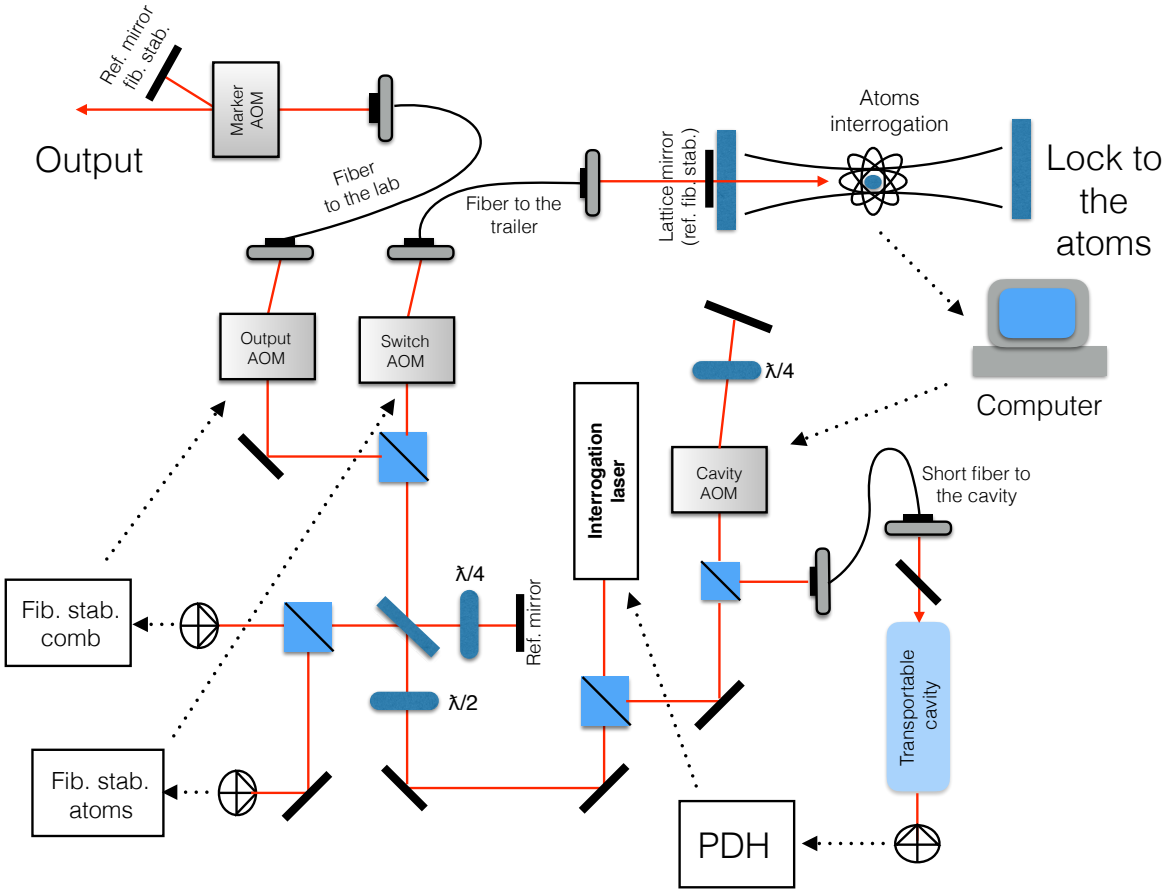

Figure 3.8: A scheme of the three outputs of the clock laser board. The output going to the atoms and the one for frequency comparison are delivered with optical fibers phase stabilized through their respective AOMs. The light going to the transportable cavity for the Pound Drever Hall lock is tuned with the double-passcavity AOM, which corrects the frequency to keep it in resonance with the atoms and subtracts the linear cavity drift as measured against the atoms.

dividers and compared to check for de-phasing between the two. When a cycle slip is detected during atom interrogation, the measured point is discharged by the computer program, because it could lead to false value for the measured clock transition frequency (if for example it causes the light going to the atoms to have one extra oscillation per second, the measured frequency is shifted by 1 Hz for evey second of interrogation time). Stabilizing the light over the pulsed path leaves the optical fiber stabilization loop without input signal during the dead time between clock pulses. To solve this problem, we synthesize an artificial beat signal by switching the input of the phase detector to the reference DDS during the dead time [Fal12].

After the atoms have been interrogated and their excitation probability has been detected, the computer program calculates the offset of the interrogation laser from the atomic transition and corrects its frequency by acting on the cavity AOM. This is a double-pass AOM that delivers the light to the fiber going to the transportable cavity for the pre-stabilization of the laser. This correction is composed of two signals that are mixed and feed to the AOM. One part corrects the drift of the cavity against the atoms with a feed-forward and and the other one set the real lock to the atoms. The fiber delivering the light to the cavity is not phase stabilized because is very short (1 m).

Finally, the third output represents the output of light that can be used for clock comparison. The light passes through the "output AOM" for optical path stabilization and the first AOM diffracted order is coupled into a fiber that delivers the output. At the end of the fiber, we make the light pass through a second AOM used as marker that works at a different frequency. The first diffracted order from this AOM is sent back through a mirror that represents the reference mirror for the phase stabilization. In this way we assure that the beat is really coming from the light back reflected by this mirror, since back reflected light from components before the marker AOM would give a beat note at a difference frequency. The zero or the same first order light are then used to generate a beat note on a photodiode or through a transfer beat using a frequency comb with an other clock for comparison.

Electronics and computer control

For the generation of the RF signals driving the AOMs and the EOMs, standard DDSs

and RF amplifiers are used. A computer program drives the system through TTL signals and USB communication ports, records the detected signals, interprets them and sends the correction feedback to the interrogation laser. It also sets and changes the magnetic fields in the various phases of the experimental cycle. The detection of the fluorescence from the atoms was initially performed collecting the light on a photodiode. During my thesis, we replaced it with a photo multiplier to improve the signal-to-noise-ratio of the detection and improve the stability of the clock (see following section).

3.2.2 Technical improvements

Here I will report the technical improvements that we made during my doctorate in order to optimize the operation of the system. Their need has become clear during the evaluation of the clock and its use in the measurement campaigns.

Lattice laser:
In the initial setup of the system, the lattice laser light was produced via a diode laser at 813 nm and a tapered amplifier (TA) chip to reach the required power ($\sim$ 1 W).
It is known that such laser systems have spectral impurities caused by amplified spontaneous emission that can represent a problem in the determination of the magic wavelength [Le 12]. However, this laser was initially chosen because of its greater compactness with respect to the other option, a Ti:Sapphire laser. To improve the laser beam quality of the light exiting from the TA, two filtering processes were performed. First a spectral filtering with a volume Bragg grating with 0.1 nm bandwidth, and then a spatial filtering with a 1 m long, large-mode-area (LMA) fiber. The bandwidth of the Bragg grating was 0.1 nm. After this the light was passed in AOM for intensity stabilization and then coupled in a second LMA fiber connecting the laser board to the physic package.

We performed a first comparison to the stationary ^{87}Sr lattice clock at PTB in which the TA system was employed for the transportable clock. The result of the comparison showed a frequency difference between the two systems of about 3×10^{-16} in fractional frequencies units, not compatible with zero considering the combined uncertainty of the

two clocks, which was below 1×10^{-16}. Moreover, the magic wavelength frequency we found resulted to be lower than expected by 101 MHz, considering the parallel alignment of the lattice polarization vector and the bias field. This value lies even outside the wavelength range expected for any lattice polarization. For this reason, we decided to repeat the comparison replacing the laser diode system with an old Ti:Sapphire system available in our laboratories. This time, the frequency difference between the clock resulted to be $-6(80) \times 10^{-18}$, compatible with zero. Also the value for the magic wavelength frequency we found was compatible with what we expected. In figure 3.9, the results for the magic wavelength frequency measurements in the two experiments are shown. In the graphs, the difference between the transportable clock frequencies measured with a deep and a shallow lattice are reported (using the stationary clock as a reference) for different values of the lattice laser frequency. The resulted magic wavelength differs by more then 100 MHz in the two cases, and only for the measurement with the Ti:Sapphire laser matches the expected value.

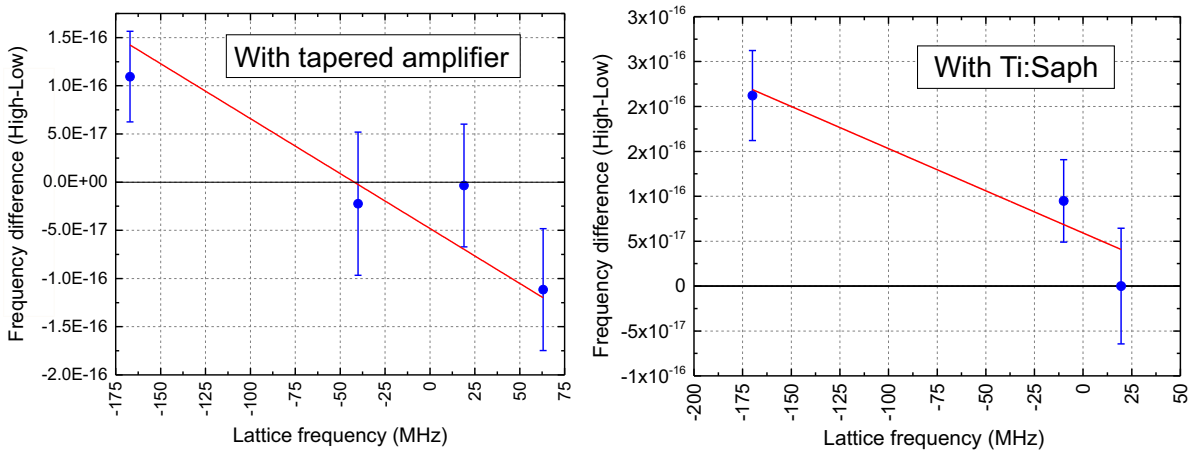

Figure 3.9: The results of the magic wavelength measurement when we used the TA laser (on the left) and when we used the Ti:Sapphire laser (on the right). The lattice frequency is reported as detuning from the stationary magic wavelength value. The blue dots are the measurement results and the red line is a linear fit (with fixed slope).

After this finding, we decided to definitively change the lattice laser for the transportable clock from the tapered amplifier system to a Ti:Sapphire one. However, we needed this laser to be compact and with short set up time. The choice fall on the Solstis

system from the M^2 company. The head of this laser is monolithic and measures only $29 \times 17 \times 7$ cm, while the power supply and cooler for the pump laser (from Lighthouse Photonics) has dimensions of $345 \times 323 \times 480$ cm. The head of this system is now installed on the lattice optical table inside the car trailer. The pump is transported separately during transport. The system can be re mounted and be ready to use in few minutes.

Thermal and humidity management inside the trailer:
One of the main problems that we experienced for the clock operation during the first measurement campaign outside PTB was the temperature management inside the trailer. The overheating of the titanium sapphire laser driving the optical lattice caused the laser to stop working in a few occasions, and to cool it down we had to switch it off.
The unstable temperature inside the trailer lead to higher instability in the lock of the cooling lasers (especially the red cooling and stirring) and to misalignment of the setup used to overlap and re-distribute the blue and red (cooling and stirring) lasers light for the three retro-reflected MOT beams. This fiber-cluster was based on free-space optic. Initially, we managed to mitigate the effect with some isolation between it and the optical table where it was placed. However, this resulted to be not enough and we decided to replace it with a fiber based one. In this way, the free-space paths susceptible to misalignment were removed. The two fiber clusters are compared in figure 3.10

Although the air conditioning system has enough power to cool the trailer considering the heat produced during the experiment, the small volume of the container causes the heat to be stuck in some particular places with low ventilation. This was the cause of the thermal instability of some delicate part like the pump laser and the fiber polarization described above. For this reason we adopted some switches to turn off the RF amplifiers for the less critical AOMs when they are not in use, since these RF amplifiers are the main source of heat. Operating the system with the switches did not affect the atom cooling process and contributed to reduce the heat production. Moreover, in very sunny and warm days during measurement campaigns outside PTB the thermal management inside the trailer was better handled with the precaution of shadowing it to protect it from direct solar light irradiation. This was achieved by placing the system in the shadow of a building or by the installation of shadowing tents.

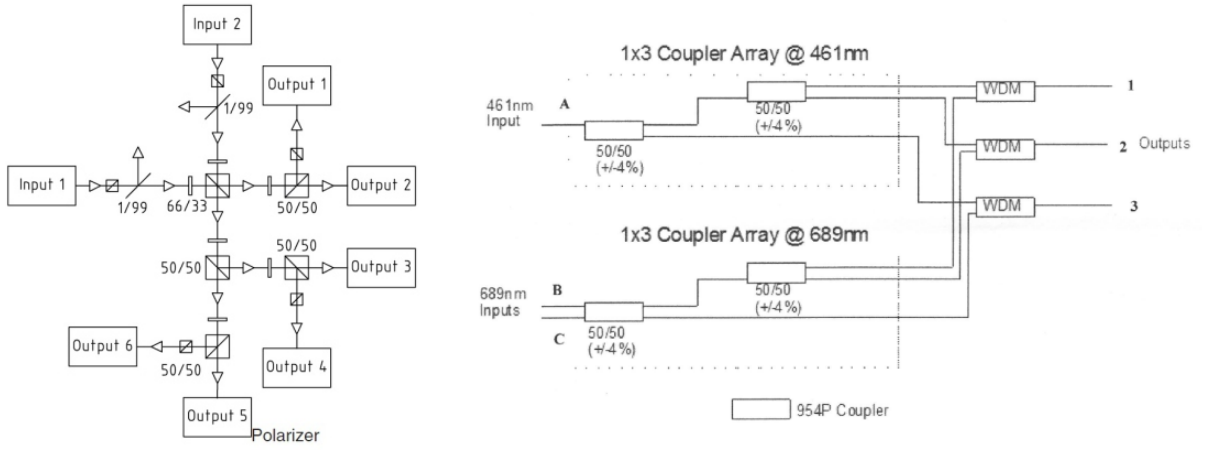

Figure 3.10: In the old fiber cluster (on the left) the light from each of the three laser (blue and red cooling, red stirring) entering in the cluster in three different inputs (1,2,3) was polarized and mixed with beam splitters and wave-plates. Three of the outputs containing all the three different laser light were the transferred for the retro-reflected MOT beams (Schäfter and Kirchhoff). On the right, the new version of the fiber cluster (from Evanescence Optics) where free-optical paths are removed. This cluster is all fiber-based.

Moreover, an other problem was also present: the AC system in the back of the trailer blows the fresh air very close to the vacuum chamber: we saw that this had a clear effect on the detected atom numbers and on the temperature of the vacuum chamber, that were changing periodically accordingly to the air flux being switched on and off by the AC system. For this reason we built a box to cover the vacuum chamber to protect it from the direct flux of air. In figure 3.11a the difference in the detected counts with and without this protection box is shown. With the box the large fluctuations in the number of atoms were removed. In the picture with the box the atom number is lower because it was taken whit a photomultiplier as a detection system (see next paragraph) that allowed us to have a good SNR also working with less atoms (and in this way reduce collision shift).

This box has also an other important positive effect: it reduces the temperature inhomogeneities inside the main vacuum chamber, thus reducing the uncertainty on the BBR shift determination. The representative temperature T for the environment of the atoms can in fact be calculated assuming the vacuum chamber as an opaque system, and measuring the highest and lower temperature T_{max} and T_{min} points of it. This measurement

is performed with calibrated Pt100 sensors placed in the hottest and coldest regions of the chamber. The BBR radiation emitted from the hot oven is considered as zero because of the use of the mechanical shutter closing the view of the atoms to the oven during the clock transition interrogation. Assuming a rectangular probability distribution for the representative temperature T between T_{min} and T_{max}, we have $T = (T_{min} + T_{max})/2$ with an uncertainty given by $(T_{max} - T_{min})/\sqrt{12}$ [GUM08].
The box reduces the temperature excursions caused from air blow of the AC system on the vacuum chamber: with the use of this box together with efficient water cooling of the MOT coils, we were able to reduce the temperature difference between T_{max} and T_{min} to 200 mK (corresponding to a BBR uncertainty of 3×10^{-18}) for several hours of measurement. In figure 3.11b are shown the temperatures measured from the various Pt100 sensors on and inside the chamber for a three hours measurement. On all the line, and especially on the one indicated with the arrow is possible to still see the effect of the periodically turning on of the AC system, but with the box this effect is now negligible.

Finally, we also realized that during days with high air humidity, water molecules were entering and accumulating in the second harmonic generation cavity needed to double the 922 nm laser light in order to obtain the 461 nm (blue) cooling and detection

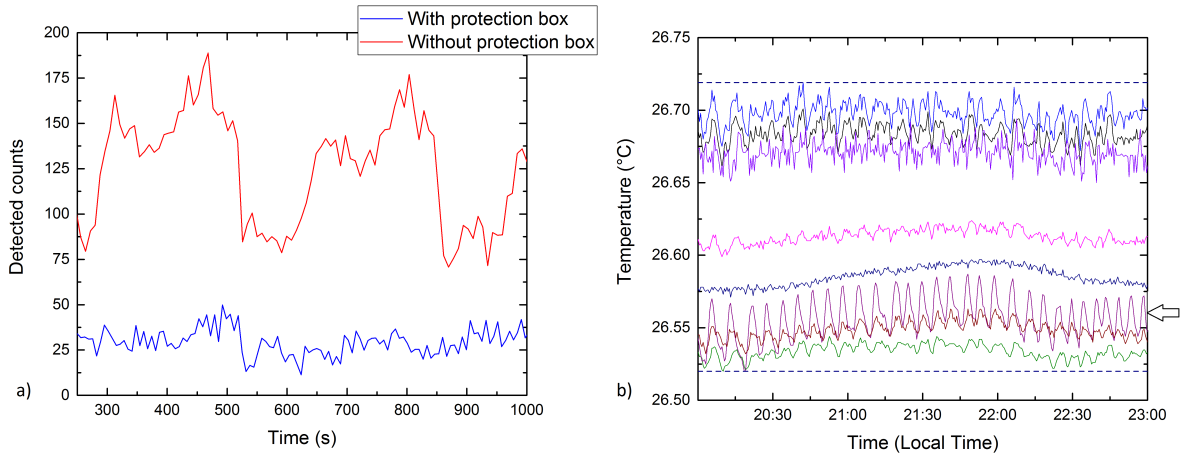

Figure 3.11: a) Fluctuations in the detected counts with and without the protection box. b) Temperatures measured by the Pt100 sensors with the protection box. On the line indicated by the arrow, the effect can still be spotted, but it is negligible.

light. Unfortunately, the water molecule has an absorption line at 922 nm exactly at the frequency we need to double to operate the Zeeman slower and the blue MOT. The problem was solved by replacing the doubling cavity with a more recent model that is sealed. In this way, the humid air cannot enter inside.
In figure 3.12 the power drop caused by the absorption of the 922 nm light by water molecules in the SHG cavity output measured is shown.

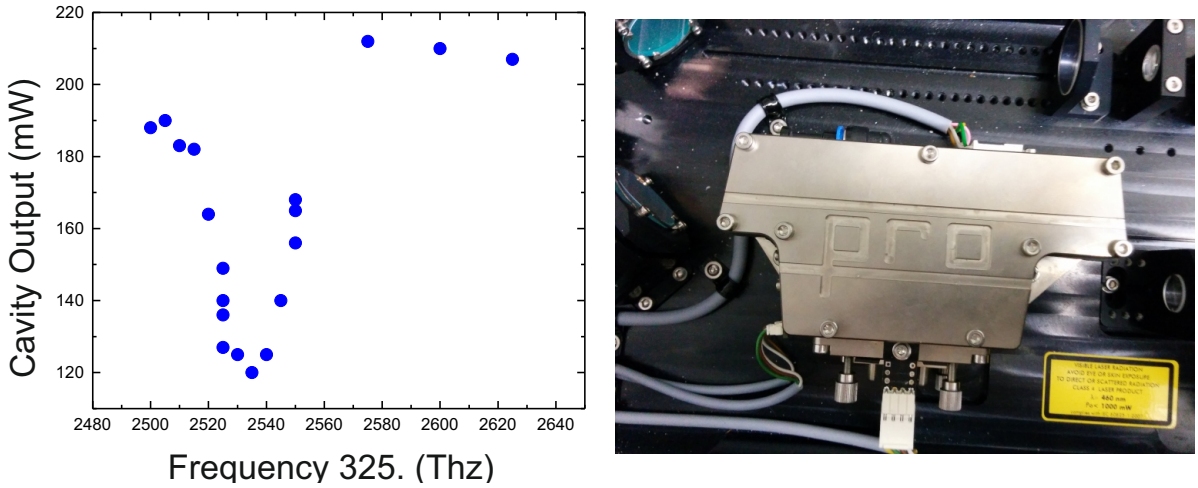

Figure 3.12: The power drop in the SHG cavity output caused by the absorption of the 922 nm light by water molecules as function of the laser frequency (left). On the right a picture of the doubling cavity itself.

Detection:

During the evaluation of the system, we realized that our stability was limited by the way in which the detection process was handled. This became clear when we had the opportunity to lock out interrogation laser to a much more stable laser present at PTB (see next section) and we did not see the expected gain in stability due to the reduction of the noise coming from the Dick effect.
In the first version of the experiment, we were using a photodiode as detection system. Moreover, the background was not recorded as a separate pulse after the excited and ground state detections, but a single background for each of the two pulses was recorded after the atoms florescence was gone. We saw that this was the cause of false values for the detected excitation probability, and it made us decided to adopt the three pulses detection.

In addition, we decided to exchange the photodiode with a photomultiplier, because of its much better signal to noise ratio for small signals. This allowed us to increase the SNR from 30:1 to 300:1, with two positive effects: the reduction of the detection noise contribution to the instability of the clock (see section 3.3.1) and the possibility to work with smaller atomic densities without degrading the fluorescence signal to reduce the collision shift (see section 3.3.2).

3.3 Clock performances characterization

The evaluation of the transportable clock performances proceeded through various steps during my doctorate. Here, I will report the latest and most accurate uncertainty budget evaluation we performed at PTB for the transportable clock.
Initially, the clock was placed in the laboratory, but later we moved it into the car trailer. Now, the transportable clock at PTB is arranged as in figure 3.13: the trailer is placed in the parking lot of our building, while the interrogation laser cavity and breadboard are in a room in the basement. Two phase stabilized 50 meter fibers deliver the laser light from the basement to the trailer to interrogate the atoms and to the stationary ^{87}Sr clock's laboratory of our group. There, a beat note between the interrogation lasers of the two clocks is detected on a photodiode.

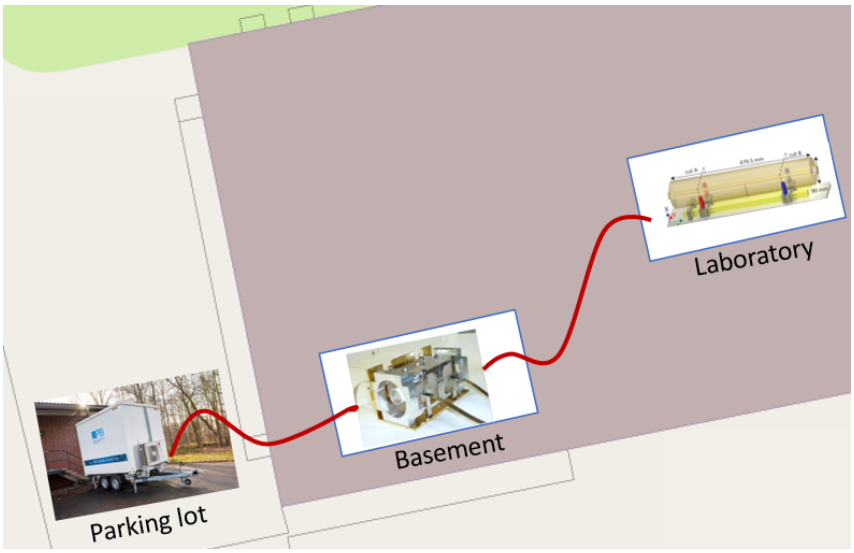

Figure 3.13: Arrangement of the transportable clock at PTB. The trailer is located in the parking lot, the transportable interrogation laser and cavity (see picture) are placed in the a room in the basement and its light is delivered to the trailer by a 50 meter long fiber. A second fiber delivers its light to the laboratory where the interrogation laser and cavity (see picture) of the stationary clock are and where their beat note is recorded.

3.3.1 Uncertainty budget evaluation

Here I will described how we evaluate the value of the systematic effects that shifts the clock frequency (see section 2.2.1). This procedure has been the same for every uncertainty budget evaluation done in the experiment described in this thesis.

To evaluate independently some systematics effects like the lattice light shift or the collision shift, it is possible to run the transportable clock in interleaved mode. In this operational mode, two independent experimental cycles are operated interleaved one to the other, as is depicted in figure 3.14. One parameter, for example the lattice intensity o the atomic density, is set differently in cycle A and cycle B. It is possible then to measure the different locking frequency of the two cycles, that gives a measure of the systematic

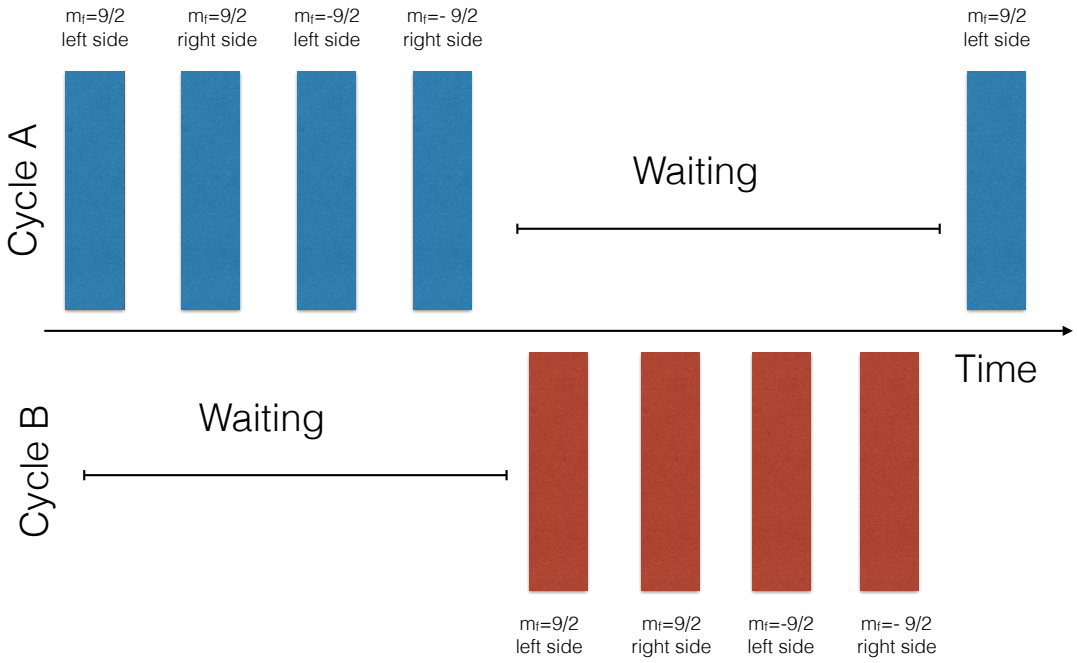

Figure 3.14: In the interleaved operation of the clock two cycles are run independently. When cycle B is running, cycle B is stopped and vice-versa. This dead time increases the noise coming from the Dick effect (see instability characterization section).

effect being tested. The difference in locking frequency A and B is detected at every step against the clock laser cavity which has a better short term stability then the lock to the atoms.

The scheme for interleaved operation showed in figure 3.14 is in reality not the best choice to reach the best instability of the system during interleaved operation. It was showed that a better arrangement would be to interleaved each of the eight cycles on to the other, instead of interleaving them in block of four [Al-15a]. We do not yet use this configuration in our system because it requires some major changes in the computer program that run the experiment, but in the near future we will implement this scheme.

AC Stark shift:

The AC Stark shift from the lattice light is given by equation 3.4. The shift is evaluated by operating the clock in interleaved mode with two very different lattice depths U_0. The lattice depth is converted in the effective lattice depth U experienced by the atoms. This is calculated by supposing that only a small fraction (5%) of the atomic population is in longitudinal states different from $n_z = 0$ and by approximating the thermally averaged energy for the radial degrees of freedom as its classical value ($2\mathrm{K}_B T$) [Dör18]. This is justified by the small temperature (few μK) and trap frequency ($\sim$ 100 Hz) in the radial direction: the energy spectrum can be approximated as a continuum. Making use of the virial theorem, we have:

$$U \sim U_0 - \frac{1}{2}\left(\frac{1}{2}h\nu_z + 2k_B T_r\right) \tag{3.9}$$

In our system we interleave the clock operation between 65 E_r and 185 E_r effective lattice depth. The measured shift between the two cycles is used to calculate the actual shift on both of them via equation 3.4 [Kat15], where the coefficients for the differential hyperpolarisability and differential E2/M1 polarisability are taken from [Le 13] and [Wes11] respectively. We operate the clock at shallow lattice depth during normal operation.

The interrogation laser light causes also an AC Stark shift. However this shift is very small and negligible: for usual Rabi pulse duration (130 ms) and interrogation laser intensity (5 W/cm^2) the shift is in the order of 2×10^{-20}.

Light from other lasers is prevented from entering the vacuum chamber by switching

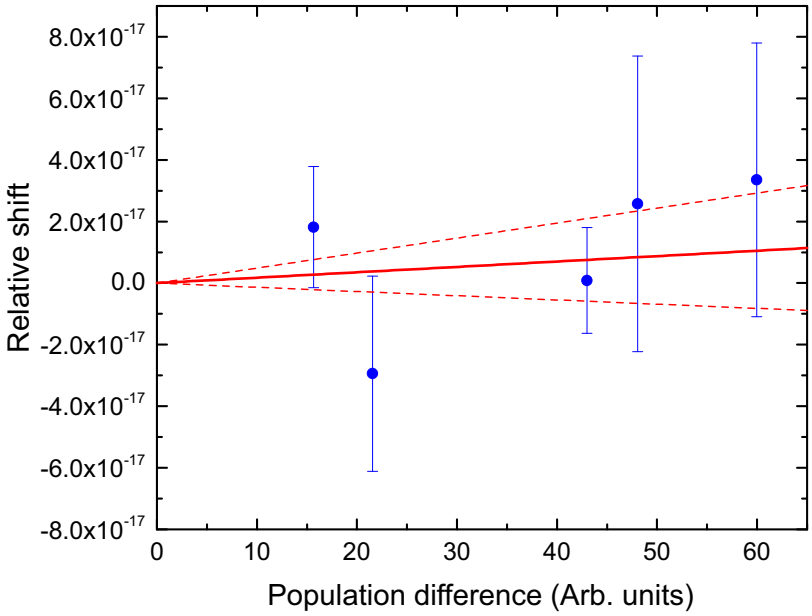

Figure 3.15: Relative shift between the two cycles during the interleaved operation of the clock as a function of the atomic population difference in the two cycles. The continuous red line is a linear fit without an offset and the dashed lines represent its statistical error.

AOMs and using mechanical shutters during atomic interrogation.

Collisions shift:

As introduced in section 2.2.1, the collision shift can be divided in two contributions: cold collisions between atoms in the lattice (also called density shift) and collision from the background gas (hot collisions).

The first contribution can be experimentally evaluated by interleaving two cycles with different atomic density (see figure 3.15). This is done by loading for a longer or shorter time the blue MOT: the atom numbers is then greater or lower depending on the interleaved cycle. We suppose that the volume they occupy in the lattice trap is the same in the two cycles: the lattice depth does not change, as well as the detection light intensity.

Collision with the background hot atoms are also possible. We estimated this shift following reference [Gib13] and using the coefficients from [Mit10]. We derive the background pressure from the measurement of the lattice lifetime (3 s). We valuate the shift

from hot atoms and its uncertainty both as half of the highest estimated possible shift.

Blackbody radiation shift:

As already said, one of the most important effect to be evaluated is the blackbody radiation shift, that depends on the temperature of the environment where the atoms sit during interrogation. This shift can be calculated from equation 2.10 with the coefficients from [Mid12a]. To recover the atom's environment temperature we continuously monitor the temperature value of the hottest and coldest points in the vacuum chamber with eight calibrated Pt100 sensors (see section 3.2.2). Keeping as small as possible the difference between the highest and lowest temperatures measured by these sensors is fundamental to reduce the uncertainty on the determination of the shift.

A big source of BBR is the oven. To eliminate its effect we use a shutter that closes the view from the atoms to the oven during interrogation. When it is used, the BBR shift coming from the oven is considered zero (with negligible uncertainty). However, in the last part of my doctorate, the shutter mechanical actuator broke. Since it is placed inside the vacuum chamber, its replacement is not immediate. For this reason, some of the uncertainty budgets that I report include a correction for the BBR shift from the oven. This is calculated by knowing the oven temperature, the solid angle of the view form the oven to the atoms and the vacuum chamber dimension and emissivity [Fal11].

Tunneling shift:

The tunneling shift in our system is negligible. The lattice is tilted by approximately 50° against gravity, and together with the use of deep lattice depth tunneling is strongly suppressed.

DC stark shift:

To estimate the DC stark shift, we considered the separation of the vacuum chamber windows which is 54 mm and we allow for possible patch potentials of up to 100 mV. These windows are the closest surfaces to the atoms, and are coated on the inside with a conducting ITO layer to avoid patch charges. Using the coefficients from [Mid12b], we estimate a maximum shift far below 10^{-18}.

Second order Zeeman shift:

The second order Zeeman shift is evaluated using equation 2.5 and the coefficient from [Fal11]. A precise measurement of the magnetic filed B can be determined by the measure of the frequency separation between the two interrogated (extreme) m_f components (see section 3.1.4). We can usually measure this splitting with a 0.02 Hz accuracy. Setting the bias magnetic field in order to keep the separation between the interrogated m_f components at the order of 500 Hz allows to have an uncertainty on the determination of the second order Zeeman shift in the order of 5×10^{-18}.

Servo error shift:

If the drift rate of the cavity used to stabilize the laser changes too rapidly, a locking error can occur that shifts the detected frequency. This shift is called servo error shift. We suppose the shift to be zero with an uncertainty that can be estimated by evaluating the maximum second order drift of the cavity, $\ddot{\nu}_{cav}$ and by knowing the cycle time of the experiment is τ_{cycle}.

$$\Delta\nu_{lock} = \ddot{\nu}_{cav}\frac{\tau_{cycle}^2}{\beta} \tag{3.10}$$

with β gain of the lock, [Fal11]. In our system usually we have $\ddot{\nu}_{cav}$ in the order of 2-4 Hz/s^2, $\beta = 0.05$ and $\tau_{cycle} = 3.6$ s

AOM efficiency shifts:

This shift comes from the fact that to switch the clock laser frequency in order to interact with the different Zeeman components we use an AOM. The laser intensity may then vary and systematically different excitation probability can be detected. This effect must be estimated measuring the light power trough the fiber as a function of the AOM frequency [Fal11]. In our case we suppose the shift to be zero and we estimated an uncertainty on it of 2×10^{-18}.

Line pulling:

Line pulling between atomic population in a neighbouring m_F spectroscopy line can be present due to not perfect operation of the clean-up pulse. To estimate this effect we

evaluate the population remained in the unwanted state and its distance in frequency from the resonance of the interrogated line, which depends on the chosen bias field.

3.3.2 Instability evaluation

To evaluate the instability of our clock is possible to compare the instability of its output with respect the one of the stationary clock. This is done by simply measuring the beat note between the two outputs on a photodiode (their frequency is very close since they work with the same atomic species) and recording the values with a counter (see figure 3.17).

The stationary interrogation laser is normally stabilized to a 48 cm ULE cavity at 698 nm, which has an instability below 1×10^{-16} for averaging times between 1 to

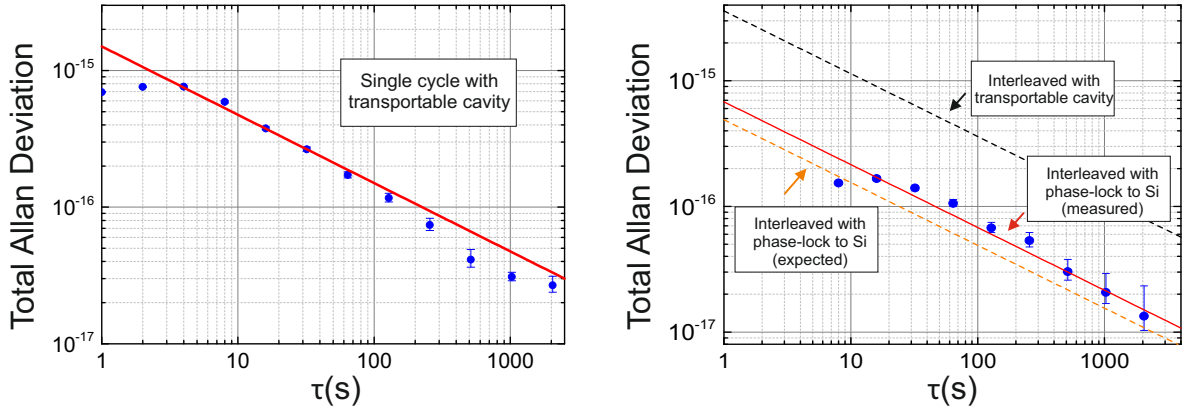

Figure 3.16: Left: The instability ($1.3 \times 10^{-15}/\sqrt{\tau}$) of the transportable clock when only the transportable cavity is used to pre-stabilize the interrogation laser, expressed as the total Allan deviation of the beat note between the transportable and stationary clock, which reflects the instability of out system. Right: The interleaved instability of the transportable clock alone in interleaved operation ($3.6 \times 10^{-15}/\sqrt{\tau}$, black dashed line) in comparison to the instability that can be reached when phase-locking the transportable laser to the stationary one (stabilized on the Silicon cavity).The red line and the blue dots represent the measured instability with the phase-lock ($6.8 \times 10^{-16}/\sqrt{\tau}$) and the orange dashed line the expected one from the model ($4.9 \times 10^{-16}/\sqrt{\tau}$). The discrepancy between model and measurement indicates that we were limited by detection noise, because the model we used accounts only for the contribution to the noise coming from the clock laser.

1000 s [Häf15b]. Moreover, in the last year an even more stable cryogenic Silicon cavity has been developed and is now available at PTB [Mat17b]. The laser locked to this cavity reported an instability of 4×10^{-17} for interrogation times between 0.1 s and a few tens of seconds. A commercial Er-doped DFB (ditribuded feedback) fiber laser at 1542 nm is locked to the Silicon cavity. The stationary interrogation laser at 698 is normally pre-stabilzed on the long ULE cavity and phase-locked to the 1542 nm laser. The gap between the two laser frequencies is bridged with an optical frequency comb. In this way, the stability of the Silicon cavity is transferred to the interrogation laser of the stationary ^{87}Sr lattice clock (see figure 3.17). In this configuration the stationary has demonstrated to have an instability below $10^{-16}/\sqrt{\tau}$.
For this reason, the instability of the beat note is then limited by our system and reflects the one of the transportable clock. This resulted to be $1.3 \times 10^{-15}/\sqrt{\tau}$ (see figure 3.16, left graph and reference [Kol17]), and represents the best instability that the transportable clock can reach when used in measurement campaign outside PTB.

As said in the previous paragraph, to evaluate systematic effects like AC Stark shift

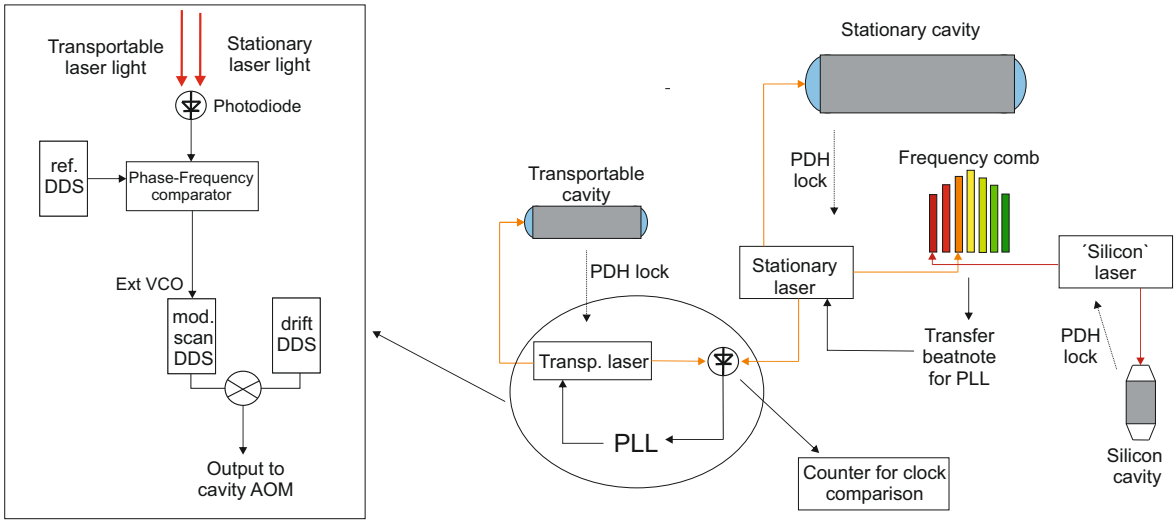

Figure 3.17: Left: insight of the PLL used to lock the transportable interrogation laser to the stationary one. Right: schematic view of the three lasers (and the respective cavity) involved in the phase-lock of the transportable interrogation laser to the ultra-stable Silicon cavity. The beatnote between the transportable and stationary interrogation lasers is recorded also on a counter for the comparison of the two clocks.

from the lattice or cold atom collisions it is necessary to run the system in interleaved mode. During the interleaved operation, the instability of the clock is worsen (by a factor of two in a very crude approximation) with respect to the stability of the clock operated in single cycle: the cycle time and the dead time of each cycle is in fact much longer during interleaved operation, leading to a greater instability due to the Dick effect.

On the other hand, when we are at PTB the same beatnote used to compare the frequency of the two clocks can also be used to phase lock the transportable interrogation laser to the stationary one to improve the stability of our clock. In this case, the beatnote signal is sent to a phase frequency comparator (PFC) that compares this frequency with a stable signal generated by a DDS. The output of the PFC is then used as an external reference for the voltage controlled oscillator (VCO) of the DDS that generates the signal that, after mixing with the signal to follow the cavity drift, steers the laser frequency going to the transportable cavity trough the cavity AOM (see figure 3.17 and A2 for more details).
Reducing the clock instability is particularly helpful during the interleaved operation for systematics evaluation, since even just a factor of two gain in the instability results in a factor of four shorter measurement time (the statistical uncertainty scales with $(1/\sqrt{\tau})$.

It is possible to calculate the expected gain in instability for the transportable clock operated in interleaved mode when the the transportable interrogation laser is phase-lock to the stationary one (that is pre-stabilized on the 48 cm cavity and phase-locked to the Si cavity though the virtual beat note on the comb. see figure 3.17), by knowing the noise spectrum of the involved lasers and the parameter of the experimental cycle (dead time and duration of the interrogation). This results to be $4.9 \times 10^{-16}/\sqrt{\tau}$ under ideal conditions (when all the other noise contribution are lower, see orange dashed line in right figure 3.16), almost a factor of ten better then the instability of the transportable clock operated with the transportable cavity alone (black dashed line in right figure 3.16).
However, experimentally this gain resulted slightly less the what we expected (see red line and blue measured points in right figure 3.16): $6.8 \times 10^{-16}/\sqrt{\tau}$. This means that our system was at this point limited by detection noise (see section 2.1.3). This is one of the reasons why we decided to change the detection device from a photodiode to a PMT (see setion 3.2.2), in order to improve the signal to noise ratio of the detected signal and reduce the detection noise.

3.3.3 Comparison to PTB stationay ^{87}Sr lattice clock

When the clock was at PTB, we performed two frequency comparison between the transportable clock and the stationary system of our group, both based on ^{87}Sr to check the agreement between the two systems.

The first comparison was done at the beginning of my doctorate, with the clock still placed in the laboratory. It is the one already introduced in section 3.2.2 and described in reference [Kol17]. It was performed with a total fractional uncertainty for the transportable clock of 7.4×10^{-17}. This comparison resulted in a frequency difference between the two clocks of $\nu_{stat}/\nu_{trans} - 1 = 6(80) \times 10^{-18}$ including a redshift correction of $-9.0(6) \times 10^{-18}$ (with a total fractional uncertainty of 2.6×10^{-17} for the stationary system and of 7.4×10^{-17} for the transportable one).

After that, the clock was moved into the trailer and technical improvements were done as described in the previous section. This allowed to reduce the uncertainty of the transportable system to 3.5×10^{-17} during the second comparison at PTB. This

Effects	Correction to be applied	Uncertainty
Lattice, scalar/tensor:	2.65	2.59
Lattice, hyperpolarizability:	0.39	0.18
Lattice, E2/M1:	0.00	0.34
Probe light:	0.017	0.017
BBR, ambient:	517.11	1.66
BBR, oven:	0.94	0.94
Second-order Zeeman:	10.90	0.44
Cold collisions:	0.53	1.16
Background gas collisions:	0.5	0.5
Efficiency AOM:	0.00	0.20
Tunnelling:	0.00	0
DC Stark shift:	0.000	0.034
Total (fractional):	**532.5**	**3.5**

Figure 3.18: Corrections and uncertainties of the transportable clock in parts per 10^{17}.

uncertainty budget is shown in the table of figure 3.18.
With the total uncertainty of the the stationary clock reduced to 2×10^{-17}, in the new comparison the frequency difference resulted to be $\nu_{stat}/\nu_{trans} - 1 = -3.7(41) \times 10^{-17}$, including a redshift correction of $-3.3(1) \times 10^{-17}$. This result is shown in the graph of figure 3.19, where is also compared to the previous one.

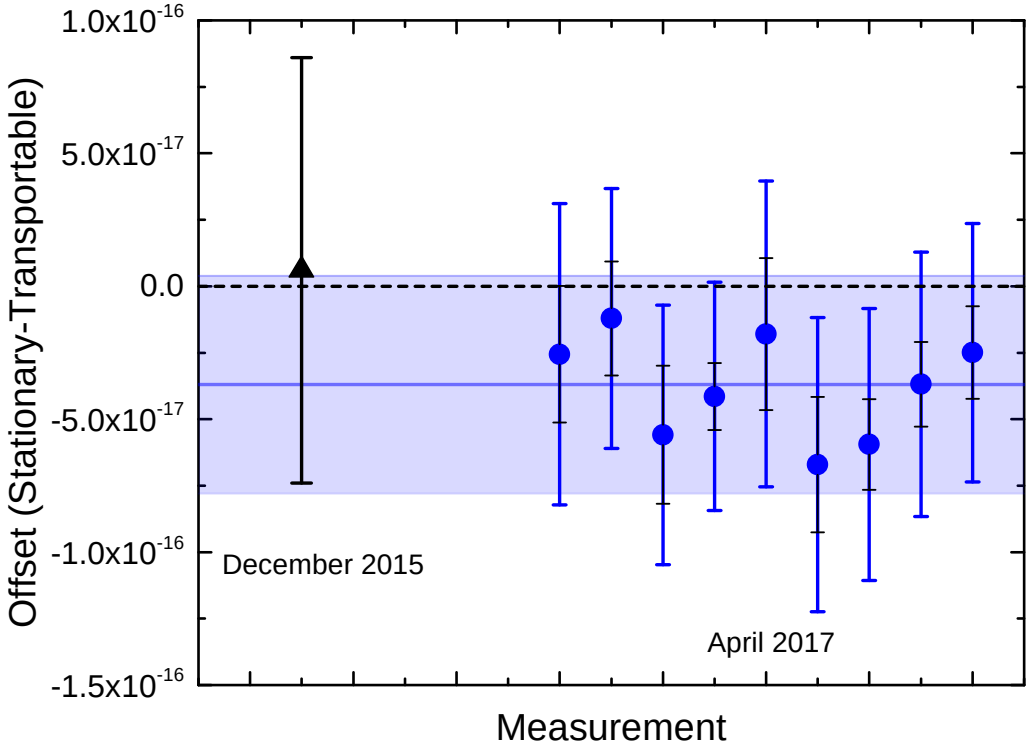

Figure 3.19: The result of the two comparisons to the stationary ^{87}Sr lattice clock performed in December 2015 and April 2017.

In figure 3.19, the first comparison (performed in the December of 2015) is reported as a black triangle with error bars representing its total uncertainty. The new comparison (performed in the April of 2017) is represented by the blue dots. For these points, the blue error bars represent the total uncertainty (systematic plus statistical) for every measurement, while the black lines represent only the statistical part. The blue horizontal

line represent the weighted mean of the newest comparison, and the colored area the total error on this weighted mean. The dashed black line represents the zero frequency between the two clocks, which is the expected result. In both cases, the comparison results are compatible with a zero frequency difference between the two clocks.

To calculate the weighted mean and its uncertainty, we considered the statistical errors of every measurement as fully uncorrelated and the systematics as correlated, following the procedure described in Appendix A1.

Chapter 4

Measurement campaigns outside PTB

To test the use of the transportable clock for metrology and geodesy applications, we performed two measurement camapigns during my doctorate. We transported and operated the system in three different locations in Europe: the Laboratoire Soutterrain de Modane located in Modane (French Alps) and the Italian national metrology institute (Inrim) in Turin during the first campaign, and the French metrology institute Syrte-Observatoire de Paris during the second.

These campaigns represent the first time ever that an optical clock was transported and operated outside a laboratory, and the experiments we performed are testbeds and proof of principles of the use of such a highly accurate transportable optical frequency reference. They will be described in this chapter.

4.1 First campaign

4.1.1 Campaign motivations

This campaign took part in the framework of the ITOC (International Timescales with Optical Clock) project [Mar13]. This project's goals were the comparison of the optical

clocks developed in Europe and the evaluation of the relativistic effects influencing these comparisons. In this framework, the transportable clock contributed in two ways.

Metrological contribution:
First, we contributed as one of the methods to compare clocks of distant institutes: we use the transportable clock to measure the optical frequency ratio between the reference transition of the ^{171}Yb Inrim lattice clock in Turin [Piz17] and the one of the ^{87}Sr transportable optical lattice clock by transporting and operating it directly at the Italian institute.
This optical ratio that we call $R = {}^{171}\mathrm{Yb}/{}^{87}\mathrm{Sr}$, has been previously measured in only three other experiments. Moreover, all the reported measurements were performed between clocks developed in the same institute: One was performed at the National Metrology Institute of Japan (NMIJ) in 2014 [Aka14b] while the other two were performed at RIKEN (also in Japan) in 2015 and 2016 [Tak15, Nem16]. The results of these experiments are reported in figure 4.1, where it is also reported the value for the ratio that obtained by the CIPM recommended values for ^{171}Yb and ^{87}Sr absolute frequencies.

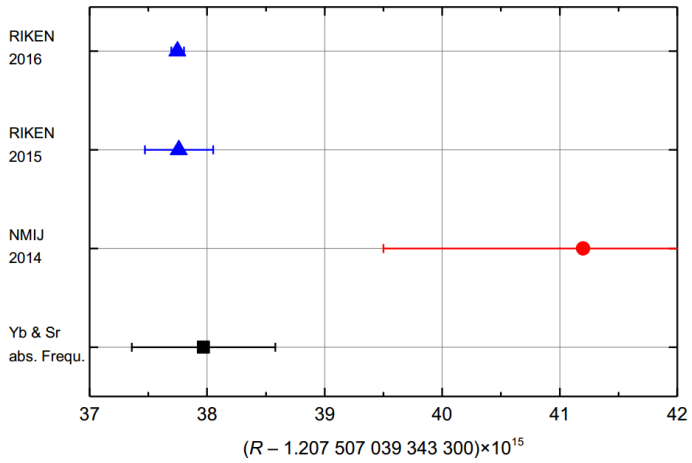

Figure 4.1: The three measurement of the ^{171}Yb/^{87}Sr optical frequency ratio reported before our experiment and the ratio obtained by the CIPM recommended values for ^{171}Yb and ^{87}Sr absolute frequencies.

Details on the ^{171}Yb Inrim optical lattice clock can be found in [Piz17]. At the time of the measurement campaign, this clock reported an interleaved stability between

$1 \times 10^{-14}/\sqrt{\tau}$ and $3 \times 10^{-14}/\sqrt{\tau}$ and an uncertainty of 12×10^{-17}.

Relativistic geodesy contribution:
As a second contribution, we used our clock to measure the gravity potential difference between Inrim and the Laboratoire Soutterrain de Modane via chronometric leveling; this was conceived as a proof of principle experiment of the use of a transportable optical clock for this purpose.
The two chosen locations are connected via a 150 km long fiber link that allows optical frequency transfer and have height difference of approximately 1000 m. LSM is located in the transitional zone between two countries (France and Italy) in an mountain range (Alps). All these aspects make it particularly interesting for a proof of principle application of chronometric leveling. As a final consideration, LSM is not an atomic physics or metrology laboratory: it represents a realistic testbed for the use of a transportable optical clock in an uncommon environment.

4.1.2 Campaign background

Laboratoire Soutterrain de Modane:
The Laboratoire Soutterrain de Modane (Modane Underground Laboratory, or Fréjus Underground Laboratory) is a subterranean particle physics laboratory (see [lsm]). It is located in the middle of the 12.6-kilometer Fréjus road tunnel, a motorway connecting Italy to France and 1700 meters below the Fréjus Peak. A sketch representing the position of the laboratory inside the tunnel and the laboratory interior dimension are shown in figure 4.2.

The experiments usually performed in this laboratory are faraway from optical frequency metrology, and the conditions of the laboratory are very different from what is usually experienced by optical atomic clocks. The temperature inside has a short-term stability of 2 K, and is kept between 25 °C - 28 °C. The humidity is quite low, about 20%-30% all the year. The fresh air for the laboratory is taken from the top of the mountain. Dust and dirt are also more present then in an usual metrological laboratory and, on the

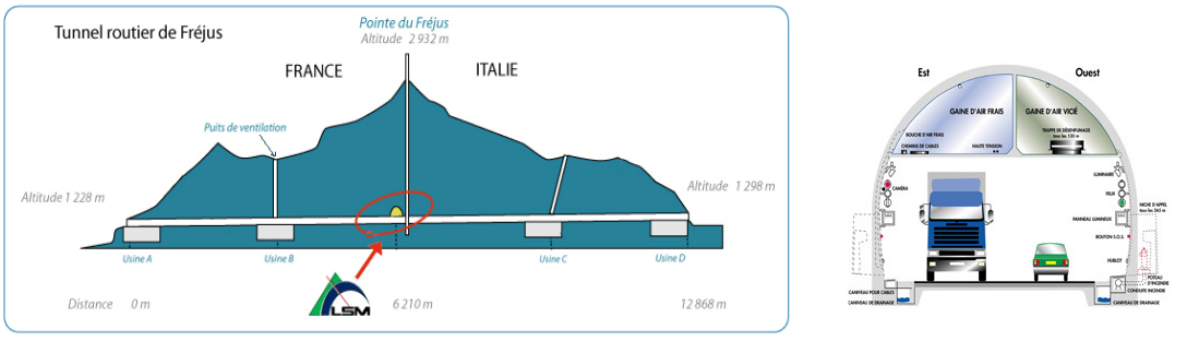

Figure 4.2: The location of LSM in the middle Fréjus road tunnel and the interior of the lab. Pictures from www-lsm.in2p3-fr.

logistic side, it has strict working hours (from 9:00 to 11:30 and from 13:30 to 16:30) and strict safety rules: not trained workers are not allowed to stay inside the laboratory alone, and they enter the laboratory only with the local staff.

Fiber link connection to Inrim:
LSM and Inrim are connected via a 150 km noise-compensated optical fiber link transmitting a laser light at 1542.14 nm. The transportable ^{87}Sr optical clock at LSM and the ^{171}Yb laboratory clock at Inrim were connected to this link laser via two (local) fiber frequency combs. The comb at LSM was a transportable system provided and operated by National Physical Laboratory (NPL) scientists.
The link laser was stabilized to a high-finesse cavity at Inrim. The long term drift of the cavity was removed by a loose frequency-lock to a H-maser via a fiber frequency comb. In this way, the beat notes of the clock with the respective comb remained inside a small frequency interval, giving the possibility for long-term operation. Moreover in this way potential errors arising from any counter de-synchronization between Inrim and LSM are reduced.

For this link laser the "dark channel" approach is used (see section 2.2.1): a multiplexed channel of a telecom fiber was equipped with two dedicated bidirectional Erbium-doped fibre amplifiers. The phase stability of the signal was controlled with a Doppler noise cancellation technique.

At Inrim, the cryogenic Cs fountain primary clock of the institute was also connected to the comb serving as an additional reference [Lev14].
Given the impossibility of having a GNSS-disseminated signal in the underground laboratory, a 100 MHz high-quality RF signal was provided from Inrim to guarantee and was needed as a frequency reference to operate the frequency shifters and counters of the transportable clock and the transportable comb. It was delivered by amplitude modulation of a second 1542.14 nm laser beam that was transmitted through a parallel optical fiber. At LSM, this amplitude modulation was detected on a fast photodiode, amplified and regenerated by an oven-controlled quartz oscillator (OCXO) at 10 MHz to improve signal-to-noise ratio.

Geopotentail difference:
The height difference between the two sites is approximately 1000 m. The gravity potential difference has been previously determined with advanced geodetic methods to provide an accurate reference to compare with the chronometric leveling experiment result. This measurement has been performed by geodesists of the Instut für Erdmessung (IfE) of Leibniz university of Hannover in collaboration with Politecnico di Torino. A state-of-the-art evaluation with the best possible uncertainty at each clock site was obtained involving a combination of GNSS based ellipsoid heights at Inrim and near the tunnel portal at LSM, spirit leveling between the GNSS stations and reference points near the clock location, and a geoid model refined by local gravity measurements [Den13]. For the latter, separate gravity surveys were carried around Inrim and LSM providing 36 and 123 new gravity points respectively (including one absolute gravity observation at Inrim and another one at LSM; the reaming ones were measured with relative gravimeters respect to the absolute ones). Eleven of the gravity points are located inside the Fréjus tunnel (near LSM). This new gravity points enabled the existing gravity database to be evaluated and improved. The result is a 10 029.7(6) m^2/s^2 gravity potential difference between two markers one at LSM and one at Inrim. The height differences between the markers and the actual transportable clock position (less then 10 m apart from the reference markers) were determined for convenience (and in view of the uncertainty of the chronometric leveling experiment) with a simple spirit leveling rather then by geodetic leveling. The geopotential difference between the two clock positions resulted then 10 032.1(16) m^2/s^2, where the largest uncertainty contribution comes from this last height determination.

Experiment schematic configuration:

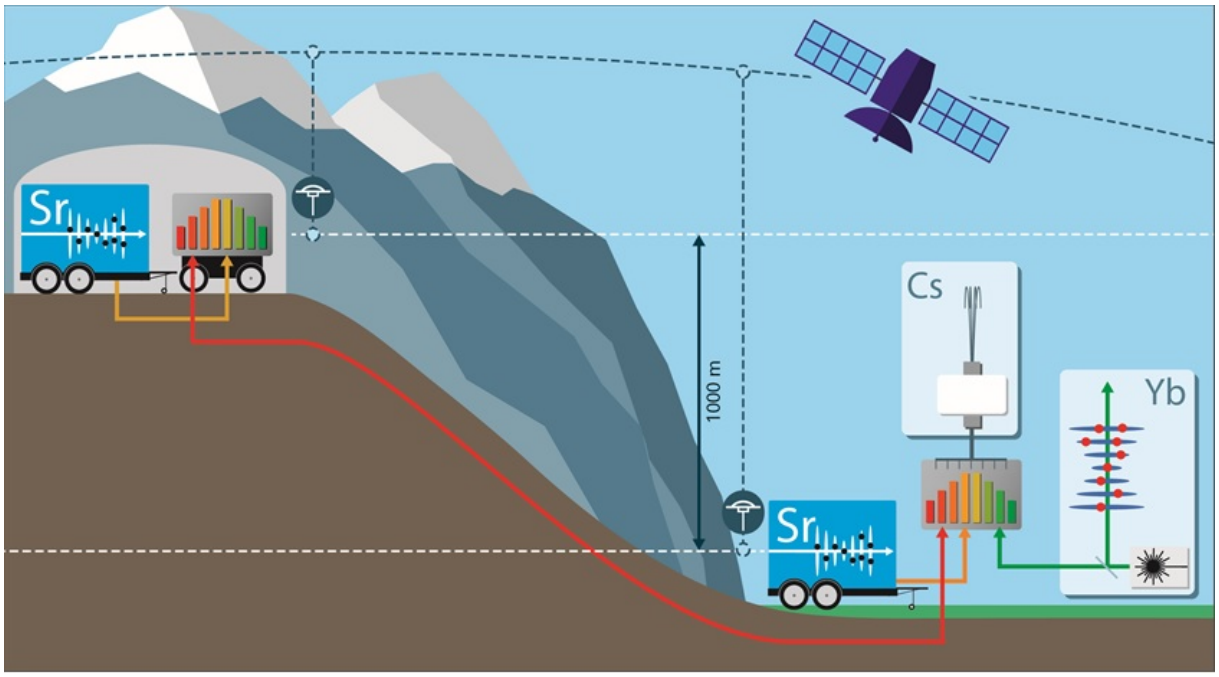

Figure 4.3: A scheme of the measurement campaign. The gravity potential difference between two markers (one at LSM and one at IRIM) was known thanks to a measure by geodesists of IfE and Politecnico di Torino with state-of-the-art classical methods, including GNSS, geoid modeling and spirit leveling. At LSM the 698 nm reference laser of the transportable ^{87}Sr clock was connected to the NPL transportable comb. The optical fiber was used to connect via the link laser at 1.5 μSm the comb at LSM to the one at Inrim, to which were connected the ^{171}Yb lattice reference laser at 578 nm, and the Cs fountain primary clock of the Italian institute. At INIRIM the 698 nm reference laser was directly connected to the comb to measure the ^{171}Yb/^{87}Sr.

In figure 4.3 a schematic representation of the experiment is given. For a pure chronometric leveling measurement, two comparisons are needed: one remote (the transportable clock located at LSM compared to the reference clock at INIRM) and one local (the transportable clock located at Inrim compared side-by-side to the reference clock). Only the difference between these two measurements gives a value of the gravity potential difference of the two locations where potential clock errors are eliminated, because very few optical clocks uncertainty budget have been verified independently at the level they can operate.

4.1.3 Experiment execution

At the beginning of February 2016, the transportable clock was moved out from PTB and transported to Modane using a van (see figure 4.4). Inside the van were placed the ultra-stable interrogation laser, its reference cavity and the various equipment needed in the campaign.

Figure 4.4: The transportable clock leaving PTB for the first time.

Experiment in Modane:
After the clock was allocated inside the LSM laboratory, we spent the first week to "re-activate" the system. At the end of this first week, all the cooling and trapping processes were working: atoms were trapped in the lattice. After ten days, we were able to perform spectroscopy on the clock transition: we recorded the transition sideband spectrum of the atoms in the lattice. Included in this setup time were general logistic, the powering and thermalisation of the equipment, installation of reference frequency equipment, re-alignment of optical fiber coupling, individual testing of all subcomponents and coarse background magnetic field compensation.

The ultra-stable interrogation laser was placed next to the trailer to avoid is performances being degraded by the vibrations induced in the trailer by the air conditioning system. The comb from NPL was also placed and operated next to the trailer. A picture of the whole arrangement inside LSM is showed in figure 4.5

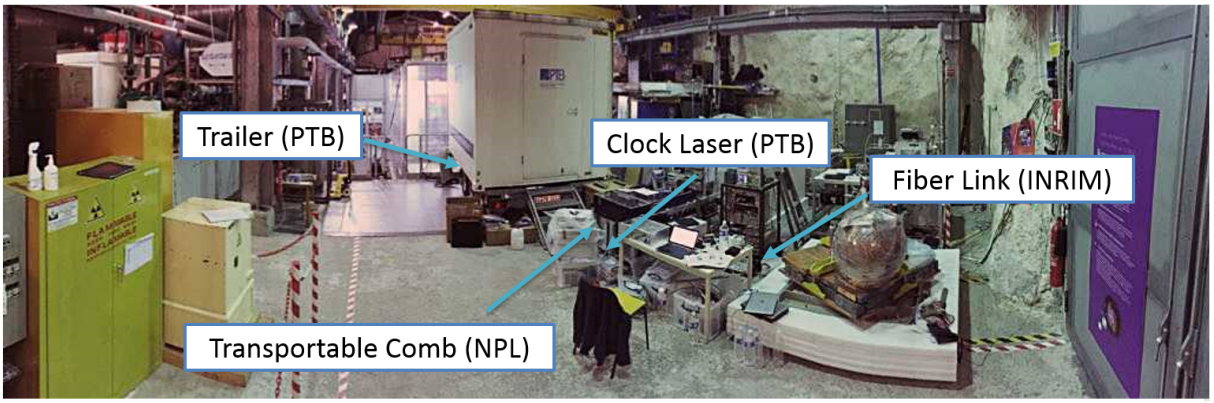

Figure 4.5: A panoramic picture of the arrangement at Inrim

After this positive start, certain problems have arisen and affected the reliability of the transportable clock. The thermal management inside the trailer did not work as well as expected, probably because the very low humidity of LSM hampered the cooling of the air conditioning. In particular the heat was stuck in hot spots with low ventilation, like in the corner were the titanium sapphire laser driving the optical lattice was placed. This caused the pump laser to stop working in a few occasions, and the only way to cool it down was to switch it off every time. To help the air ventilation inside the trailer, we had to work with the main door of the trailer open, as can be seen in figure 4.6. This, together with the less stable temperature inside the trailer as compared to the tests at PTB, lead to higher instability in the lock of the cooling lasers (especially the red cooling and stirring) and to misalignment of the setup used to overlap and re-distribute the blue and red laser light for the three retro-reflected MOT beams. This fiber-cluster was still based on free-optics (see section 3.2.2), and suffered the temperature instability. We managed to mitigate the effect with some isolation between it and the optical table where it was placed. Furthermore, the blue laser system (a commercial one) had a big failure. The cavity in which the SHG crystal to double the light from the laser diode from 922 nm to 461 nm is placed misaligned. The alignment of the light into this crystal

is a very delicate process, and required some time to be reached again. We suspect that the cause of the misalignment were the (quite strong) vibrations of the LSM underground laboratory due to explosive used in its proximity. Workers were building a parallel road tunnel in the mountain at the time of the experiment and used explosive to open the way in the rock at the time. This not only caused strong vibrations in the laboratory, but also forced us to stop working in order to move to a safe shelter before every explosion, which occurred in a 24/7 shift and for which we were given only a 5 minutes warning. In the shelter, we had to wait for an hour or more before having the permission to continue working.
Figure 4.6 shows some of the people that contributed to the experiment and the working environment at LSM.

Figure 4.6: On the left, some of the persons that collaborate to the experiment. On the right, a working day at LSM. Note that the door of the trailer needed to be open from time to time to avoid the overheating of the titanium sapphire laser pump.

These harsh conditions influenced a lot the successive development of the measurement at LSM. We were able to lock the transportable clock to the atomic reference only for two days at the end of the LSM campaign, in mid-March, and for a total measurement time of 2.8 h. Very unfortunately, at Inrim the ^{171}Yb, which had worked reliably during the previous time, had a problem with the lattice laser during the last days of the campaign, so we reached common operation only with the Cs fountain. In this way, we were able to measure only the absolute frequency of the ^{87}Sr atoms of the transportable

clock at LSM as referred to the CS fountain at Inrim.
The higher instability (low $10^{-13}/\sqrt{\tau}$ range) of the Cs fountain [Lev14] with respect to an optical/optical comparison in combination with the short measurement time led to a high statistical uncertainty on the absolute frequency measurement result. However, we were able to reduce it by using a H-maser as a flywheel to extend the measurement time, following the method of reference [Gre16]. This will be better explained in the following section.

Experiment in Turin:
To transform this absolute frequency measurement into a chronometric leveling measurement, the next step was to move the transportable clock to Inrim, to compare it locally against the Cs fountain on a common gravity potential. Moreover, this time we had the possibility to reach common uptime with the ^{171}Yb/^{87}Sr optical frequency ratio.

At the beginning of April 2016, the transportable clock was moved from LSM to Inrim. The car trailer was placed in the parking lot of the institue and the ultra-stable laser was placed in the frequency comb laboratory. While the connection between this laser and Inrim comb was then straightforward (they ware in the same laboratory), the delivery of the interrogation light to the atoms in the trailer (in the parking lot) was done with a 50 m phase-stabilized optical fiber. As before, the ^{171}Yb optical clock and the Cs fountain were also connected to the comb.
Thanks to the experienced gained in the first part of the campaign, we decide to perform some small but important changes in our setup in a short time before the experiment in Turin. In particular, we changed the fiber cluster to distribute the light into the MOT beams with the much more stable fiber based one (see section 3.2.2) and we took more effort in controlling the ventilation inside the trailer. We also decided to place the trailer in the shadow of the building to avoid heating from the direct sun light.
With these changes, we were able to improve significantly the availability of the Sr clock. The amount of data taken increased by a factor of almost seven and at the same time we were able to shorten the duration of the experiment by almost a factor of two. It was possible to record several hours of data over a week.
Common operation with the Yb clock was reached and the ^{171}Yb/^{87}Sr optical frequency ratio measurement was performed simultaneously to the side-by-side comparison against the Cs fountain.

4.1.4 Data analysis and results

The difference in data points recorded at LSM and at Inrim is shown in figure 4.7. The improvements we made on the system between the two experiments allowed us to extend the availability of the transportable clock as can be see comparing the two graphs in figure 4.7.

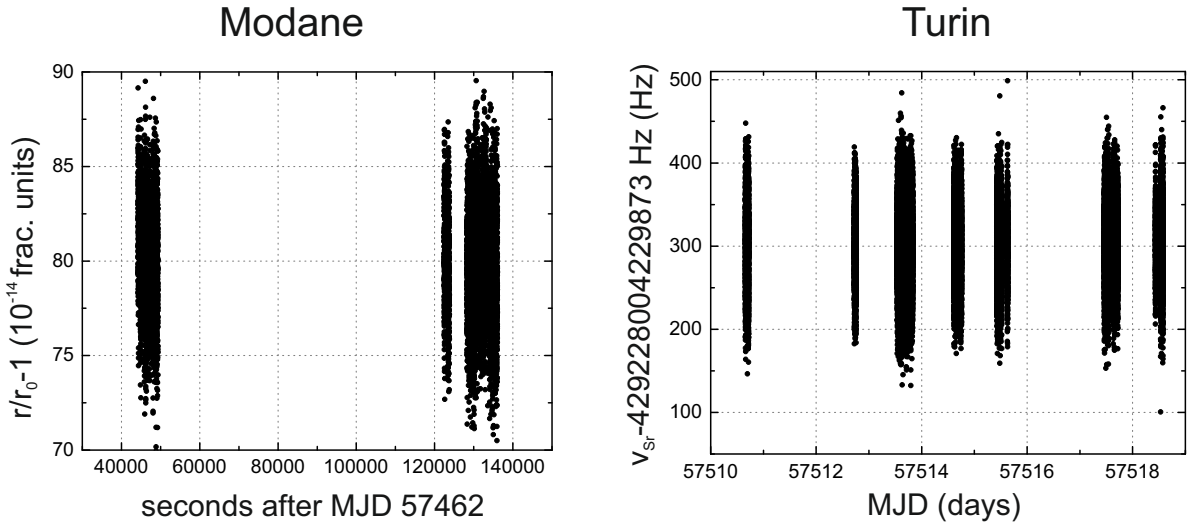

Figure 4.7: Data points recorded in Modane (left graph) versus data points recorded in Turin (right graph). The changes we made to the setup between the two experiments increased the availability of the transportable clock allowing a factor of seven increase in recored data points. In the left graph is reported that ratio r in fractional units between the transportable clock transition and the fiber link laser, while for the right left is reported the deviation in Hz of the transportable clock transition from a fixed value.

However, the availability of the transportable clock in this first on-field campaign was not sufficient to evaluate the systematics at the same level of uncertainty that we had in the first test in the laboratory at PTB (7×10^{-17}, see section 3.2.3). Although in the experiment in Turin the total uncertainty of the clock was slightly improved, both there and in the Modane experiment this uncertainty remained at the low 10^{-16} level (see tables in figure 4.8).

The main contribution to the uncertainty budget comes from the determination of the magic wavelength for the lattice laser. Due to the poor availability of the system, we cold

not properly evaluate this frequency, and we decided to use the frequency value we determined earlier at PTB. We allowed for a possible change in the frequency of the reference resonator of 50 MHz caused by vibrations and shocks during transport.
To test this hypothesis, during the experiment in Turin (where the transportable clock was more reliable) we performed two set of measurements, one with a shallow thermally averaged lattice depth and one with a deep effective depth. The optical ratio measurement result for the two set of measurements showed no difference inside the estimated total uncertainty of the two data sets, proofing our hypothesis. This is showed in figure 4.12.
The uncertainty on the lattice shift includes also possible variations of the scalar and tensor light shift caused by geometrical changes or change in the residual magnetic field after compensation.

	Modane		Turin	
Systematic effect	**Correction**	**Uncertainty**	**Correction**	**Uncertainty**
Linear lattice light shift	0	24	0	17
Higher-order lattice shifts	-1.0	0.7	-0.5	0.7
Density shift	-1.2	3.0	-2.2	5.3
2^{nd}-order Zeeman shift	34.2	0.5	11.7	0.2
BBR	500.3	3.4	515.3	1.8
Probe light shift	0.2	0.2	0.3	0.3
DC Stark shift	0	0.1	0	0.1
Servo error	0	9.4	0	3.7
Line pulling	0	4.1	0	1.1
Optical path length	0	0.8	0	1.3
AOM switching	-		-	-
Total	**532**	**27**	**524**	**18**

Figure 4.8: Uncertainty budget of the transportable clock in Modane and in Turin in 10^{-17} fractional units.

All the other systematic contributions were evaluated following the procedure described earlier in this thesis. The density shift was evaluated applying the coefficient we measured during the tests at PTB. It should be noted that although the problems we experienced with the temperature management inside the trailer, we were able to control

the fractional uncertainty on the BBR shift to the low 10^{-17} level.

Graviational redshift determination:
In the Modane part of the campaign, the short availability of our system allowed to perform only an absolute frequency measurement of the optical transition through a comparison to the Inrim Cs fountain and not an optical ratio measurement against the ^{171}Yb clock. To measure the gravitational redshift, we had to repeat the same absolute frequency measurement locally, even if in Turin we were indeed able to measure the optical ratio. The comparison of two absolute frequency measurements has considerably worsened the statistical uncertainty on the gravitational redshift determination, since they showed an instability in the low $10^{-13}/\sqrt{\tau}$ range (limited by the Cs fountain), ten times worse then the optical ratio measurement we performed in Turin.

However, to reduce the total statistical uncertainty is possible to use the method described in [Gre16], where an H-maser is used as a stable reference to extend the measurement time of the absolute optical frequency measurement. Hydrogen masers have a good short-term stability, better then Cs fountains for periods up to 10^5 s, and they are highly reliable. They are used to continuously generate the UTC time scale, by regularly steering their frequency in respect to a Cs fountain that acts as primary frequency standard. For the same reason, they are used as a flywheel between the Cs fountain and the optical frequency comb during optical absolute frequency measurements. In this way the optical clock (through the comb) and the Cs fountain are simultaneously compared to the H-maser. Is possible then to make use of the high short term stability of the H-maser to extend the comparison time between the optical clock and H-maser, and as a consequence, to the Cs fountain.

In our case let us call T_{Sr} the time duration of the comparison between the Sr clock and the maser (that coincides with the transportable clock uptime). The Cs clock was then compared against the maser for a longer time T_{ext}, extended over the T_{Sr} time interval, to reduce the statistical uncertainty. As explained in [Gre16], however, this method adds to the overall statistical measurement uncertainty u_A a term u_{ext} due to the lack of knowledge about the potential difference between the maser frequency averaged over T_{Sr}

and over T_{ext}. This uncertainty u_{ext} can be calculated by the knowledge of the spectrum of the maser frequency fluctuations $S(f)$ and a weighting function $g(t) = g_{Sr} - g_{ext}$, with g_{Sr} (g_{ext}) being the weighting function for the normal (extended) average. Using $g(t)$ is possible to define u_{ext} through the difference δy_{ext} between the maser frequency averages over the two intervals, and with Parseval's theorem is possible to relate it to $S(f)$:

$$u_{ext}^2 = \langle (\delta y_{ext})^2 \rangle = \int_0^\infty S(f) \mid G(f) \mid^2 df \tag{4.1}$$

with $G(f)$ the Fourier transform of $g(t)$.

The maser spectrum can be reconstructed from the maser frequency fluctuations after removing a linear drift. The noise on the maser frequency can then be modeled by three contributions added in quadrature: flicker phase noise, white frequency noise and flicker noise. For the Inrim maser characterization, a flicker phase noise of $6 \times 10^{-14}/\tau$ ($1 \times 10^{-13}/\tau$), white frequency noise of $5 \times 10^{-14}/\sqrt{\tau}$ ($4.5 \times 10^{-14}/\sqrt{\tau}$) and a flicker noise of 1.7×10^{-15} (1×10^{-15}) were inferred in March (May) 2016 for the Modane (Turin) frequency measurement. The stability of the Cs fountain was $2.2 \times 10^{-13}/\sqrt{\tau}$ during the measurement in Modane and $3.6 \times 10^{-13}/\sqrt{\tau}$ during the one in Turin.

We used these numbers to find the best T_{ext} which minimizes the overall statistical uncertainty. For the Modane experiment, the best T_{ext} resulted in a 48 hr extended single data set over the two days of measurement, with total $u_A = 17 \times 10^{-16}$, while the systematic uncertainty of the Sr clock and the Cs fountain were respectively 2.7×10^{-16} (table 4.7) and 3×10^{-16}, giving a total uncertainty on the measurement of 18×10^{-16}. In this way, we obtained a Sr absolute frequency of 429 228 004 229 921.05(79) Hz for the transportable clock operated in Modane.

For the measurement in Turin, we took seven different data sets, one for each day of measurement: They are depicted in figure 4.9. We applied to each of them the H-maser flywheel approach to extend each data set averaging time. Since in every single data set the stastical uncertainty is much higher then the systematic, the weighted average of the data set and its total statistical uncertainty were simply calculated via linear fit.

This fit gave a total statistical uncertainty on the measurement of 8.6×10^{-16}. The Sr clock systematic uncertainty was slightly improved to 1.8×10^{-16} (table 4.7). With the systematic uncertainty of the Cs fountain being again 3×10^{-16}, the total uncertainty on the absolute frequency measurement performed in Turin was 9×10^{-16}.

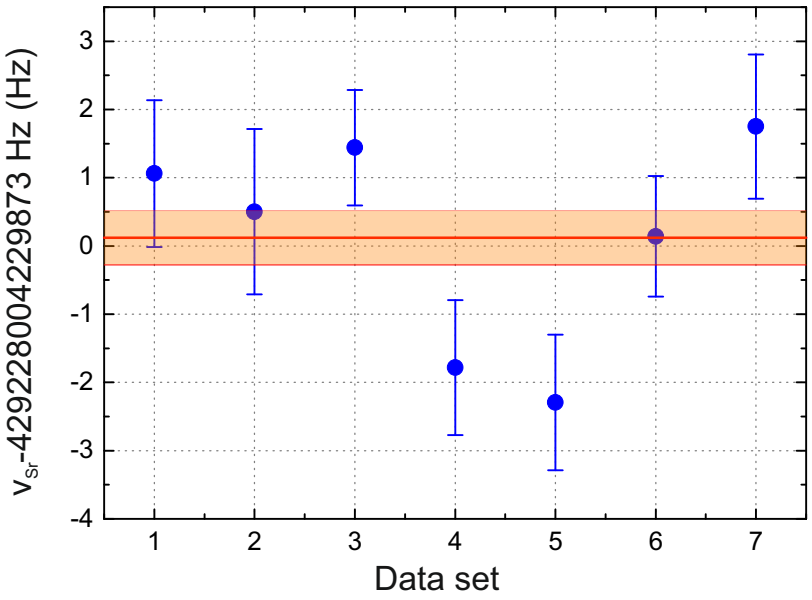

Figure 4.9: Transportable clock absolute frequency values (blue dots with error bars the statistical uncertainty on the measurement) obtained in different measurements (days) at INIRM and their weighted average (red line). The colored area represent the total uncertainty on the weighted average (statistical plus systematic) reported as 1σ deviation from the mean.

This time we obtained a Sr absolute frequency of 429 228 004 229 873.12(39) Hz for the transportable clock operated in Turin.

We can report the two absolute frequency measurements in Modane and Turin as a function of the local geopotential, as it is done in the left graph of figure 4.10. Here, the red line is the expected variation of the clock frequency with the potential. The two measurements fit very well with the model.
The difference between the two measurements gives the geopotential difference between the two remote locations measured via chronometric leveling: this results to be 10 034(174) m^2/s^2, which is in excellent agreement with the result measured with the conventional

geodesy methods (10 032.1(16) m^2/s^2).

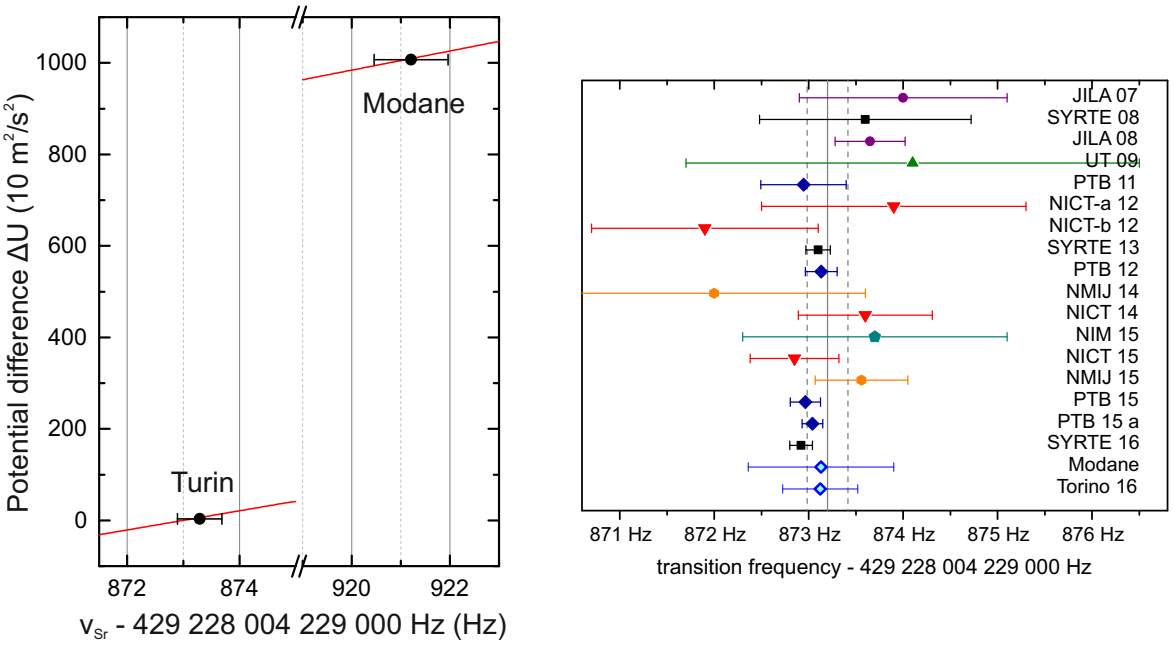

Figure 4.10: The two absolute frequency measured in Modane and Turin as a function of the geopotential difference between the two locations (left), where the red line represent the expected frequency variation. On the right, a comparison of our measurements (after redshift correction) o other recently reported frequency values.

.

We were able to measure the height difference between the two locations with an accuracy of approximately 17 m. This is off course much worse that wath state-of the-art gedoesist methods can do (the potential difference LSM-Inrim was measured with a few cm accuracy). However, few things should be noted. The main error contribution is statistical and stems by the use of the Cs fountain as reference, that considerably worsen the stability of the comparison. As will be shown in the next paragraph (see figure 4.11), already in Turin thanks to the small but important changes we made to our system we were able to increase its availability and reach common uptime with the Yb optical clock. The optical-optical comparison had a 10 times better stability, and this would have reduced the statistical contribution below the clocks systematics, leading to a 10 times more accurate result. Moreover, the systematic uncertainty at which the clock

was operated is far from its design limit ($\sim 1 \times 10^{-17}$). This measurement represented the first time we operated the clock in an uncommon environment outside PTB, and even of the measurement accuracy is not great, all this considered, we are confident that we should be able to use it in the future to measure height differences with few tens of cm accuracy.

As an additional check, we can see the measurement from a metrology point of view. If we subtract the redshift correction measured via conventional methods on both measurements we can compare them to other recently reported frequency values: they result in very good agreement, as can be observed in the right graph of figure 4.10, giving and additional proof of the validity of the result.

^{171}Yb/^{87}Sr optical ratio measurement:

The increased availability of the transportable clock during the experiment at Inrim allowed to reach common operation with the Yb lattice clock and to measure the ^{171}Yb/^{87}Sr clock frequency ratio R. The instability of the frequency ratio resulted to be $2.2 \times$

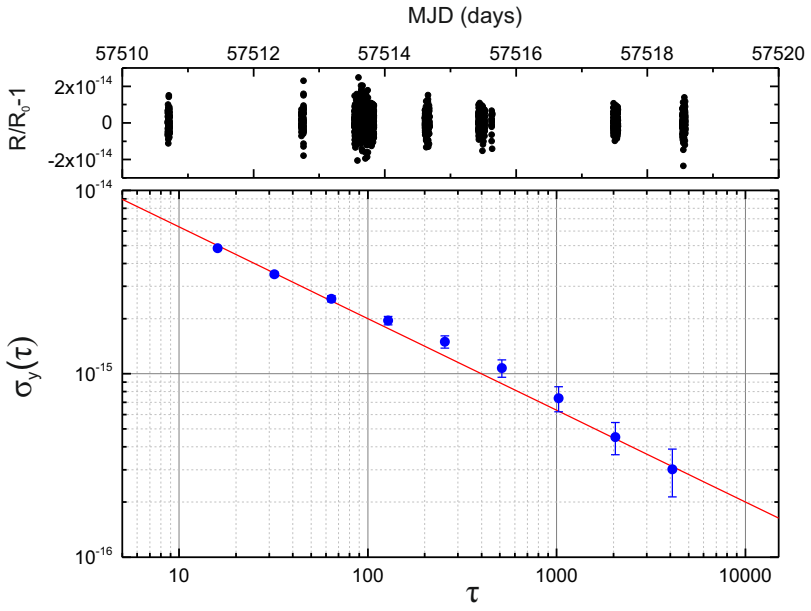

Figure 4.11: Top graph: Measured ratio R/R_0 averaged over 16 s intervals as a function of the modified Julian date(MJD). Graph below: Allan deviation of the ratio R/R_0, where $R_0 = 01.207507039343338122$ is the value derived from the CIPM recommended value for the two optical clocks absolute frequency values.

$10^{-14}/\sqrt{\tau}$, as expressed by the Allan deviation (see figure 4.11), ten time better then the comparison to the microwave clock.

We acquired eight different optical frequency ratio measurements with a total measurement time of approximately 30 000 s over a period of one week in May 2016.
As a said before, to check our hypothesis on the magic wavelength frequency, we performed three of these measurement with a deeper lattice of about 160 E_r. We did not see any significant variation of the ratio value R between the two cases, and that confirmed our assumption.
The results for each data sets are reported in figure 4.12 left graph. The data sets represented as diamonds (circles) denote operation with a shallow(deep) lattice. A weighted average of the different data sets (with its uncertainty) is represented by the red line (the orange area represents a 1 σ deviation). Thanks to the better stability of this measurement, this time the statistical error of most data sets was smaller and comparable to its systematic one. For this reason to calculate the weighted mean of the series we adopted the method described in the Appendix. The systematic uncertainty for the transportable clock are reported in figure 4.7. The Yb clock was operated with a total systematic uncertainty of 16×10^{-17} in fractional units.

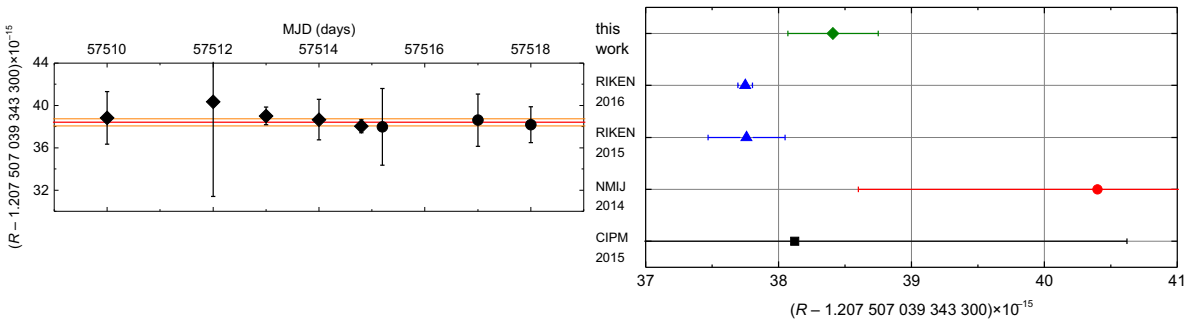

Figure 4.12: On the left: Ratio results for different data sets with their weighted average. On the right: our result as compared to the previous measurements

In figure 4.12 is also reported the comparison between our result and the previous measurements of this ratio that were presented in section 4.1.1. The uncertainty on our result is two orders of magnitude higher then the best reported measurement, but comparable

or better with respect to the others. It is the only one performed with a transportable system and between two clocks developed independently in different institutes. Our result differs from the most accurate previous measurement by two standard deviations, and the origin of this difference will require further investigation by the research groups involved, pointing out the importance of this kind of comparisons.

4.1.5 Observations and conclusion about the first campaign

This first campaign showed the possibility to use the transportable optical clock outside PTB in real measurements campaign [Gro18]. It was the first time that an optical clock was transported and operated in conditions very far from usual.
Remarkably, the result we obtained (although not as good as hoped and not yet challenging conventional techniques) represents a significant milestone to shows the potential of such a transportable system [Lud18].

The quite large uncertainty on the result is due to some technical problems coming from the fact that it was the first time we operated the transportable clock outside PTB. We solved them after the experience gained in this first campaign. As I will show in the next section, in the second campaign (that we did one year after this first one), most of the problems that worsened our result were gone.
Technology advancement in optical clocks are going on in many laboratories around the globe, and new transportable clock will probably be developed. Chronometric leveling measurements are expected to become complementary or even outperform conventional methods .

The total systematic uncertainty reached by our clock during this campaign ($\sim 2\times10^{-16}$ fractional units) was still worse the the first evaluation we performed at PTB before leaving ($\sim 7\times10^{-17}$, [Kol17]) and far from the design limit ($\sim 1\times10^{-17}$). The main limitation in reducing this uncertainty was the availability of our clock: it was not enough to evaluate systematic effects at the best accuracy.
The thermal management inside the trailer was the main factor that affected the availability of the system. For this reason, when we were back at PTB we adopted the solutions

described in section 3.2.2.

The next step was then to operate the clock in a second on-field campaign, with the goal to increase the availability of the system and to reduce the total uncertainty of the system. This second campaign will be described in the next section.

4.2 Second campaign

The second campaign was performed at the end of my doctorate. It was done in the framework of the *geo-Q* project (already presented in section 2.3.2), that is a collaboration between physicist and geodesists at the university of Hannover for the integration of quantum metrology sensors in geodetic modeling.

4.2.1 Campaign background

The motivation of this second campaign was to use the transportable clock for a chronometric leveling experiment over a long distance. This is in fact the application where the chronometric leveling approach can be competitive and integrative with the standard geodetic methods, that are limited to a few cm accuracy over long distances. To perform the experiment, a fiber link connecting the reference clock to the remote location is needed. This was identified in the 1415 km long international fiber link presented in section 2.2.1 that connects PTB to LNE-SYRTE in Paris. The two institutes are approximately 700 km far apart from each other. The link was already used in a previous experiment involving the stationary clocks of the two institute [Lis16]. I introduced this link in section 2.1.2 (see figure 2.7) and is described in more details in [Rau15, Chi15].

We decided then to use the stationary ^{87}Sr lattice clock at PTB as the reference clock and to perform a local and a remote comparison to it by moving the transportable clock in Paris. This time the goal was to improve the availability of the transportable clock during the mission and to reduce its total uncertainty to the low $\sim 10^{-17}$ level.
The local comparison to PTB clock is the one presented at the end of chapter 3. We performed it in April 2017, before moving the clock to Paris. This local comparison gave the following result:

$$\frac{\nu_{stationary}}{\nu_{transportable}} - 1 = -3.7(41) \times 10^{-17} \tag{4.2}$$

We moved the clock to Syrte-Observatoire de Paris in May 2017 for the remote comparison. The weather was very warm during this period, especially in the early afternoon

when the sun was shining. For this reason the transportable clock was placed in the shadow of some trees and we used tents to repair it from the direct sun light (see figure 4.13).

Figure 4.13: The transportable clock location at Syrte-Observatoire de Paris outside the Cs fountain laboratory.

The transportable clock was located outside the laboratory of one of the Cs fountain clocks of the institute. The transportable interrogation laser and its reference cavity were placed inside this laboratory, because as already said the cavity best performances are reached in a quite environment. A phase-stabilized fiber was used as a connection between the laser and the experimental apparatus. A second phase-stabilized fiber, 100 m long, was used to deliver the interrogation laser light to the frequency comb of the French institute, where the beat note to the link laser was recorded. A 100 MHz high-quality RF signal was also provided from the comb laboratory to operate the frequency shifters and counters of the transportable clock.

The geopotential difference between the atoms interrogated in the transportable clock in Paris and the ones interrogated in the stationary clock in Paris sites has been determined by geodesist with conventional state-of.the-art methods in order the have a reference to

compare the chronometric leveling result, as in the previous campaign. The height distance between a marker at PTB and one at Syrte-Observatoire de Paris was determined by scientists of the IfE (Leibniz University of Hannover) by a combination of GPS ellipsoid height and geoid model refined by local gravity measurements inside the ITOC project for previous measurement campaigns.

This time the height of the atoms in the transportable clock in respect to the chosen marker at Syrte was done with proper state-of-the-art methods, because in respect to the previous campaign here the goal was to reach a few tens of cm accuracy for the chronometric leveling result. The result of the geodetic methods should gave a comparable or lower accuracy to be used as a reference. This height difference was the determined by spirit leveling by geodesist of the Institut National de l'Information Géocraphique et Forestiére (ICN), as it is showed in figure 4.14. They measuredthe height of a reference point close to the atoms (chosen on the top of the Zeeman slower beam window on vacuum chamber) over a marker close to the transportable clock location (marker 200 in figure 4.14 . We assumed then the atom to be in line with the Zeeman laser beam direction orthogonal to the window and passing trough ts center, 2 mm away from the chosen point (we know the radius of the window). All considered, the geopotential difference between the atoms

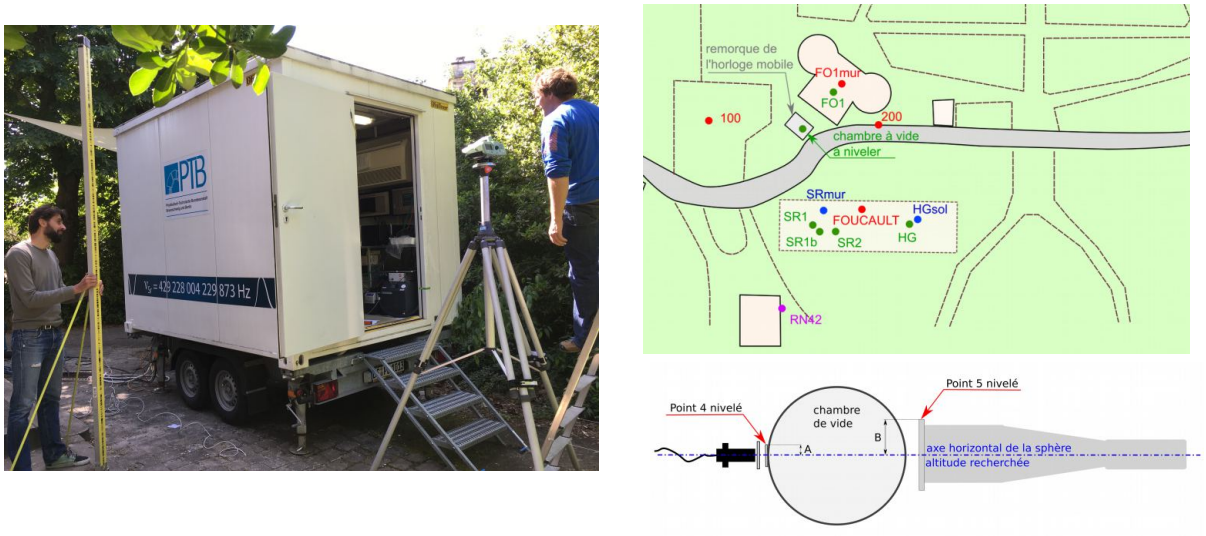

Figure 4.14: On the left: the spirit leveling measurement performed by geodesist of the Institut National de l'Information Géocraphique et Forestiére (ICN). On the right: a map showing the position of the transportable clock in respect to marker 200 and a picture of th vacuum chamber highlighting the reference point (point 4) chosen on the top of the Zeeman slower window.

at PTB and at Syrte resulted in 146.9(4) m^2/s^2.

4.2.2 Transportable clock performances

As in the first campaign, after ten working days dedicated to general logistic, powering and thermalization of the equipment, small re-alignments of laser boards, individual tests of all subcomponents and coarse background magnetic field compensation, we were able to perform clock spectroscopy with the transportable system.

Thanks to the changes we made (reported in section 3.2.2) and the experience we gained after the first campaign, this time the transportable clock worked much more reliable. The total uptime of the transportable clock during this campaign was 120 000 seconds over two weeks of measurement, with several thousands of seconds taken per day (see figure 4.15). In approximately 3/4 of the total uptime we reached common operation with the stationary optical clock in Braunschweig to perform the comparison.

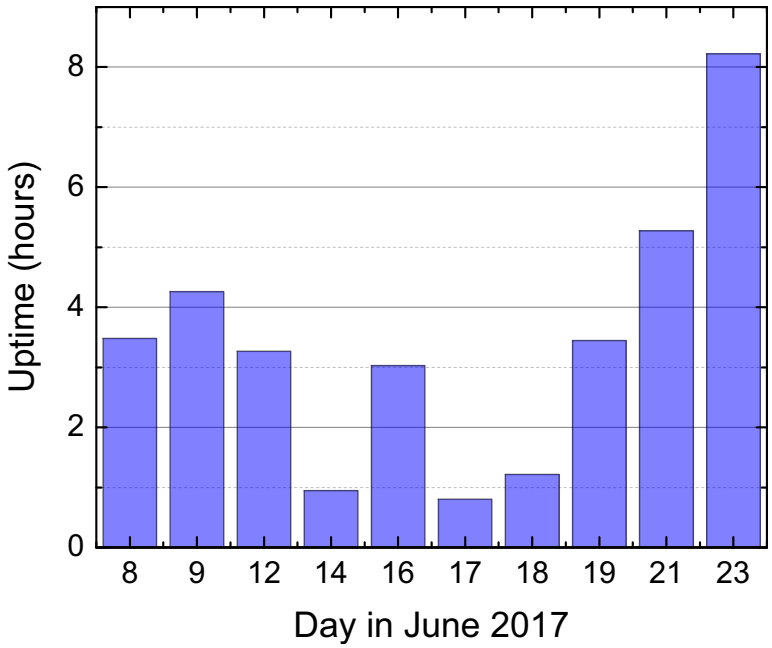

Figure 4.15: Transportable clock uptimes during the campaign in different days.

To calibrate the accuracy of the system, we run it in interleaved mode. Basically, the only effect that needs to be re-evaluated after the transport is the lattice light shift. The reference cavity of the lattice laser in fact can change its resonance frequency due to the transport, and as a consequence the knowledge on the magic wavelength frequency is lost. Moreover, small geometrical changes in the lattice beam propagation or the change of the environmental magnetic fields can change the lattice light shift (see equation 3.4). To evaluate the lattice shift we operated the clock switching between cycles with shallow (thermally average lattice depth 64 E_{rec}) and deep (thermally average lattice depth 184 E_{rec}).
The increased availability of the clock, allowed us to reduce the statistical uncertainty of the measurements to the low 10^{-17} fractional uncertainty region. The total Allan deviation for the clock interleaved operation is reported in 4.16 and shows a $5.5\times10^{-15}/\sqrt{\tau}$ instability.

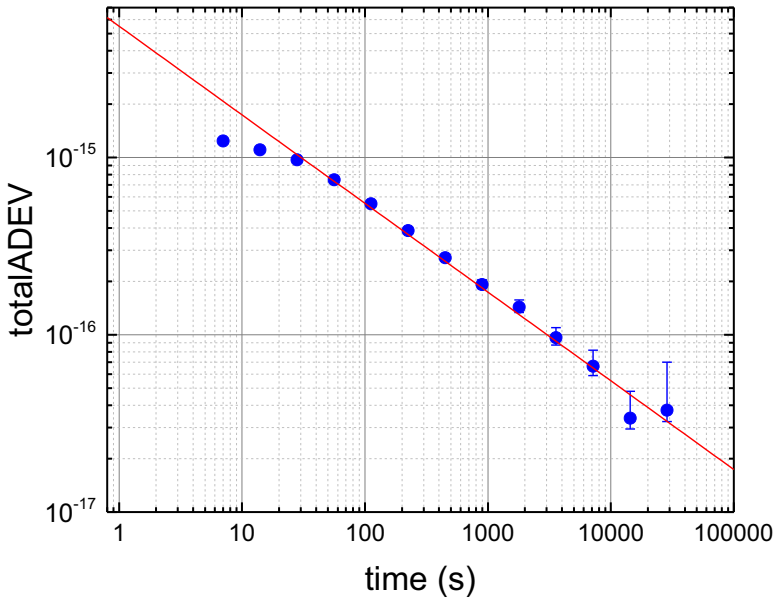

Figure 4.16: Total Allan Deviation for the interleaved operation of the transportable clock (instability $5.5 \times 10^{-15}/\sqrt{\tau}$).

This instability is not as good as the best expected from the transportable cavity ($3.6 \times 10^{-15}/\sqrt{\tau}$, see left graph in figure 3.16.). We could not reach in fact the best working condition for the cavity. This was mainly due to the fact that the cooling system of

the wooden box we put on top of the cavity for sound isolation worked not as good as expected. This box was new and it was the first time we used it in a campaign. However, the clock instability was good enough to reach after 10 000 seconds of measurement the low 10^{-17} statistical uncertainty for the lattice light shift characterization.

The collision light shift has been calculated measuring the employed atom number and using the coefficients determined previously during the comparison at PTB. All the other systematics are determined following the procedures explained in chapter 3.

In particular, we were able to control the blackbody radiation shift below 1×10^{-17} for most of the measurement time. However, during the last week of the campaign (third week of June), the temperature outside was reaching very high level especially in the early afternoon (almost 40 °C) for then rapidly decreasing in the evening. This affected also the temperature inside the trailer, but thanks to the changes we made (see section 3.2.2) we were able to control it much better then during the previous campaign: the transportable clock never stopped working for this reason. In particular, to limit the influence of this temperature changes on the blackbody radiation shift, we were able to follow the change

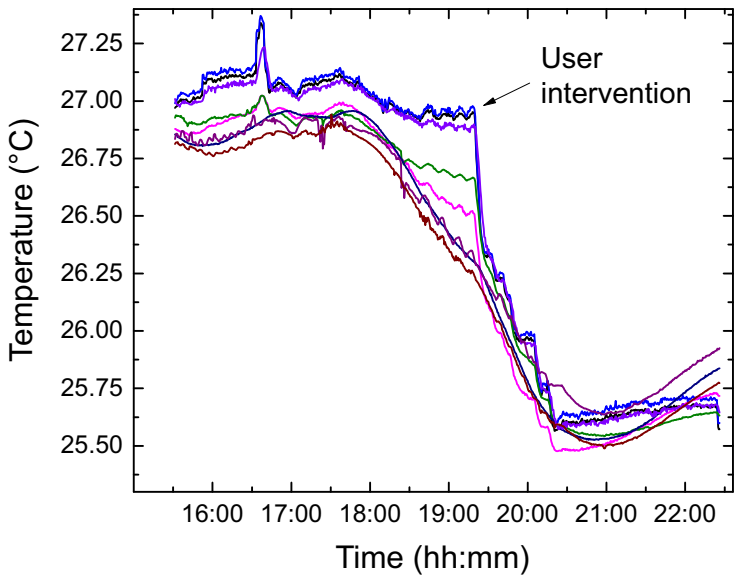

Figure 4.17: Temperature variations of the vacuum chamber during the warmest days of the campaign. By manually changing the temperature of the cooling water we were able to follow them and control the temperature gradient.

in temperature of the vacuum chamber by manually changing the temperature of the cooling water (see figure 4.17).

A typical uncertainty budget for the transportable clock in Paris operated at low lattice is showed in the table of figure 4.18. Reaching a total systematic uncertainty of 2×10^{-17}, this represents the best uncertainty budget (in term of accuracy) ever reached with the system.

Systematic effect	Correction	Uncertainty
Lattice light shift	0.17	0.96
BBR Ambient	534.05	0.68
BBR oven	0.98	0.98
2nd-order Zeeman shift	11.21	0.46
Collision	0.43	0.79
Probe light shift	0.036	0.036
DC Stark shift	0	<0.1
Servo error	0	0.97
Optical path length	0	<0.1
AOM switching	0	0.2
Background gas collision	0.5	0.5
Total	**547.4**	**2.1**

Figure 4.18: Transportable clock uncertainty budget during the campaign in Paris (10^{-17} fractional units) for the clock operated at shallow lattice depth.

4.2.3 Data analysis and result

For more then half of common uptime between the two clocks and the link laser, the transportable clock was operated in interleaved mode, because we needed to characterize the magic wavelength frequency to the low 10^{-17} level.

When the clock is operated in interleaved mode, in our configuration the frequency of the output signal (sent through the link for clock comparison) is switched between the different locking frequencies of the two interleaved cycles. This is because the tuning of

the interrogation laser frequency for locking to the atoms is done on the cavity AOM (see figure 3.8). The correction for the systematic shifts is different for the two cycles and a combined systematic correction with uncertainty needs to be calculated. This results to be the mean of the two cycle corrections, with an uncertainty that is also given by the mean of the two different uncertainties: the justification comes from the fact that the main contribution to the total lattice shift uncertainty stems from the statistic error in the determination of the linear part of the shift. This is explained in more details in Appendix A2.

The results for all the days in which we reached common uptime with the stationary clock are reported in figure 4.19. The red shift correction is applied, so it is easier to compare them with the expected result (zero frequency difference). The total uncertainty on every measurement (systematic plus statistic) is reported as the blue error bars, while the black show only the statistical part of the uncertainty. The transportable system worked at a total systematic uncertainty between 2.3 and 3.9 at 10^{-17} units, with the stationary reporting uncertainties between 1.7 and 2.2.

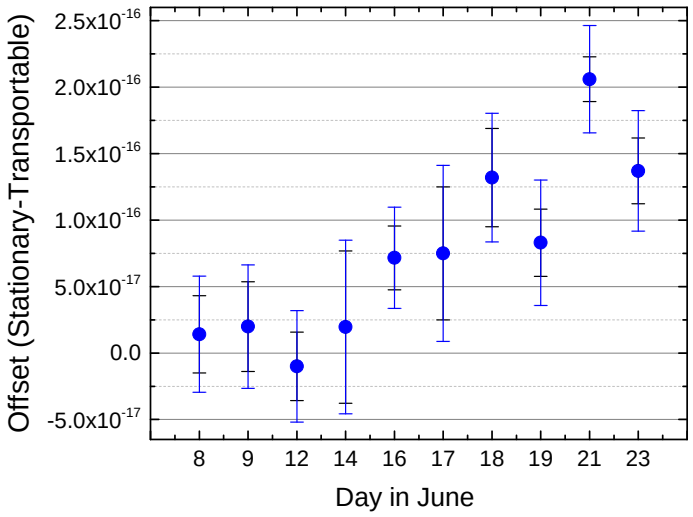

Figure 4.19: Results for the remote comparison for different days of the campaign. The blue error bars represent the total error of each measurement, and the black ones just the statistical contribution to the error.

Looking at the data showed in figure 4.19, it is obvious to see that during the last days of measurement the results are much more scattered and show a significant offset, with changes at the 10^{-16} level, a factor four times bigger then the reported total uncertainty.

This is also shown by plotting the Allan deviation of the data in 4.19, and is done in the left graph of figure 4.20. The Allan deviation stops to average down at the low 10^{-17}, suggesting that an uncontrolled systematic effect degraded the consistency of the measurements. If we limit the analysis at the days of the comparison (until June 14th) and we plot the Allan deviation, we do not see this effect. The statistical uncertainty averages down below 2×10^{-17}. This is done in the left graph of figure 4.20.

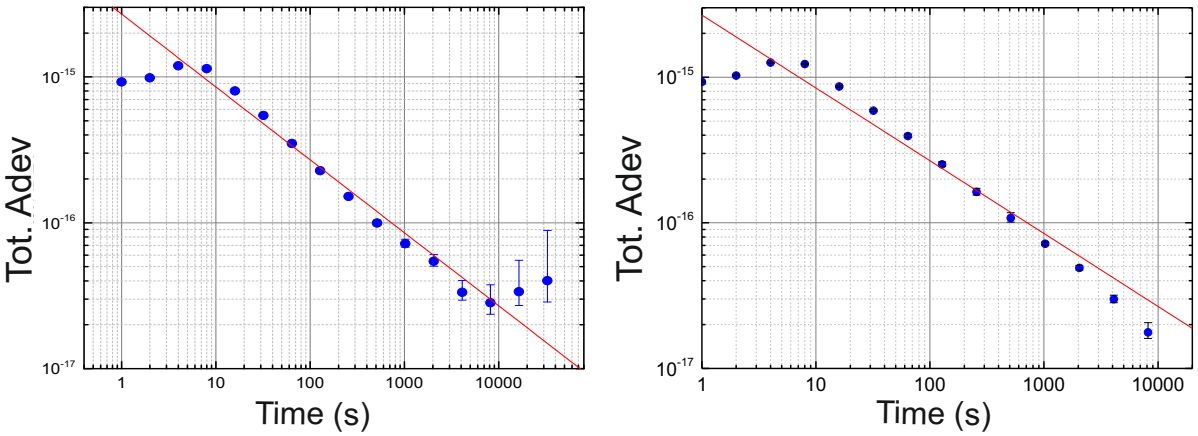

Figure 4.20: Left: Total Allan deviation for all the data recorded in the measurement campign for the remote comparison between the two clock. The Allan deviation point stop to average down at the low 10^{-17}, suggesting that an uncontrolled systematic effect degraded the consistency of the measurements. Right: if we limit the analysis to the data recorded until June 14, the total Allan deviation averaged down 2×10^{-17} statistical uncertainty as expected, showing an instability for the comparison of $2.7 \times 10^{-15}/\sqrt{\tau}$.

The instability of the ratio with the stationary clock reflects the instability of our system because the latter can make use of the stationary ultra-stable reference cavities introduced in section 3.2.3, and resulted in $2.7 \times 10^{-15}/\sqrt{\tau}$.

To test the consistency of the measurement we can also perform a weighted average on them and a χ^2 test following the procedure explained in Appendix A.1.

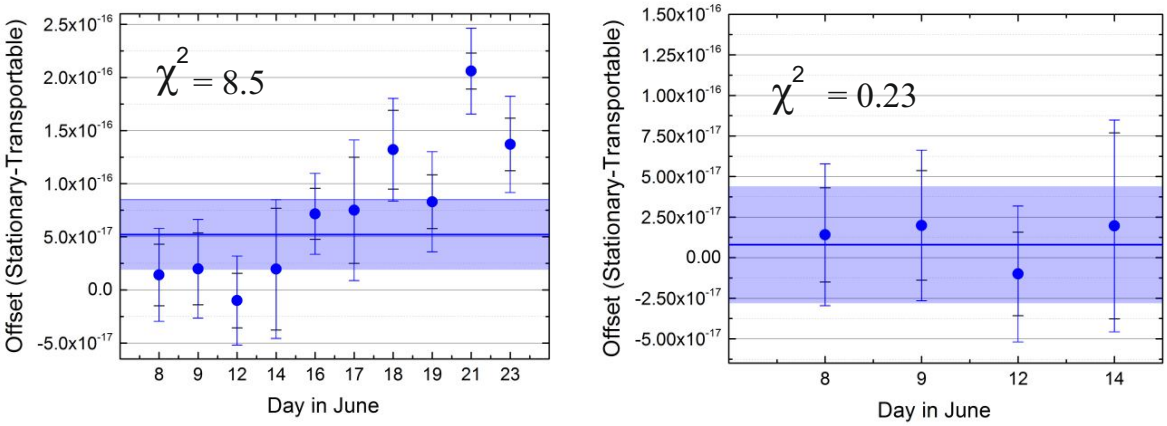

Figure 4.21: On the left: the shadowed blue region covering a 1 σ area,represent the weighted mean resulting from the full set of measurement. The result is not compatible with zero and the χ^2 test on this set measurement a result in 8.5, giving an hint for a not good statistical consistency in the data that suggests a not controlled systematic hidden in the result. On the right: if we limit the analysis to the first part of data sets the result is compatible with zero and we have $\chi^2 = 0.23$.

If we take all the measurement of figure 4.19, this results in a mean value for the remote comparison of $5.1(3.3)\times10^{-17}$ (not consistent with zero) with a $\chi^2 = 8.5$. This value is high, and is in the same way as before and indication that a not controlled systematic effect deteriorating the consistency of the measurements.
If we repeat the analysis limiting it to the first part of the data, until June 14th, we obtain a result for the comparison of $0.8(3.6)\times10^{-17}$ with a $\chi^2 = 0.23$. The measurements are in extremely good agreement between each others and the result is very well compatible with zero, pointing again in the direction that some uncontrolled systematic effect has risen after this day of the campaign. Results on these analysis are reported in figure 4.21.

For all the motivations pointed out before we decided to consider as trustworthy only the data recorded until June 14th. We can be sure that the systematic that scattered the results and introduced a considerable offset after this day was indeed introduced by a malfunction of our system. In fact, when we were performing the remote comparison to PTB stationary system, this clock was at the same time involved in an other measurement campaign between stationary optical clocks of different national metrology institutes, and

this jump resulted to be only in the comparison against the transportable clock.
We believe that the cause of the shift are undetected cycle slips on the phase stabilization for the fiber delivering light from the interrogation laser board to the vacuum chamber in the trailer. The cycle slip detector did not work properly in the last part of the experiment. An other possible cause could have been a wrong value given by the reference resistor in the bridge to read the values of the Pt100 sensors monitoring the vacuum chamber during the warm days of the campaign. However, a check on this resistor after the measurement campaign made us discharge this hypothesis.

We can now compare the local and remote offset between the transportable system and the stationary clock at PTB to have a result on the geopotential difference between the two locations.

First we can compare the local and remote measurements after applying the redshift correction as inferred from the measurement performed by geodesist. We have $\nu_{stat} - \nu_{trans} = -3.7(41) \times 10^{-17}$ for the local comparison and $\nu_{stat} - \nu_{trans} = 0.8(36) \times 10^{-17}$ for the remote one. The results are reported in the left graph of figure 4.22. They are both compatible with zero difference between the clock and are in agreement with each other inside the error bars.

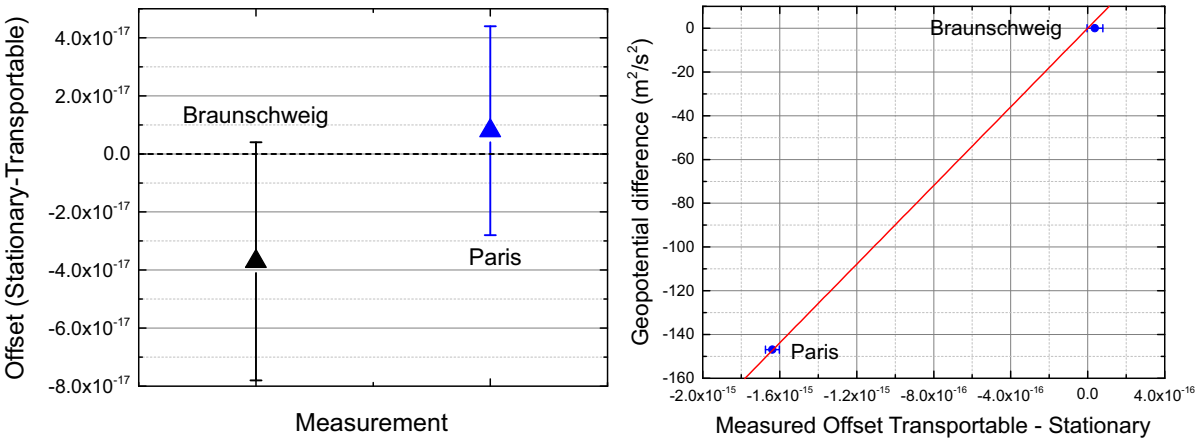

Figure 4.22: Left: Comparison between the locally and remote measured offset of the two clocks including the redshift correction on the Paris measurement using the data given by goedesists. The two comparisons agree between each other and with a zero offset between the clocks. Right: the two measurement as a function of the geopotential difference between the them. The red line represent the expected change in the offset between the two clocks as is predicted by the theory of general relativity.

Then, as done for the chronometric leveling result for the first campaign, we can use the two measurements to calculate the geopotential difference between the two locations. We can use the local comparison as a validation of zero offset between the two clocks with an uncertainty of 4.1×10^{-17} and use it to infer the geopoetential difference from the remote comparison not red shift corrected.
The measured geopotential difference measured via chronometric leveling results then in 150.5(37) m^2/s^2, and is in good agreement with the one done via the conventional geodetic methods, 146.9(4)m^2/s^2.
The graph on the right in figure 4.21, reports the two measurement as a function of the geopotential difference between them. The red line represent the expected change in the offset between the two clocks as it is predicted by the theory of general relativity. The result is in very good agreement with the expectation.

4.2.4 Conclusions and observations

The biggest improvement we obtained during this second measurement campaign with respect to the previous one is a much higher reliability of the transportable clock. As showed in figure 4.15, the clock was up for several hours each day, and most of the time it operated continuously without the need of an external intervention from the user.
This was due to the actions we took to better control the management of the heat produced inside the trailer, like the use of the switches for the amplifiers, the use of the box for the vacuum chamber (so that the air blown by the conditioning system did not disturb the loading of atoms in the lattice stabilizing at the and and the same time the temperature inside the trailer) and the precautions we took in the positioning and shadowing of the trailer. This time the clock operation was never stopped as a consequence of over heating.
On the other hand, we realized that, as can be seen in figure 4.17, big changes in the external temperature during the day (like the temperature difference between night and day in summer days) affect the temperature inside the trailer and the stability of the vacuum chamber temperature. Although this problem can be solved by following the temperature by manually steering the cooler temperature, we think that a better solution

can and should be found for next campaigns.

The high reliability of the clock allowed to perform a characterization of the systematics to a level that was ten times better then during the previous measurement campaign, and also better then any previous systematic characterization even at PTB. However, the probable scattering of the measurement during the last week of the campaign suggests that the control of the systematics did not work always as expected. We suspect this to have been caused by an undetected cycles slip in the phase stabilization of the interrogation light going to the atoms. We have to investigate more this problem and solve it.

This time, the measured geopotential difference between the local and remote comparison is given with a total uncertainty of 3.7 m^2/s^2, that is 50 times smaller with respect to the one obtained in the previous campaign. The main reason for this improvement comes again from the improved reliability of the clock that allowed an optical-optical comparison to be performed.
This means that we were able to measure the height difference between the two locations with an accuracy of less then 40 cm. The result is in agreement with the one obtained with state-of-the-art conventional methods, and this time only ten times less accurate.
These results, considering that they are the first tries to use a transportable clock outside a metrology laboratory, are encouraging about the use of such instruments for chronometric leveling. When these clocks reach an uncertainty equal or below 1×10^{-17} (a result that could be reached in the near future already by our system) they can be use in experiment where the accuracy they offer for the determination of geopotential differences could be complementary or even competitive with conventional methods.

Chapter 5

Summary and Outlook

In this thesis, I presented the characterization of PTB transportable optical lattice clock and its employment in the first measurement campaign ever done with a transportable optical clock , showing possible applications of such an instrument in optical frequency metrology and relativistic geodesy.
The uncertainty budget characterization of the system was improved from 7×10^{-17} during the first comparison to PTB stationary ^{87}Sr optical lattice clock of the clock still placed the laboratory, to 2×10^{-17} for the second comparison with system operated inside a car trailer during a measurement campaign (very close to the design limit of the system, $\sim 1 \times 10^{-17}$).

The first campaign in which the clock has been used, was a proof of principle chronometric leveling experiment to measure the gravity potential difference between two distant locations: The Instituto Nazionale di RIcerca Metrologica (Inrim), the Italian metrological institute in Turin and the Laboratoire Soutterrain de Modane (LSM) in Modane, a particle physics laboratory in the France Alps. The two sites have an eight difference of approximately 1000 m and were connected connected via a 150 km fiber link for the optical frequency transfer.
In this campaign the clock operated at a higher uncertainty then expected ($\sim 2 \times 10^{-16}$ total systematic uncertainty), because the poor reliability of the system did not allow to properly evaluate the systematics. For the same reason we could not reach common operation with the optical clock at INRIM during the remote comparison but only with

the microwave Cs fountain. The chronometric leveling result, although in excellent agreement with the one obtained with state-of-the-art geodesy methods, has as a consequence a large uncertainty of $\sim 1 \times 10^{-15}$. However, when we moved the clock at INRIM for the local comparison, common operation with the optical clock of the institute was reached allowing to determine the optical ratio $^{171}\mathrm{Yb}/^{87}\mathrm{Sr}$ with a 2.8×10^{-16} total fractional uncertainty. This was the first measurement of this optical ratio between optical clock developed by two independent institutes.

For the second campaign, the transportable clock was moved to Syrte-Observatoire de Paris, French national metrology institute, to perform a chronometric leveling experiment making use of the 1400 km fiber link between the French institute and PTB and using PTB stationary $^{87}\mathrm{Sr}$ optical lattice clock as a reference.
In this campaign, the clock showed an highly increased reliability thanks to the changes

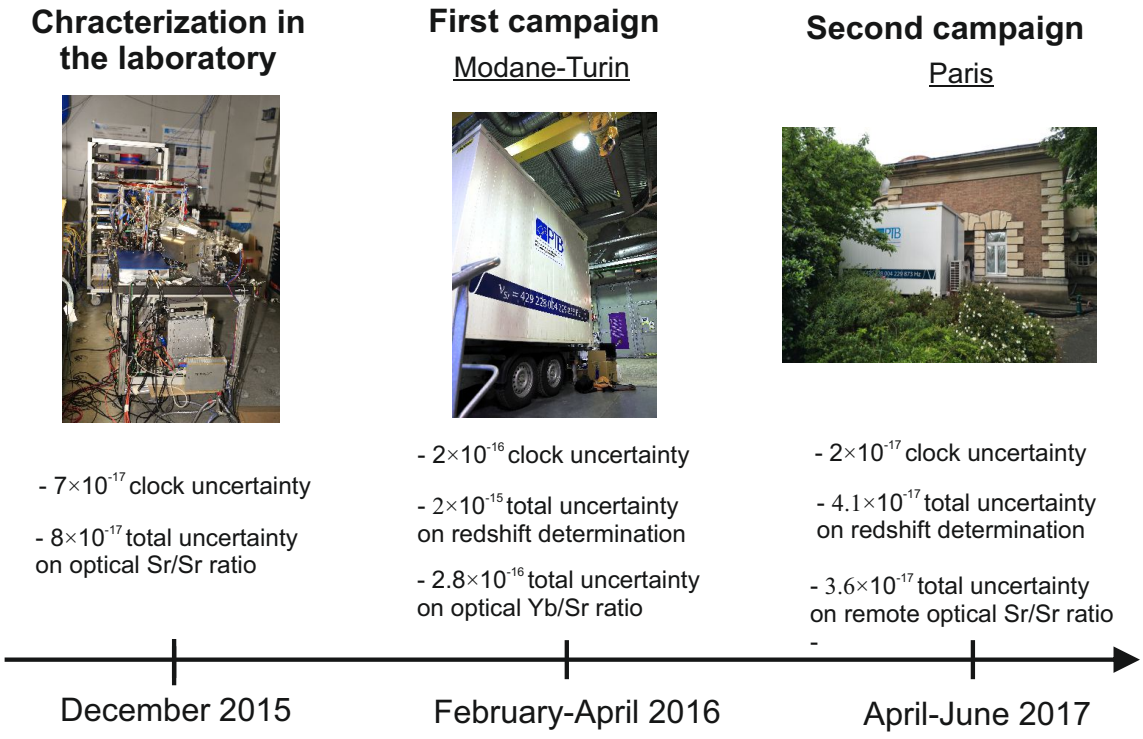

Figure 5.1: Summary of the experiments performed with the transportable clock during my doctorate.

we made on the system between the two campaigns. This allowed its characterization at a 2×10^{-17} total systematic uncertainty and even more important the possibility to reach a long common uptime with the stationary clock in Braunschweig. The relativistic redshift between the transportable clock location in Paris and the stationary clock in Braunschweig was determined with a 4.1×10^{-17} uncertainty via chronometric leveling.
Figure 5.1 summarizes all these steps performed during my doctorate work in a time-frame.

The uncertainty reached by the system is now close to its design limit. The uncertainty on the determination of the black body radiation shift is probably the one that will limit the system in the future. Although we demonstrated that under optimal conditions we are able to reduce the uncertainty on this shift at the low 10^{-18} level (see figure 3.11), when the the temperature of the environment outside the trailer changes rapidly, the control on this systematic effect is more difficult (see figure 4.17). The uncertainty on the other systematic shifts can still be improved by a more accurate determination of their components. The limit on the BBR shift uncertainty comes from the design of the vacuum chamber for which is not possible to further reduce its temperature inhomogeneity. In this vision, a future upgrade of the clock in which the atoms are interrogated in a cryogenic environment would solve this problem [Ush15].
The best stability reached with the system is currently $1.5 \times 10^{-15}/\sqrt{\tau}$ and its limited by the short time stability of the ultra-stable transportable reference cavity we use for the interrogation laser. A new version of this cavity with smaller instability is under development. This would allow a faster characterization of the lattice shift, which is the systematic that needs to be re-evaluated after each transport. Moreover, the new version of the interrogation laser plus its cavity is much smaller then the current one, and can fit inside the car trailer. For this to be done during clock operation however a way to reduce or cancel the effect of the trailer vibration on the laser stability is needed.
Changing the program control to allow to have a distributed instead of lumped distribution of the cycles during interleaved operation (see section 3.3.1) would allow to reach a better stability when the system is operated in this mode.
Finally, an other technical improvement which would increase even more the reliability of the system is the generation of the stirring light for the red MOT via as sideband frequency of the cooling red laser trough an EOM. This is currently under development and will allow to remove the need of a second laser phase-locked to the cooling one to

generate the stirring light.

Already now the increased availability and low accuracy reached by the system (2×10^{-17}) demonstrates the possibility to use the transportable optical lattice clock outside a laboratory with an uncertainty comparable with the best laboratory systems in Europe, and it is an important milestone to show the potential of this kind of instruments.

From a metrological point of view, the transportable clock can serve as a bridge to connect and compare independent optical clocks around the world at the low 10^{-17} uncertainty level, even if a stable frequency transfer link is not available. This is an important step in vision of an optical redefinition of the second.

Moreover, operating at this accuracy it is possible to use the clock to realize chronometric leveling experiment. Optical clocks are reaching for the first time the required performances to make the idea of using accurate clock in geodesy to measure gravitational potential have a practical relevance. Our system has the advantage the be transportable so that is possible to employ it in region of particular geodesy interest even if the condition where it has to operate are far from the laboratory one. We showed this during this thesis work. It can measure potential difference over long distances with a few tens of cm uncertainty at the moment, approximately an order of magnitude worse of what can be done using state-of-the-art geodesy conventional techniques. Considering that is the first prototype of transportable clock used outside the laboratory, is a remarkable result, and lights the path for the development of similar and better apparatus, which could be use to investigate the discrepancy between heights determined with leveling or GNSS/Geoid modeling approach across Europe (see figure 1.2 in the introduction) or, with a possible future definition of the second over isochronometric surfaces [Phi17], contribute to define the local geoid.

Appendix A

Appendix

A.1 Weigthed mean calculation

To calculate the weighted mean and uncertainty of a series of N ratio measurements y_i, we adopted the following procedure based on references [Cow98, Mar15].

In this calculation the main problem arises from the fact that the uncertainty u_i of every measurement in the series is composed by two parts: statistical u_A and systematic u_B. While the statistical uncertainty of different measurements can be considered fully uncorrelated, the same can not be said for the systematics, since they are always the same in every measurement. In particular, we decided to considered the systematic uncertainties as fully correlated.
To calculate the weighted mean and its uncertainty, we first need to calculate the covariance matrix V, which is defined as:

$$V_{ij} = cov[y_i, y_j] = \rho\sigma_i\sigma_j \tag{A.1}$$

where ρ is the correlation coefficient. In our case, $\rho = 0$ for the u_A and $\rho = 1$ for the u_B. The diagonal elements of V are then given by $\sigma_i\sigma_i = u_{Ai}^2 + u_{Bi}^2$ and the off diagonal elements are $\sigma_i\sigma_j(i \neq j) = u_{Bi}u_{Bj}$.
The weighted mean $\bar{y}$ is then given by the following equation (where V^{-1} is the inverted matrix of V):

$$\bar{y} = \sum_{i=1}^{N} w_i y_i \tag{A.2}$$

with the weights w_i given by:

$$w_i = \frac{\sum_{j=1}^{N}(V^{-1})_{ij}}{\sum_{k,l=1}^{N}(V^{-1})_{kl}} \tag{A.3}$$

The uncertainty on the mean is given by:

$$u_{\bar{y}} = \sum_{i,j=1}^{N} w_i V_{ij} w_j \tag{A.4}$$

A.2 Systematic uncertainty for a comparison during interleaved operation

During an interleaved measurement for the determination of a systematic correction, we operate the clock in two parallel cycles and one parameter is switched between two values in the two cycles. This means that during each cycles the atomic clock transition is at a different frequency: the difference of the two frequencies is exactly what we want to measure to evaluate the effect of the parameter changes on the clock transition.
On the other hand it is useful to make use of the uptime of the clock operated in interleaved mode to perform a clock comparison. This is particularly true during measurement campaigns, when the campaign duration is fixed and we want to use all the data we have. To use the output of the system for clock comparison during interleaved operation we need to calculate the correction (and the correction uncertainty) we have to apply to it.

As depicted in figure 3.8, in our system the lock of the interrogation laser to the atomic transition is done by steering the laser frequency via the "cavity" AOM. This AOM acts on the laser light going to the reference cavity. This correction is composed by two parts (see figure 3.17, left): one corrects the drift of the cavity in respect to the atoms and the other one tunes the frequency to lock exactly on the atomic line. In this way the output frequency of the system is different depending on which interleaved cycle we are on. A combined correction and uncertainty needs to be calculated.
To do this, we can consider the fact that half of the time the output is at the frequency determined by the first cycle and for the other half at the one of the second cycle. The total correction is then clearly the mean of the correction for the two cycles. Less obvious is how to calculate the combined systematic uncertainty during the interleaved operation of the clock.
We can limit the analysis to our actual cause. As reported in the thesis, in a measurement campaign the only systematic effect that needs to be reevaluated with interleaved operation of the clock is the lattice light shift.To evaluate the shift we run cycle A with lattice intensity I_1 and cycle B with intensity I_2 and we measure an offset between the two cycles of $\Delta\nu$ to evaluate the lattice light shift. If the main contribution in the uncertainty on the determination of this shift comes from the linear part of the AC Stark shit (as it was in the measurements reported in this thesis), the combined uncertainty can be easily

determined.
Let us call C_{MWL} the combined correction:

$$C_{MWL} = \frac{1}{2}\Big(\frac{I_1}{\Delta I} + \frac{I_2}{\Delta I}\Big)\Delta\nu \tag{A.5}$$

where $\Delta I = I_2 - I_1$. The uncertainty on the correction $u_{C_{MWL}}$ is then given by:

$$u_{C_{MWL}} = \frac{\delta C_{MWL}}{\delta\Delta\nu}u(\Delta\nu) = \frac{1}{2}\Big(\frac{I_1}{\Delta I} + \frac{I_2}{\Delta I}\Big)u(\Delta\nu) \tag{A.6}$$

Under the previous hypothesis, $u(\Delta\nu)$ is just the statistical uncertainty on the determination of $\Delta\nu$.

Bibliography

[Abg12] Michel Abgrall, "FREQUENCY COMPARISON (H_MASER 140 0889) - (LNE-SYRTE-FOM) For the period MJD 56154 to MJD 56169", (2012).

[Aka14a] Daisuke Akamatsu, Hajime Inaba, Kazumoto Hosaka, Masami Yasuda, Atsushi Onae, Tomonari Suzuyama, Masaki Amemiya and Feng-Lei Hong, "Spectroscopy and frequency measurement of the ^{87}Sr clock transition by laser linewidth transfer using an optical frequency comb", Appl. Phys. Express **7**, 012401 (2014).

[Aka14b] Daisuke Akamatsu, Masami Yasuda, Hajime Inaba, Kazumoto Hosaka, Takehiko Tanabe, Atsushi Onae and Feng-Lei Hong, "Frequency ratio measurement of ^{171}Yb and ^{87}Sr optical lattice clocks", Opt. Express **22**, 7898 (2014) see erratum Optics Express Vol. 22, Iss. 26, pp. 32199–32199 (2014).

[Al-15a] Ali Al-Masoudi, Sören Dörscher, Sebastian Häfner, Uwe Sterr and Christian Lisdat, "Noise and instability of an optical lattice clock", Phys. Rev. A **92**, 063814 (2015).

[Al-15b] Ali Al-Masoudi, Sören Dörscher, Sebastian Häfner, Uwe Sterr and Christian Lisdat, "Noise and instability of an optical lattice clock", Phys. Rev. A **92**, 063814 (2015) is now alm15.

[All66] D. W. Allan, "Statistics of Atomic Frequency Standards", Proc. IEEE **54**, 221 (1966).

[Ash78] A. Ashkin, "Trapping of Atoms by Resonance Radiation Pressure", Phys. Rev. Lett. **40**, 729 (1978).

[Bai08] X. Baillard, M. Fouché, R. Le Targat, P. G. Westergaard, A. Lecallier, F. Chapelet, M. Abgrall, G. D. Rovera, P. Laurent, P. Rosenbusch, S. Bize, G. Santarelli, A. Clairon, P. Lemonde, G. Grosche, B. Lipphardt and H. Schnatz, "An optical lattice clock with spin-polarized ^{87}Sr atoms", Eur. Phys. J. D **48**, 11 (2008).

[Bau15] Andreas Bauch, "Time and frequency comparisons using radiofrequency signals from satellites", C. R. Physique **16**, 471 (2015) Special Issue: The measurement of time / La mesure du temps.

[Bav86] E. Bava, A. Godone and G. Rietto, "Rabi and Ramsey Interrogations of Metastable Beams", Appl. Phys. B **41**, 187 (1986).

[Ber99] J. E. Bernard, A. A. Madej, L. Marmet, B. G. Whitford, K. J. Siemsen and S. Cundy, "Cs-based Frequency Measurement of a Single, Trapped Ion Transition in the Visible Region of the Spectrum", Phys. Rev. Lett. **82**, 3228 (1999).

[Ber14] Anthony Bercy, Fabio Stefani, Olivier Lopez, Christian Chardonnet, Paul-Eric Pottie and Anne Amy-Klein, "Two-way optical frequency comparisons at 5×10^{-21} relative stability over 100-km telecommunication network fibers", Phys. Rev. A **90**, 061802 (2014).

[Biz04] S. Bize, P. Laurent, M. Abgrall, H. Marion, I. Maksimovic, L. Cacciapuoti, J. Grünert, C. Vian, F. Pereira dos Santos, P. Rosenbusch, P. Lemonde, G. Santarelli, P. Wolf, A. Clairon, A. Luiten, M. Tobar and C. Salomon, "Advances in atomic fountains", C. R. Physique **5**, 829 (2004).

[Bje85] Arne Bjerhammar, "On a relativistic geodesy", Bulletin Géodésique **59**, 207 (1985).

[Bla08] S. Blatt, A. D. Ludlow, G. K. Campbell, J. W. Thomsen, T. Zelevinsky, M. M. Boyd, J. Ye, X. Baillard, M. Fouché, R. Le Targat, A. Brusch, P. Lemonde, M. Takamoto, F.-L. Hong, H. Katori and V. V. Flambaum, "New Limits on Coupling of Fundamental Constants to Gravity Using ^{87}Sr Optical Lattice Clocks", Phys. Rev. Lett. **100**, 140801 (2008).

[Blo29] Felix Bloch, "Über die Quantenmechanik der Elektronen in Kristallgittern", Z. Phys. **52**, 555 (1929).

[Bon12] Ruxandra Bondarescu, Mihai Bondarescu, György Hetényi, Lapo Boschi, Philippe Jetzer and Jayashree Balakrishna, "Geophysical applicability of atomic clocks: direct continental geoid mapping", Geophys. J. Int. **191**, 78 (2012).

[Bon15a] Mihai Bondarescu, Ruxandra Bondarescu, Philippe Jetzer and Andrew Lundgren, "The Potential of Continuous, Local Atomic Clock Measurements for Earthquake Prediction and Volcanology", EPJ Web of Conferences **95**, 04009 (2015).

[Bon15b] Ruxandra Bondarescu, Andreas Schärer, Andrew Lundgren, György Hetényi, Nicolas Houlié, Philippe Jetzer and Mihai Bondarescu, "Ground-based optical atomic clocks as a tool to monitor vertical surface motion", Geophysical Journal International **202**, 1770 (2015).

[Bon15c] K. Bongs, Y. Singh, L. Smith, W. He, O. Kock, D. Swierad, J. Hughes, S. Schiller, S. Alighanbari, S. Origlia, S. Vogt, U. Sterr, Ch. Lisdat, R. Le Targat, J. Lodewyck, D. Holleville, B. Venon, S. Bize, G. P. Barwood, P. Gill, I. R. Hill, Y. B. Ovchinnikov, N. Poli, G. M. Tino, J. Stuhler, W. Kaenders and the SOC2 team, "Development of a strontium optical lattice clock for the SOC mission on the ISS", C. R. Physique **16**, 553 (2015) Special Issue: The measurement of time / La mesure du temps.

[Boy07a] Martin M. Boyd, *High Precision Spectroscopy of Strontium in an Optical Lattice: Towards a New Standard for Frequency and Time*, PhD thesis Graduate School of the University of Colorado 2007.

[Boy07b] Martin M. Boyd, Andrew D. Ludlow, Sebastian Blatt, Seth M. Foreman, Tetsuya Ido, Tanya Zelevinsky and Jun Ye, "^{87}Sr lattice clock with inaccuracy below 10^{-15}", Phys. Rev. Lett. **98**, 083002 (2007).

[Bra03] B.H. Bransden and C.J. Joachain, *Physics of Atoms and Molecules*, (Prentice Hall, 2003).

[Cal14] D. Calonico, E. K. Bertacco, C. E. Calosso, C. Clivati, G. A. Costanzo, M. Frittelli, A. Godone, A. Mura, N. Poli, D. V. Sutyrin, G. Tino, M. E. Zucco and F. Levi, "High-accuracy coherent optical frequency transfer over a doubled 642-km fiber link", Appl. Phys. B **117**, 979 (2014).

[Cam08] Gretchen K. Campbell, Andrew D. Ludlow, Sebastian Blatt, Jan W. Thomsen, Michael J. Martin, Marcio H. G. de Miranda, Tanya Zelevinsky, Martin M. Boyd, Jun Ye, Scott A. Diddams, Thomas P. Heavner, Thomas E. Parker and Steven R. Jefferts, "The absolute frequency of the ^{87}Sr optical clock transition", Metrologia **45**, 539 (2008).

[Cam09] G. K. Campbell, M. M. Boyd, J. W. Thomsen, M. J. Martin, S. Blatt, M. D. Swallows, T. L. Nicholson, T. Fortier, C. W. Oates, S. A. Diddams, N. D. Lemke, P. Naidon, P. Julienne, Jun Ye and A. D. Ludlow, "Probing Interactions between Ultracold Fermions", Science **324**, 360 (2009).

[Cao16] Jian Cao, Ping Zhang, Junjuan Shang, Kaifeng Cui, Jinbo Yuan, Sijia Chao, Shaomao Wang, Hualin Shu and Xueren Huang, "A transportable $^{40}Ca^{+}$ single-ion clock with 7.7×10^{-17} systematic uncertainty", arXiv:1607.03731 (2016).

[CCT04] "Recommendation CCTF1 (2004): Secondary representations of the second, Report of the 16th Meeting of the CCTF (April 2004)", www.bipm.org/utils/common/pdf/CCTF16.pdf (2004).

[Chi15] Nicola Chiodo, Nicolas Quintin, Fabio Stefani, Fabrice Wiotte, Emilie Camisard, Christian Chardonnet, Giorgio Santarelli, Anne Amy-Klein, Paul-Eric Pottie and Olivier Lopez, "Cascaded optical fiber link using the Internet network for remote clocks comparison", Opt. Express **23**, 33927 (2015).

[Chu85] S. Chu, L. Hollberg, J. E. Bjorkholm, A. Cable and A. Ashkin, "Three-Dimensional Viscous Confinement and Cooling of Atoms by Resonance Radiation Pressure", Phys. Rev. Lett. **55**, 48 (1985).

[Cla91] A. Clairon, C. Salomon, S. Guellati and W. D. Phillips, "Ramsey Resonance in a Zacharias Fountain", Europhys. Lett. **16**, 165 (1991).

[Cou05] Irene Courtillot, Audrey Quessada-Vial, Anders Brusch, Dmitri Kolker, Giovanni D. Rovera and Pierre Lemonde, "Accurate spectroscopy of Sr atoms", Eur. Phys. J. D **33**, 161 (2005).

[Cow98] G. Cowan, *Statistical Data Analysis*, (Clarendon Press, 1998).

[Den13] Heiner Denker, in *Regional gravity field modeling: Theory and practical results.*, edited by Xu G., (2013).

[Den17] Heiner Denker, Ludger Timmen, Christian Voigt, Stefan Weyers, Ekkehard Peik, Helen S. Margolis, Pacôme Delva, Peter Wolf and Gérard Petit, "Geodetic methods to determine the relativistic redshift at the level of 10^{-18} in the context of international timescales: a review and practical results", Journal of Geodesy (2017).

[Des16] Jean-Daniel Deschênes, Laura C. Sinclair, Fabrizio R. Giorgetta, William C. Swann, Esther Baumann, Hugo Bergeron, Michael Cermak, Ian Coddington and Nathan R. Newbury, "Synchronization of Distant Optical Clocks at the Femtosecond Level", Phys. Rev. X **6**, 021016 (2016).

[Dic53] R. H. Dicke, "The Effect of Collisions upon the Doppler Width of Spectral Lines", Phys. Rev. **89**, 472 (1953).

[Dic88] G. John Dick, "Local oscillator induced instabilities in trapped ion frequency standards", in , *Proceedings of* 19^{th} *Annu. Precise Time and Time Interval Meeting, Redendo Beach, 1987* (U.S. Naval Observatory, Washington, DC, 1988) , S. 133–147.

[Dje10] Khelifa Djerroud, Ouali Acef, André Clairon, Pierre Lemonde, Catherine N. Man, Etienne Samain and Peter Wolf, "Coherent optical link through the turbulent atmosphere", Opt. Lett. **35**, 1479 (2010).

[Dör18] Sören Dörscher, Roman Schwarz, Ali Al-Masoudi, Stephan Falke, Uwe Sterr and Christian Lisdat, "Lattice-induced photon scattering in an optical lattice clock", ArXiv:1802.02956v1 (2018).

[Dre83] R. W. P. Drever, J. L. Hall, F. V. Kowalski, J. Hough, G. M. Ford, A. J. Munley and H. Ward, "Laser Phase and Frequency Stabilization Using an Optical Resonator", Appl. Phys. B **31**, 97 (1983).

[Eck78] J. N. Eckstein, A. I. Ferguson and T. W. Hänsch, "High-Resolution Two-Photon Spectroscopy with Picosecond Light Pulses", Phys. Rev. Lett. **40**, 847 (1978).

[Fal11] St. Falke, H. Schnatz, J. S. R. Vellore Winfred, Th. Middelmann, St. Vogt, S. Weyers, B. Lipphardt, G. Grosche, F. Riehle, U. Sterr and Ch. Lisdat, "The ^{87}Sr optical frequency standard at PTB", Metrologia **48**, 399 (2011).

[Fal12] Stephan Falke, Mattias Misera, Uwe Sterr and Christian Lisdat, "Delivering pulsed and phase stable light to atoms of an optical clock", Appl. Phys. B **107**, 301 (2012).

[Fal14] Stephan Falke, Nathan Lemke, Christian Grebing, Burghard Lipphardt, Stefan Weyers, Vladislav Gerginov, Nils Huntemann, Christian Hagemann, Ali Al-Masoudi, Sebastian Häfner, Stefan Vogt, Uwe Sterr and Christian Lisdat, "A strontium lattice clock with 3×10^{-17} inaccuracy and its frequency", New J. Phys. **16**, 073023 (2014).

[Fis04] M. Fischer, N. Kolachevsky, M. Zimmermann, R. Holzwarth, T. Udem, T. W. Hänsch, M. Abgrall, J. Grünert, I. Masimovic, S. Bize, H. Marion, F. Pereira Dos Santos, P. Lemonde, G. Santarelli, P. Laurent, A. Clairon, C. Salomon, M. Haas, U. D. Jentschura and C. H. Keitel, "New Limits on the Drift of Fundamental Constants from Laboratory Measurements", Phys. Rev. Lett. **92**, 230802 (2004).

[Flu16] Jakob Flury, "Relativistic geodesy", J. Phys.: Conf. Ser. **723**, 012051 (2016).

[For07] T. M. Fortier, N. Ashby, J. C. Bergquist, M. J. Delaney, S. A. Diddams, T. P. Heavner, L. Hollberg, W. M. Itano, S. R. Jefferts, K. Kim, F. Levi, L. Lorini, W. H. Oskay, T. E. Parker, J. Shirley and J. E. Stalnaker, "Precision Atomic Spectroscopy for Improved Limits on Variation of the Fine Structure Constant and Local Position Invariance", Phys. Rev. Lett. **98**, 070801 (2007).

[Fuj14] M. Fujieda, D. Piester, T. Gotoh, J. Becker, M. Aida and A. Bauch, "Carrier-phase two-way satellite frequency transfer over a very long baseline", Metrologia **51**, 253 (2014).

[Fuj16] Miho Fujieda, Tadahiro Gotoh and Jun Amagai, "Advanced two-way satellite frequency transfer by carrier-phase and carrier-frequency measurements", Journal of Physics: Conference Series **723**, 012036 (2016).

[Gib09] Kurt Gibble, "Decoherence and Collisional Frequency Shifts of Trapped Bosons and Fermions", Phys. Rev. Lett. **103**, 113202 (2009).

[Gib13] Kurt Gibble, "Scattering of Cold Atom Coherences by Hot Atoms: Frequency Shifts from Background Gas Collisions", Phys. Rev. Lett. **110**, 180802 (2013).

[Gil11] Patrick Gill, "When should we change the definition of the second?", Phil. Trans. R. Soc. A **369**, 4109 (2011).

[Gre16] C. Grebing, A. Al-Masoudi, S. Dörscher, S. Häfner, V. Gerginov, S. Weyers, B. Lipphardt, F. Riehle, U. Sterr and C. Lisdat, "Realization of a timescale with an accurate optical lattice clock", Optica **3**, 563 (2016).

[Gro18] Jacopo Grotti, Silvio Koller, Stefan Vogt, Sebastian Häfner, Uwe Sterr, Christian Lisdat, Heiner Denker, Christian Voigt, Ludger Timmen, Antoine Rolland, Fred N. Baynes, Helen S. Margolis, Michel Zampaolo, Pierre Thoumany, Marco Pizzocaro, Benjamin Rauf, Filippo Bregolin, Anna Tampellini, Piero Barbieri, Massimo Zucco, Giovanni A. Costanzo, Cecilia Clivati, Filippo Levi and Davide Calonico, "Geodesy and metrology with a transportable optical clock", Nature Physics (2018).

[Gru09] Thomas Gruber, "Evaluation of the EGM2008 Gravity Field by Means of GPS Leveling and surface topography solution. External quality evaluation reports of EGM08", Bureau Gravimetrique International (BGI)/ International Geoid Service (IGeS) **Newtons Bulletin 4**, 012051 (2009).

[Gru14] Thomas Gruber, Rummel Reiner, Johannes Ihde, Gunter Liebsch, Alex Rülke, Uwe Schäfer, Michael Sideris, Elena Rangelova, Philip Woodwoth and Chris Hughes, "Height System Unification with GOCE", ESA report GO-HSU-PL-0021 (2014).

[Gué12] J. Guéna, M. Abgrall, D. Rovera, Ph. Laurent, B. Chupin, M. Lours, G. Santarelli, P. Rosenbusch, M. E. Tobar, R. Li, K. Gibble, A. Clairon and S. Bize, "Progress in Atomic Fountains at LNE-SYRTE", IEEE Trans. Ultrason. Ferroelectr. Freq. Control **59**, 391 (2012).

[Gui99] L. Guidoni and P. Verkerk, "PhD Tutorial: Optical lattices: cold atoms ordered by light", J. Opt. B: Quantum Semiclass. Opt. **1**, R23 (1999).

[GUM08] "Evaluation of measurement data – Guide to the expression of uncertainty in measurement", JCGM 100:2008 2008.

[Hac14] H. Hachisu, M. Fujieda, S. Nagano, T. Gotoh, A. Nogami, T. Ido, St. Falke, N. Huntemann, C. Grebing, B. Lipphardt, Ch. Lisdat and D. Piester, "Direct comparison of optical lattice clocks with an intercontinental baseline of 9 000 km", Opt. Lett. **39**, 4072 (2014).

[Hac17a] Hidekazu Hachisu, Gérard Petit and Tetsuya Ido, "Absolute frequency measurement with uncertainty below 1×10^{-15} using International Atomic Time", Appl. Phys. B **123**, 34 (2017).

[Hac17b] Hidekazu Hachisu, Gérard Petit, Fumimaru Nakagawa, Yuko Hanado and Tetsuya Ido, "SI-traceable measurement of an optical frequency at the low 10^{-16} level without a local primary standard", Opt. Express **25**, 8511 (2017).

[Häf15a] Sebastian Häfner, *Ultrastabile Lasersysteme für Weltraum- und Boden-Anwendungen*, PhD thesis Leibniz Universität Hannover 2015.

[Häf15b] Sebastian Häfner, Stephan Falke, Christian Grebing, Stefan Vogt, Thomas Legero, Mikko Merimaa, Christian Lisdat and Uwe Sterr, "8×10^{-17} fractional laser frequency instability with a long room-temperature cavity", Opt. Lett. **40**, 2112 (2015).

[Hän75] T. W. Hänsch and A. L. Schawlow, "Cooling of gases by laser radiation", Opt. Commun. **13**, 68 (1975).

[Hap72] William Happer, "Optical Pumping", Rev. Mod. Phys. **44**, 169 (1972).

[Hin13] N. Hinkley, J. A. Sherman, N. B. Phillips, M. Schioppo, N. D. Lemke, K. Beloy, M. Pizzocaro, C. W. Oates and A. D. Ludlow, "An atomic clock with 10^{-18} instability", Science **341**, 1215 (2013).

[Hol01] Leo Hollberg, Chris W. Oates, E. Anne Curtis, Eugene N. Ivanov, Scott A. Diddams, Thomas Udem, Hugh G. Robinson, James C. Bergquist, Robert J. Rafac, Wayne M. Itano, Robert E. Drullinger and D. J. Wineland, "Optical Frequency Standards and Measurements", IEEE J. Quantum Electron. **37**, 1502 (2001).

[Hon09] F.-L. Hong, M. Musha, M. Takamoto, H. Inaba, S. Yanagimachi, A. Takamizawa, K. Watabe, T. Ikegami, M. Imae, Y. Fujii, M. Amemiya, K. Nakagawa, K. Ueda and H. Katori, "Measuring the frequency of a Sr optical lattice clock using a 120 km coherent optical transfer", Opt. Lett. **34**, 692 (2009).

[Hun14] N. Huntemann, B. Lipphardt, Chr. Tamm, V. Gerginov, S. Weyers and E. Peik, "Improved limit on a temporal variation of m_p/m_e from comparisons of Yb^+ and Cs atomic clocks", Phys. Rev. Lett. **113**, 210802 (2014).

[Hun16] N. Huntemann, C. Sanner, B. Lipphardt, Chr. Tamm and E. Peik, "Single-Ion Atomic Clock with 3×10^{-18} Systematic Uncertainty", Phys. Rev. Lett. **116**, 063001 (2016).

[Ita93] W. M. Itano, J. C. Bergquist, J. J. Bollinger, J. M. Gilligan, D. J. Heinzen, F. L. Moore, M. G. Raizen and D. J. Wineland, "Quantum projection noise: Population fluctuations in two-level systems", Phys. Rev. A **47**, 3554 (1993) See Also: Erratum Phys. Rev. A 51, 1717 (1995).

[Jef99] S. R. Jefferts, D. M. Meekhof, J. H. Shirley, T. E. Parker and F. Levi, "Preliminary Accuracy Evaluation of a Cesium Fountain Primary Frequency Standard at NIST", in , *Proceedings of the 1999 Joint Meeting of the European Frequency and Time Forum and The IEEE International Frequency Control Symposium* (1999) , S. 12–15.

[Kat02] Hidetoshi Katori, "Spectroscopy of strontium atoms in the Lamb-Dicke confinement", in , *Proceedings of the Sixth Symposium on Frequency Standards and Metrology, 9–14 September 2001, St. Andrews, Scotland*, edited by P. Gill, (World Scientific, Singapore, 2002) , S. 323–330.

[Kat15] Hidetoshi Katori, V. D. Ovsiannikov, S. I. Marmo and V. G. Palchikov, "Strategies for reducing the light shift in atomic clocks", Phys. Rev. A **91**, 052503 (2015).

[Kel17] J. Keller, D. Kalincev, T. Burgermeister, A. Kulosa, A. Didier, T. Nordmann, J. Kiethe and T. E. Mehlstäubler, "Optical clocks based on linear ion chains with high stability and accuracy", arXiv:1712.02335 [physics.atom-ph] (2017).

[Kol17] S. B. Koller, J. Grotti, St. Vogt, A. Al-Masoudi, S. Dörscher, S. Häfner, U. Sterr and Ch. Lisdat, "Transportable Optical Lattice Clock with 7×10^{-17} Uncertainty", Phys. Rev. Lett. **118**, 073601 (2017).

[Lau15] Philippe Laurent, Didier Massonnet, Luigi Cacciapuoti and Christophe Salomon, "The ACES/PHARAO space mission", Comptes Rendus Physique **16**, 540 (2015).

[Le 12] Rodolphe Le Targat, Luca Lorini, Mikhail Gurov, Michal Zawada, Rafal Gartman, Bartlomiej Nagorny, Pierre Lemonde and Jérôme Lodewyck, "Comparison of two Strontium optical lattice clocks in agreement at the 10^{-16} level", in , *European Frequency and Time Forum (EFTF), 2012* (IEEE, Gothenburg, 2012) , S. 19–22 Contribution to European Frequency and Time Forum 2012, Gothenburg, Sweden,.

[Le 13] R. Le Targat, L. Lorini, Y. Le Coq, M. Zawada, J. Guéna, M. Abgrall, M. Gurov, P. Rosenbusch, D. G. Rovera, B. Nagórny, R. Gartman, P. G. Westergaard, M. E. Tobar, M. Lours, G. Santarelli, A. Clairon, S. Bize, P. Laurent, P. Lemonde and J. Lodewyck, "Experimental realization of an optical second with strontium lattice clocks", Nature Com. **4**, 2109 (2013).

[Lem05] Pierre Lemonde and Peter Wolf, "Optical lattice clock with atoms confined in a shallow trap", Phys. Rev. A **72**, 033409 (2005).

[Lev04] F. Levi, L. Lorini, D. Calonico and A. Godone, "IEN-CsF1 Accuracy Evaluation and Two-Way Frequency Comparison", IEEE Trans. Ultrason. Ferroelectr. Freq. Control **51**, 1216 (2004).

[Lev14] Filippo Levi, Davide Calonico, Claudio E Calosso, Aldo Godone, Salvatore Micalizio and Giovanni A Costanzo, "Accuracy evaluation of ITCsF2: a nitrogen cooled caesium fountain", Metrologia **51**, 270 (2014).

[LI09] Tian chu LI, Ping wei LIN, Ming shou LI, Ping WANG, Wei liang CHEN, Nian feng LIU and Yi ge LIN, "The transportable cesium fountain clock NIM5: its construction and performance", Frontier of Physics in China **4**, 155 (2009).

[Li16] Lin Li, Qiu-Zhi Qu, Bin Wang, Tang Li, Jian-Bo Zhao, Jing-Wei Ji, Wei Ren, Xin Zhao, Mei-Feng Ye, Yuan-Yuan Yao, De-Sheng Lü and Liang Liu, "Initial Tests of a Rubidium Space Cold Atom Clock", Chinese Physics Letters **33**, 063201 (2016).

[Lin15] Yi-Ge Lin, Qiang Wang, Ye Li, Fei Meng, Bai-Ke Lin, Er-Jun Zang, Zhen Sun, Fang Fang, Tian-Chu Li and Zhan-Jun Fang, "First Evaluation and Frequency Measurement of the Strontium Optical Lattice Clock at NIM", Chin. Phys. Lett. **32**, 090601 (2015).

[Lio17] G. Lion, I. Panet, P. Wolf, C. Guerlin, S. Bize and P. Delva, "Determination of a high spatial resolution geopotential model using atomic clock comparisons", Journal of Geodesy **online first**, 1 (2017).

[Lis16] C. Lisdat, G. Grosche, N. Quintin, C. Shi, S.M.F. Raupach, C. Grebing, D. Nicolodi, F. Stefani, A. Al-Masoudi, S. Dörscher, S. Häfner, J.-L. Robyr, N. Chiodo, S. Bilicki, E. Bookjans, A. Koczwara, S. Koke, A. Kuhl, F. Wiotte, F. Meynadier, E. Camisard, M. Abgrall, M. Lours, T. Legero, H. Schnatz, U. Sterr, H. Denker, C. Chardonnet, Y. Le Coq, G. Santarelli, A. Amy-Klein, R. Le Targat, J. Lodewyck, O. Lopez and P.-E. Pottie, "A clock network for geodesy and fundamental science", Nature Com. **7**, 12443 (2016).

[Lod16] Jérôme Lodewyck, Sławomir Bilicki, Eva Bookjans, Jean-Luc Robyr, Chunyan Shi, Grégoire Vallet, Rodolphe Le Targat, Daniele Nicolodi, Yann Le Coq, Jocelyne Guéna, Michel Abgrall, Peter Rosenbusch and Sébastien Bize, "Optical to microwave clock frequency ratios with a nearly continuous strontium optical lattice clock", Metrologia **53**, 1123 (2016).

[Lop12] Olivier Lopez, Adil Haboucha, Bruno Chanteau, Christian Chardonnet, Anne Amy-Klein and Giorgio Santarelli, "Ultra-stable long distance optical frequency distribution using the Internet fiber network", Opt. Express **20**, 23518 (2012).

[Lop13] Olivier Lopez, Amale Kanj, Paul-Eric Pottie, Daniele Rovera, Joseph Achkar, Christian Chardonnet, Anne Amy-Klein and Giorgio Santarelli, "Simultaneous remote transfer of accurate timing and optical frequency over a public fiber network", Appl. Phys. B **110**, 3 (2013).

[Lop15] Olivier Lopez, Fabien Kéfélian, Haifeng Jiang, Adil Haboucha, Anthony Bercy, Fabio Stefani, Bruno Chanteau, Amale Kanj, Daniele Rovera, Joseph Achkar, Christian Chardonnet, Paul-Eric Pottie, Anne Amy-Klein and Giorgio Santarelli, "Frequency and time transfer for metrology and beyond using telecommunication network fibres", C. R. Physique **16**, 531 (2015) Special Issue: The measurement of time / La mesure du temps.

[lsm] "www-lsm.in2p3.fr", .

[Lud08] Andrew D. Ludlow, *The Strontium Optical Lattice Clock: Optical Spectroscopy with Sub-Hertz Accuracy*, PhD thesis University of Colorado, Boulder 2008.

[Lud18] Andrew D. Ludlow, "An optical clock to go", Nature Physics (2018).

[Mai13] Enrico Mai, *Time, Atomic Clocks, and Relativistic Geodesy*, *Reihe A*, Vol.124, (Verlag der Bayrischen Akademie der Wissenschaften, 2013).

[Mar13] H. S. Margolis, R. M. Godun, P. Gill, L. A. M. Johnson, S. L. Shemar, P. B. Whibberley, D. Calonico, F. Levi, L. Lorini, M. Pizzocaro, P. Delva, S. Bize, J. Achkar, H. Denker, L. Timmen, C. Voigt, S. Falke, D. Piester, C. Lisdat, U. Sterr, S. Vogt, S. Weyers, J. Gersl, T. Lindvall and M. Merimaa, *International timescales with optical clocks (ITOC)*, (2013).

[Mar14] Helen Margolis, "Timekeepers of the future", Nature Physics **10**, 82 (2014).

[Mar15] H. S. Margolis and P. Gill, "Least-squares analysis of clock frequency comparison data to deduce optimized frequency and frequency ratio values", Metrologia **52**, 628 (2015).

[Mat12] Kensuke Matsubara, Hidekazu Hachisu, Ying Li, Shigeo Nagano, Clayton Locke, Asahiko Nohgami, Masatoshi Kajita, Kazuhiro Hayasaka, Tetsuya Ido and Mizuhiko Hosokawa, "Direct comparison of a Ca^+ single-ion clock against a Sr lattice clock to verify the absolute frequency measurement", Opt. Express **20**, 22034 (2012).

[Mat17a] D. G. Matei, T. Legero, S. Häfner, C. Grebing, R. Weyrich, W. Zhang, L. Sonderhouse, J. M. Robinson, J. Ye, F. Riehle and U. Sterr, "1.5 μm lasers with sub 10 mHz linewidth", Phys. Rev. Lett. **118**, 263202 (2017).

[Mat17b] Michael Matus, Veselin Gavalyugov, Denita Tamakyarska, Nasser Alqahtani, Mohammad Alfohaid, Girija Moona, Rina Sharma, Asep Hapiddin, Ahmad Mohamad Boynawan, Monludee Ranusawud, Anusorn Tonmueanwai, Feng-Lei Hong, Jun Ishikawa and Lennart Robertsson, "The CCL-K11 ongoing key comparison. Final report for the year 2014", Metrologia **54**, 04001 (2017).

[Mei08] D. Meiser, Jun Ye and M. J. Holland, "Spin squeezing in optical lattice clocks via lattice-based QND measurements", New J. Phys. **10**, 073014 (17pp) (2008).

[Mid12a] Thomas Middelmann, Stephan Falke, Christian Lisdat and Uwe Sterr, "High Accuracy Correction of Blackbody Radiation Shift in an Optical Lattice Clock", Phys. Rev. Lett. **109**, 263004 (2012).

[Mid12b] Thomas Middelmann, Stephan Falke, Christian Lisdat and Uwe Sterr, "Long range transport of ultra cold atoms in a far-detuned one-dimensional optical lattice", New J. Phys. **14**, 073020 (2012).

[Mit10] J. Mitroy and J. Y. Zhang, "Dispersion and polarization interactions of the strontium atom", Mol. Phys. **108**, 1999 (2010).

[Muk03] Takashi Mukaiyama, Hidetoshi Katori, Tetsuya Ido, Ying Li and Makoto Kuwata-Gonokami, "Recoil-Limited Laser Cooling of Sr Atoms near the Fermi Temperature", Phys. Rev. Lett. **90**, 113002 (2003).

[Mül17] J. Müller, D. Dirkx, S. M. Kopeikin, G. Lion, I. Panet, G. Petit and P. N. A. M. Visser, "High Performance Clocks and Gravity Field Determination", arXiv: 1702.06761 Will be published in Space Science Reviews as special issue on High Performance Clocks which is organized by ISSI (2017).

[Nem16] Nils Nemitz, Takuya Ohkubo, Masao Takamoto, Ichiro Ushijima, Manoj Das, Noriaki Ohmae and Hidetoshi Katori, "Frequency ratio of Yb and Sr clocks with 5×10^{-17} uncertainty at 150 s averaging time", Nature Photonics **10**, 258 (2016).

[Nic12] T.L. Nicholson, M.J. Martin, J.R. Williams, B.J. Bloom, M. Bishof, M.D. Swallows, S.L. Campbell and J. Ye, "Comparison of Two Independent Sr Optical Clocks with 1×10^{-17} Stability at 10^3 s", Phys. Rev. Lett. **109**, 230801 (2012).

[Nic15] T. L. Nicholson, S. L. Campbell, R. B. Hutson, G. E. Marti, B. J. Bloom, R. L. McNally, W. Zhang, M. D. Barrett, M. S. Safronova, G. F. Strouse, W. L. Tew and J. Ye, "Systematic evaluation of an atomic clock at 2×10^{-18} total uncertainty", Nature Com. **6**, 6896 (2015).

[Nie00] M. Niering, R. Holzwarth, J. Reichert, P. Pokasov, Th. Udem, M. Weitz, T. W. Hänsch, P. Lemonde, G. Santarelli, M. Abgrall, P. Laurent, C. Salomon and A. Clairon, "Measurement of the Hydrogen 1S – 2S Transition Frequency by Phase Coherent Comparison with a Microwave Cesium Fountain Clock", Phys. Rev. Lett. **84**, 5496 (2000).

[Ori16] S. Origlia, S. Schiller, M. S. Pramod, L. Smith, Y. Singh, W. He, S. Viswam, D. Świerad, J. Hughes, K. Bongs, U. Sterr, Ch. Lisdat, S. Vogt, S. Bize, J. Lodewyck, R. Le Targat, D. Holleville, B. Venon, P. Gill, G. Barwood, I. R. Hill, Y. Ovchinnikov, André Kulosa, W. Ertmer, E.-M. Rasel, J. Stuhler and W. Kaenders, "Development of a strontium optical lattice clock for the SOC mission on the ISS", Proc. SPIE **9900**, 990003 (2016).

[Pai11] Roland Pail, Helmut Goiginger, Wolf-Dieter Schuh, Eduard Höck, Jan Martin Brockmann, Thomas Fecher, Reinhard Mayrhofer, Ina Krasbutter and Torsten Mayer-Gürr, "GOCE-only gravity field model derived from 8 months of goce data", in , *Proceedings 4th International GOCE User Workshop Frascati, Italy, ESA Publication SP-696*, edited by L. Ouwehand, (2011) http://www.iapg.bv.tum.de/medialab/1733001/1733002/p11_pail.pdf.

[Par11] Christian G. Parthey, Arthur Matveev, Janis Alnis, Birgitta Bernhardt, Axel Beyer, Ronald Holzwarth, Aliaksei Maistrou, Randolf Pohl, Katharina Predehl, Thomas Udem, Tobias Wilken, Nikolai Kolachevsky, Michel Abgrall, Daniele Rovera, Christophe Salomon, Philippe Laurent and Theodor W. Hänsch, "Improved Measurement of the Hydrogen 1S-2S Transition Frequency", Phys. Rev. Lett. **107**, 203001 (2011).

[Pav03] Nikolaos K. Pavlis and Marc A. Weiss, "The relativistic redshift with 3×10^{-17} uncertainty at NIST, Boulder, Colorado, USA", Metrologia **40**, 66 (2003).

[Pet15a] Gérard Petit, Felicitas Arias and Gianna Panfilo, "International atomic time: Status and future challenges", C. R. Physique **16**, 480 (2015) Special Issue: The measurement of time / La mesure du temps.

[Pet15b] Gérard Petit, Amale Kanj, Sylvain Loyer, Jérôme Delporte, Flavien Mercier and Félix Perosanz, "1×10^{-16} frequency transfer by GPS PPP with integer ambiguity resolution", Metrologia **52**, 301 (2015).

[Phi85] William D. Phillips, Jon V. Prodan and Harold J. Metcalf, "Laser cooling and electromagnetic trapping of neutral atoms", J. Opt. Soc. Am. B **2**, 1751 (1985).

[Phi17] Dennis Philipp, Volker Perlick, Dirk Puetzfeld, Eva Hackmann and Claus Lämmerzahl, "Definition of the relativistic geoid in terms of isochronometric surfaces", Phys. Rev. D **95**, 104037 (2017).

[Piz17] Marco Pizzocaro, Pierre Thoumany, Benjamin Rauf, Filippo Bregolin, Gianmaria Milani, Cecilia Clivati, Giovanni A. Costanzo, Filippo Levi and Davide Calonico, "Absolute frequency measurement of the $^1S_0$ - $^3P_0$ transition of ^{171}Yb", Metrologia **54**, 102 (2017).

[Pol13] N. Poli, C. W. Oates, P. Gill and G. M. Tino, "Optical atomic clocks", Rivista del Nuovo Cimento **36**, 555 (2013).

[Pre12] K. Predehl, G. Grosche, S. M. F. Raupach, S. Droste, O. Terra, J. Alnis, Th. Legero, T. W. Hänsch, Th. Udem, R. Holzwarth and H. Schnatz, "A 920-Kilometer Optical Fiber Link for Frequency Metrology at the 19th Decimal Place", Science **336**, 441 (2012).

[Raa87] E. L. Raab, M. Prentiss, A. Cable, S. Chu and D. E. Pritchard, "Trapping of Neutral Sodium Atoms with Radiation Pressure", Phys. Rev. Lett. **59**, 2631 (1987).

[Rau15] Sebastian M. F. Raupach, Andreas Koczwara and Gesine Grosche, "Brillouin amplification supports 1×10^{-20} accuracy in optical frequency transfer over 1400 km of underground fibre", Phys. Rev. A **92**, 021801(R) (2015).

[Rie15] Fritz Riehle, "Towards a redefinition of the second based on optical atomic clocks", C. R. Physique **16**, 506 (2015) Special issue: The measurement of time / La mesure du temps.

[Rie17] Fritz Riehle, "Optical clock networks", Nature Photonics **11**, 25 (2017).

[Rob16] Clelia Robert, Jean-Marc Conan and Peter Wolf, "Impact of turbulent phase noise on frequency transfer with asymmetric two-way ground-satellite coherent optical links", Journal of Physics: Conference Series **723**, 012039 (2016).

[Ros12] M. Rost, D. Piester, W. Yang, T. Feldmann, T. Wübbena and A. Bauch, "Time transfer through optical fibers over a distance of 73 km with an uncertainty below 100 ps", Metrologia **49**, 772 (2012).

[Sam14] E. Samain, P. Vrancken, P. Guillemot, P. Fridelance and P. Exertier, "Time transfer by laser link (T2L2): characterization and calibration of the flight instrument", Metrologia **51**, 503 (2014).

[Sch96] H. Schnatz, B. Lipphardt, J. Helmcke, F. Riehle and G. Zinner, "First Phase-Coherent Frequency Measurement of Visible Radiation", Phys. Rev. Lett. **76**, 18 (1996).

[Sch01] Harald Schnatz and Friedhelm Mensing, in "Iodine-stablized, frequency-doubled Nd:YAG lasers at $\lambda = 532$ nm; design and performance", *Proceedings of SPIE: Laser Frequency Stabilization, Standards, Measurement, and Applications*, edited by John L. Hall and Jun Ye, (SPIE, P.O. Box 10, Bellingham, Washington 98227–0010 USA, 2001) , S. 239–247.

[Sch17] M. Schioppo, R. C. Brown, W. F. McGrew, N. Hinkley, R. J. Fasano, K. Beloy, T. H. Yoon, G. Milani, D. Nicolodi, J. A. Sherman, N. B. Phillips, C. W. Oates and A. D. Ludlow, "Ultra-stable optical clock with two cold-atom ensembles", Nature Photonics **11**, 48 (2017).

[Śli13] Łukasz Śliwczyński, Przemysław Krehlik, Albin Czubla, Łukasz Buczek and Marcin Lipiński, "Dissemination of time and RF frequency via a stabilized fibre optic link over a distance of 420 km", Metrologia **50**, 133 (2013).

[Ste02] Jörn Stenger, Harald Schnatz, Christian Tamm and Harald R. Telle, "Ultra-Precise Measurement of Optical Frequency Ratios", Phys. Rev. Lett. **88**, 073601 (2002).

[Ste11] Uwe Sterr, "Frequenzstabilisierungsvorrichtung", German patent DE 10 2011 015 489 (2011).

[Szy05] K. Szymaniec, W. Chalupczak, P. B. Whibberley, S. N. Lea and D. Henderson, "Evaluation of the primary frequency standard NPL-CsF1", Metrologia **42**, 49 (2005).

[Tak03] Masao Takamoto and Hidetoshi Katori, "Spectroscopy of the $^1S_0 \rightarrow ^3P_0$ Clock Transition of ^{87}Sr in an Optical Lattice", Phys. Rev. Lett. **91**, 223001 (2003).

[Tak05] Masao Takamoto, Feng-Lei Hong, Ryoichi Higashi and Hidetoshi Katori, "An optical lattice clock", Nature **435**, 321 (2005).

[Tak15] Masao Takamoto, Ichiro Ushijima, Manoj Das, Nils Nemitz, Takuya Ohkubo, Kazuhiro Yamanaka, Noriaki Ohmae, Tetsushi Takano, Tomoya Akatsuka, Atsushi Yamaguchi and Hidetoshi Katori, "Frequency ratios of Sr, Yb, and Hg based optical lattice clocks and their applications", C. R. Physique **16**, 489 (2015) Special Issue: The measurement of time / La mesure du temps.

[Tak16] Tetsushi Takano, Masao Takamoto, Ichiro Ushijima, Noriaki Ohmae, Tomoya Akatsuka, Atsushi Yamaguchi, Yuki Kuroishi, Hiroshi Munekane, Basara Miyahara and Hidetoshi Katori, "Geopotential measurements with synchronously linked optical lattice clocks", Nature Photonics **10**, 662 (2016).

[Tan15] Takehiko Tanabe, Daisuke Akamatsu, Takumi Kobayashi, Akifumi Takamizawa, Shinya Yanagimachi, Takeshi Ikegami, Tomonari Suzuyama, Hajime Inaba, Sho Okubo, Masami Yasuda, Feng-Lei Hong, Atsushi Onae and Kazumoto Hosaka, "Improved frequency measurement of the $^1S_0$-$^3P_0$ clock transition in ^{87}Sr using a Cs fountain clock as a transfer oscillator", J. Phys. Soc. Jpn. **84**, 115002 (2015).

[Tap04] Byron D. Tapley, Srinivas Bettadpur, John C. Ries, Paul F. Thompson and Michael M. Watkins, "GRACE Measurements of Mass Variability in the Earth System", Science **305**, 503 (2004).

[Ude97] Th. Udem, A. Huber, B. Gross, J. Reichert, M. Prevedelli, M. Weitz and T. W. Hänsch, "Phase-Coherent Measurement of the Hydrogen 1S–2S Transition Frequency with an Optical Frequency Interval Divider Chain", Phys. Rev. Lett. **79**, 2646 (1997).

[Ude02] Th. Udem, R. Holzwarth and T. W. Hänsch, "Optical frequency metrology", Nature **416**, 223 (2002).

[Ush15] Ichiro Ushijima, Masao Takamoto, Manoj Das, Takuya Ohkubo and Hidetoshi Katori, "Cryogenic optical lattice clocks", Nature Photonics **9**, 185 (2015).

[Ver83] M. Vermeer, *Chronometric Levelling*, (Geodeettinen Laitos, Geodetiska Institutet, 1983).

[Vig99] J. R. Vig, "Quartz Crystal Oscillators and Resonators", http://www.ieee-uffc.org/fc SLCET-TR-88-1 (Rev. 8.3.9) (1999).

[Vog11] Stefan Vogt, Christian Lisdat, Thomas Legero, Uwe Sterr, Ingo Ernsting, Alexander Nevsky and Stephan Schiller, "Demonstration of a Transportable 1 Hz-Linewidth Laser", Appl. Phys. B **104**, 741 (2011).

[Vog15] Stefan Vogt, *Eine transportable optische Gitteruhr basierend auf Strontium*, PhD thesis QUEST-Leibniz-Forschungsschule der Universität Hannover 2015.

[Vog16] Stefan Vogt, Sebastian Häfner, Jacopo Grotti, Silvio Koller, Ali Al-Masoudi, Uwe Sterr and Christian Lisdat, "A transportable optical lattice clock", J. Phys.: Conf. Ser. **723**, 012020 (2016).

[Wan60] Gregory H. Wannier, "Wave Functions and Effective Hamiltonian for Bloch Electrons in an Electric Field", Phys. Rev. **117**, 432 (1960).

[Wes11] P. G. Westergaard, J. Lodewyck, L. Lorini, A. Lecallier, E. A. Burt, M. Zawada, J. Millo and P. Lemonde, "Lattice-Induced Frequency Shifts in Sr Optical Lattice Clocks at the 10^{-17} Level", Phys. Rev. Lett. **106**, 210801 (2011).

[Wey00] Stefan Weyers, Andreas Bauch, Udo Hübner, Roland Schröder and Christian Tamm, "First Performance Results of PTB's Atomic Caesium Fountain and a Study of Contributions to its Frequency Instability", IEEE Trans. Ultrason. Ferroelectr. Freq. Control **47**, 432 (2000).

[Yam11] Atsushi Yamaguchi, Miho Fujieda, Motohiro Kumagai, Hidekazu Hachisu, Shigeo Nagano, Ying Li, Tetsuya Ido, Tetsushi Takano, Masao Takamoto and Hidetoshi Katori, "Direct Comparison of Distant Optical Lattice Clocks at the 10^{-16} Uncertainty", Appl. Phys. Express **4**, 082203 (2011).

[Yam12] Atsushi Yamaguchi, Nobuyasu Shiga, Shigeo Nagano, Ying Li, Hiroshi Ishijima, Hidekazu Hachisu, Motohiro Kumagai and Tetsuya Ido, "Stability Transfer between Two Clock Lasers Operating at Different Wavelengths for Absolute Frequency Measurement of Clock Transition in ^{87}Sr", Appl. Phys. Express **5**, 022701 (2012).

[Yao18] Jian Yao, Thomas E. Parker, Neil Ashby and Judah Levine, "Incorporating an Optical Clock Into a Time Scale", IEEE Trans. Ultrason. Ferroelectr. Freq. Control **65**, 127 (2018).

Acknowledgements

Many people contributed to the work described in this thesis, and I would like to thank them.
First of all I would like to thank Stefan Vogt, Silvio Koller and professor Christian Lisdat. Stefan built and assembled together almost all the components of the transportable clock during his doctorate work, and he taught me a lot during the first part of mine on how the system has to work. His presence during the first measurement campaign was also fundamental. Silvio started his post-doc on the transportable clock at PTB at the same time I started my doctorate. He has been a vary patient and helpful mentor during these three and a half years, and all the work presented here was done together with him. Professor Lisdat had the idea of building the transportable clock. He coordinated its development and the experiments performed with it. He was also very helpful with suggestion and corrections to write this thesis.
A lot of other people helped at PTB: discussing and working with them was very important in the realization of this thesis. Ali Al-Masoudi, Roman Schwarz and Sören Dörscher work on the stationary optical clock of our group and operated it during the clock comparisons. Sofia Herbers and Sebastian Häfner built and work on the ultra-stable cavities both for the transportable and stationary system. Stefano Origlia and Pramod Mysore work on the SOC (Space Optical Clock) European project hosted at PTB.
Discussion with my friend Lorenzo were also of great help in writing this work.
I thank the European Marie Curie Actions for giving me the opportunity to learn in an intentional environment, and all the other students that participated at FACT (Future Atomic Clock Technology) project, with which we shared a very nice experience. I thank professors Guglielmo Tino and Nicola Poli at Florence University for suggesting me to join this opportunity.
Finally, life exists also outside work and study, and many people were important during this time in Germany. I would like to thank Paola, Francesco, Matteo, Mohammed, Luciana, Francesco, Stefano, Matteo e Claudia for sharing the experience of living in an other country, my roomates Elena, Asha, Andreas, Jana for the nice time spent living together, and off course many thanks go to my girlfriend Nicola for supporting me. My family support was also fundamental to complete this doctorate, my father Anselmo, my mother Rossana, my brothers Jason and Alessio and Faton and my grandparents Mariuccia and Tino. This thesis is dedicated to my grandfathers Arturo and Tino.